NASA

Technical Memorandum 86183

21 Layer Troposphere- Stratosphere Climate Model

(NASA-TM-86183) 21 LAYER TROPOSPHERE-STRATOSPHERE CLIMATE MODEL (NASA) 78 p HC A05/MF A01 CSCL 04B
N85-21871
Unclas
G3/47 14575

D. Rind, R. Suozzo, A. Lacis, G. Russell, J. Hansen

December 1984

National Aeronautics and Space Administration

Goddard Space Flight Center
Institute for Space Studies
New York, New York 10025

ABSTRACT

Our global climate model (Model II) is extended through the stratosphere by increasing the vertical resolution and raising the rigid model top to the 0.01mb (75 km) level. The inclusion of a realistic stratosphere is necessary for investigation of the climate effects of stratospheric perturbations, such as changes of ozone, aerosols or solar ultraviolet irradiance, as well as for studying the effect on the stratosphere of tropospheric climate changes.

The model is integrated for 15 months with 8° x 10° resolution and 21 layers. Results are shown for the full seasonal cycle. The model realistically simulates the observed temperature and wind patterns throughout the troposphere and stratosphere. This includes latitudinal gradients, such as the reversed temperature gradient in the winter lower stratosphere and the summer stratosphere; seasonal variations, such as the change from winter westerlies to summer easterlies, and semiannual oscillations in temperature and wind in the equatorial upper stratosphere (although the west wind phase is weak); and realistic hemispheric differences, such as the colder lower winter stratosphere in the Southern Hemisphere, the greater zonal kinetic energy in the Southern Hemisphere winter stratosphere, and the greater eddy kinetic energy in the Northern Hemisphere winter stratosphere. The Southern Hemisphere has a larger transient to standing eddy kinetic energy ratio in winter than the Northern Hemisphere. The simulation develops what appear to be inertial oscillations in the equatorial upper stratosphere of the winter hemisphere.

The model also realistically reproduces the observed wave 1 and wave 2 forcing at the base of the lower stratosphere, and the long wave amplitudes and phases are similar to observations throughout most of the stratosphere. In the upper stratosphere the long wave amplitudes are too strong, possibly due to the lack of photochemical damping. Energy budget calculations show that the long waves are producing an energy cycle while propagating through the lower and mid stratosphere of the winter hemisphere. Eastward moving tropical waves display many of the properties expected of Kelvin waves throughout the stratosphere and appear to be associated with the semiannual wind oscillation. Horizontal transports of sensible heat and westerly momentum are realistic throughout the troposphere and stratosphere, except for excessive values in the upper stratosphere associated with the large wave amplitudes. The vertical transport of geopotential energy and the Eliassen-Palm (EP) flux show the expected greater penetration in the winter hemisphere, and the EP flux is directed into the core of the stratospheric jet due to the relatively large gradient of quasigeostrophic potential vorticity encountered there. The EP flux divergence is similar to that observed throughout the atmosphere. Finally, a time sequence of downward propagating minor warmings is shown which displays many of the properties associated with actual stratospheric warmings.

In addition to the excess planetary wave amplitude in the upper stratosphere, other model deficiencies include the Northern Hemisphere lower stratospheric temperatures being 5-10°C too cold in winter at high latitudes, probably due to the model's failure to allow excess water vapor to condense above 100mb. Also, temperatures at 50-60km altitude near the equator are too cold, probably as a result of excessive CO_2 cooling. This latter effect is

probably also responsible for the temperature gradient being too large at those altitudes near the equator, and thus for east winds of large magnitude in the tropical mesosphere. Methods of correcting these deficiencies are discussed.

1. Introduction

It is now recognized that the stratosphere may have a strong influence on lower atmospheric dynamics and climate on all time scales. For example, there is the possible influence of the top boundary condition on weather forecasts (Lindzen et al., 1968; Spahr et al., 1982) (thus the possible influence of the stratosphere on actual weather); the effect of the stratospheric refractive index on wave propagation from the troposphere, providing a mechanism for solar cycle effects on weather and climate (Hines, 1974); on a longer time scale, the changes that the ozone amount or vertical distribution would have on climate (Ramanathan and Dickinson, 1979). These effects are often interactive: for example, if changes in ozone were to change the tropospheric temperature, the water vapor coming into the stratosphere might also change, further altering the ozone.

Similarly, changes initiated in the troposphere may have strong impacts on stratospheric structure and composition. Short time-scale events such as blocking have been implicated in the generation of stratospheric warmings (Craig and Hering, 1959). Warming of the troposphere due to increased carbon dioxide could plausibly alter the water vapor content of the stratosphere, with the subsequent chemical alterations affecting numerous species (this is in addition to the direct effect of added CO_2 cooling in the stratosphere). These types of events are in addition to the well-known influence of the troposphere on the dynamics of the winter stratosphere.

In order to evaluate and understand these effects in a numerical model it is necessary that the model realistically simulate both tropospheric climate and the stratosphere. This paper describes one such model; it is an extension of the climate model described by Hansen et al. (1983 - hereafter referred to as I). There have been only two other primitive equation troposphere-stratosphere models published in the literature (Fels et al., 1980; Hunt, 1981). This model differs from both in that it includes full seasonal and diurnal cycles, and does not include explicit diffusion. The model contains all the detailed calculations and parameterizations necessary for climate simulation, as given in I. The differences between this model and the 9 layer "model II" discussed in I mainly concern the numerical techniques or parameterizations in the stratosphere; these are discussed in Section 2.

Selected output from the model is shown and compared with observations in Section 3. There are several purposes behind this comparison. The most obvious is to gage the acceptability of the model in simulating the current troposphere and stratosphere. To this end the comparison with observations is extensive, similar to that which was done in I for the tropospheric simulation. This has not previously been published for a full troposphere-stratosphere model, and is made possible by the continued accumulation of observations throughout the stratosphere and climatologies in the troposphere. In the course of the comparison opportunities arise to compare different sets of observations, and the degree of agreement among them is noted. Problems and choices which arise in the course of model development are discussed, again with reference to observations. Specific aspects of stratospheric dynamics are explored through the model simulations, including semiannual oscillations, apparent Kelvin wave variations, the energy cycle at various levels, the relative importance of transient versus stationary kinetic energy, and the relevance of stationary conservative wave theory and quasi-geostrophic

diagnostics in a time-varying primitive equation model. Finally, a series of minor warmings is discussed, which developed in the model during January, the first time such events have been shown in this type of model.

Model deficiencies are discussed as they appear from the comparison with observations. They are summarized in Section 4, along with a brief discussion of needed improvements.

2. Model description

In this section we will describe the model, emphasizing the differences between this version and the version published in I. The model structure is discussed in Section 2a, the fundamental equations in 2b, the numerics in 2c, radiation in 2d, convection and condensation in 2e, and other model physics in 2f.

a. Model structure

The model is global in horizontal extent. The horizontal and vertical resolutions are variable. The resolution employed here is 8° x 10° (latitude x longitude) with 21 levels in the vertical, as shown in Fig. 1. (As altitudes and pressures will be used interchangeably in the text, this figure provides the equivalence). There are approximately three levels in the boundary layer (although this varies with the diurnal cycle), an additional 6 layers up to the tropopause, 8 layers in the stratosphere, and 4 in the mesosphere. For radiation calculations there are an additional three layers at the top which do not interact with the dynamics but serve to provide a radiative equilibrium boundary at the top of the atmosphere. In the troposphere above the boundary layer, the layers are of nearly constant pressure thickness, while above the tropopause they are of nearly constant height thickness (log pressure). The vertical coordinate in the troposphere is the σ coordinate system (Phillips, 1957) so the ground is a coordinate surface, while at altitudes above 100mb the model uses constant pressure coordinates. This is necessary in the stratosphere to avoid spurious oscillations induced by σ coordinates in regions of variable topography. For example, meridional winds in the equatorial region near the Andes show large several grid point oscillations when σ coordinates are used throughout.

The model structure at each grid point is shown in detail in I. Each gridbox has appropriate fractions of land and ocean, with the ocean temperature and sea ice specified climatologically based on monthly mean values. Antarctica, Greenland and some Arctic islands are covered by ice sheets; snow is calculated by the model. The land has realistic topography. At each grid box radiative fluxes, convection and large-scale clouds are calculated, as well as sensible and latent heat fluxes between the ocean or land and the atmosphere. Temperature and soil moisture are calculated at several levels within the ground. In these respects the model corresponds to "Model II" as published in I; see I for more details.

b. Fundamental equations

The equations used are those given in I. They represent conservation of mass, momentum, energy, and water vapor, along with the equation of state. They differ in the stratosphere from those shown in Table 2 of I only due to

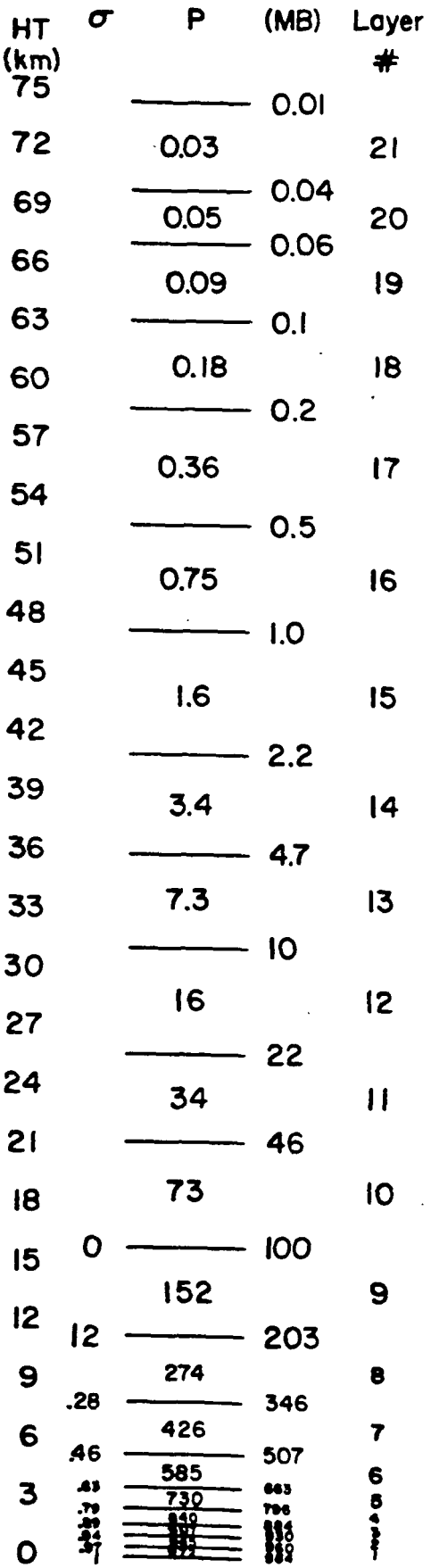

Fig. 1. Global mean pressure levels for the 21 layer model. Shown are the mean and layer edge pressures, the edge σ values for the layers in σ coordinates, the layer number and the global mean height.

the use of constant pressure coordinates. The boundary conditions are that $\sigma = 0$ at $\sigma = 1$ (the surface), and $\omega = 0$ at $p = .01$mb (the model dynamic top).

Two additional points should be made about these equations. First, there is no explicit diffusion employed, either in the vertical or the horizontal. Thus this model differs substantially from other such models (i.e., Hunt, 1981; Fels et al., 1980). Second, there is no equation for ozone photochemical feedback, the ozone values being prescribed. These points are discussed further in subsequent sections.

c. Numerics

As discussed in I, the model uses the B grid of Arakawa (1972), except that potential temperature is a prognostic variable, and the Coriolis force and metric term are included at the pole grid points. In addition, in this paper there is a major change in the advection term in the energy equation. The second order scheme used for the advection of heat in I has a tendency to produce rather noisy patterns (Russell and Lerner, 1981). This deficiency is not very noticeable in the troposphere, partly because the temperature gradients tend to be small, and partly because convection mixes heat rapidly in the vertical, destroying horizontal noise patterns. In the stratosphere the problem becomes severe. With the decreased density, wave amplitudes (wave 1 primarily) become quite large, as do horizontal temperature gradients associated with the waves. The stability of the stratosphere largely prevents any convection. Thus the noise in the temperature patterns produced by the second order scheme becomes important, and helps produce local wind gradients of large magnitude. These in turn cause difficulty in integration, especially in a model such as this with no explicit diffusion.

To alleviate this problem, the second order differencing scheme was replaced in the stratosphere (above 100mb) by the "slopes scheme" (Russell and Lerner, 1981), which produces much smoother patterns in a non-diffusive manner. In one dimension, this is a higher order upstream scheme, which represents the distribution of the advected quantity (in this case, potential temperature) within the grid box as a mean concentration and a slope. When advection takes place in two or three dimensions, the slopes may be advected laterally with an upstream scheme, as in Russell and Lerner (1981), or with second order differencing. We tried the slopes scheme in all three directions throughout the model with the spatial leapfrog splitting technique (SLF) described by Russell and Lerner. This resulted in much smoother patterns of temperature and thus height and wind, and allowed the model to be run without explicit diffusion. The derivation of this scheme, its exact formulation, and the results obtained using it compared to second and fourth order schemes, are given in Russell and Lerner (1981).

When applied to the troposphere, this scheme altered the available potential energy, and thus the eddy energy and transports. It was desired, however, for the model to produce a climatology similar to that published in I; thus it was necessary to keep the second order scheme in the troposphere. The model thus has a different numerical heat advection scheme in the horizontal above and below 100mb, which is also the level at which it switches from σ to constant pressure coordinates.

The possibility arose that using a different vertical advection scheme in the troposphere and stratosphere would introduce numerical noise at the 100mb level. Tests were run using only the vertical portion of the slopes scheme in the troposphere; they showed that this did not significantly change the tropospheric energetics or climate from that shown in I. Thus the vertical portion of the slopes scheme is used in the model throughout the atmosphere, and provides continuity through the 100mb level. The model results give no evidence of numerical perturbations generated at or near this level.

The bottom boundary condition in the model allows for zero vertical velocity at the surface, appropriate in σ coordinates. The top of the model presents a well-known difficulty: the use of an artificial lid traps energy which ought to propagate through. The result is a region of high velocity winds near the top; from the thermal wind relationship, the large shears require strong latitudinal temperature gradients. This is accomplished by inducing rising air at high latitudes, establishing an artificial circulation. Reflection of waves off the top should also affect wave transports (Kirkwood and Derome, 1977), limiting poleward heat transport.

Models with tops at around 30km and realistic topography have difficulty closing off the tropospheric jet (Tenenbaum, 1982). As the top of the model is raised, the region of excessive winds rises with it; when the top is near 50km, a level which ordinarily has strong winds, it becomes difficult to numerically integrate for any length of time. When the model top is raised out of the stratosphere, it then becomes difficult to close off the stratospheric jet (e.g., Mahlman and Sinclair, 1979).

This represents, at least to some extent, a numerical modeling difficulty. In addition, at mesospheric heights the induced diabatic circulation from summer to winter pole, theoretically on the order of 1 m s^{-1}, when acted upon by the Coriolis torques, should produce mesopheric zonal motions more than an order of magnitude larger than observed. One solution to both of these problems is to introduce friction into the mesosphere below the model top (Leovy, 1964; Schoeberl and Strobel, 1978; Holton and Wehrbein, 1980). This technique works to alleviate the problem of energy accumulation near the artificial lid, as was shown in I, when it was applied to the 30mb level. It also can be used to explain why the observed mesospheric winds decrease with altitude even in the presumed presence of the diabatic circulation. The friction is thought to result from breaking gravity waves (including tides), the adiabatic temperature changes associated with the waves producing an unstable lapse rate when combined with the already steep temperature decline with height prevalent in the mesosphere. If these waves have a low level source their (pseudo) momentum is significantly less than the ambient momentum, and as the waves break they would act as a drag on the flow.

In reality, this process, and its application, may be much more complicated. The point of absorption of these waves may be difficult to determine since it may involve critical level absorption. For this and other reasons, the parameterization of the process should differ from the simple Rayleigh friction often used (Lindzen, 1981). There is even some question as to whether other processes, such as inertial instability (Dunkerton, 1981) might not actually be more responsible for drag in equatorial regions.

In this model it is assumed that the dominant drag mechanism in the mesosphere is that associated with breaking gravity waves. Frictional drag is incorporated in layers 19-21 (approximately 65-75km); although analysis shows that the effects may occur as low as 50km in winter (Lindzen, 1981), observations show that the apparent turbulence is largest above 70km (e.g., Rottger, 1980). The form of the drag is similar to that employed at the surface (I, equations 44-49), except the variation of the drag coefficient in conditions of non-neutral stability has been altered. The stability criterion is determined by assuming that a gravity wave with a surface temperature perturbation of 0.1°C has propagated up to these heights with no attenuation (the kinetic energy density remains constant). The wave is assumed to have a 1km vertical wavelength and induces a peak to peak temperature perturbation over a 500m vertical distance. This lapse rate is added to the background lapse rate, interpolated to this scale; if the resulting total lapse rate exceeds the dry adiabatic, the drag coefficient is maximized. Insofar as the density decreases with altitude, the wave amplitude will be highest at the highest levels. The instability will also be largest in regions where the ambient lapse rate is largest, for constant wave amplitude. This parame-terization thus is an attempt to mimic the conditions under which breaking gravity waves are most likely.

The decay time associated with this drag in the winter hemisphere averages about 2 ± 1 days at 65km, about 1 ± 1/2 day at 70km, and about 1/2 ± 1/4 day at 75km (varying with wind speed, and thus latitude). These are somewhat faster than those employed by Holton and Wehrbein (1980) in their symmetric model (in which the decay times ranged from 5 days to 2 days at these altitudes), although the use of a more realistic infrared radiation algorithm would require that model to use stronger mechanical dissipation, more like the values used here (Wehrbein and Leovy 1982; Holton, 1983). Various values and forms of the drag were tried, including some with longer decay times. The winds and temperatures in the stratosphere were only slightly altered by the different magnitudes.

An additional question which arises is what to do with the energy removed by the drag. The same question can of course be asked about the energy lost to friction at the earth's surface, but that is insignificant compared to the energy in the troposphere. In the mesosphere, however, the results are quite different. Several runs were made in which the energy removed by the drag was put back in the form of heat, to be lost eventually by radiative fluxes. The resulting temperature differences at 70°N, where the drag is strongest in winter, between these runs and runs in which the energy was simply discarded, ranged between 10°-30°C, with the highest values at the greatest altitudes (75km). At 70°N including the energy back into the model produced results which were strongly at variance with the (somewhat uncertain) observations in the mesosphere. At other latitudes, where the effects were less, it was not obvious which formulation compared better with observations. It also appeared as if the change in stability resulting from the different formulations affected the long wave amplitudes throughout the stratosphere, although this could not be proved as the model has not been run sufficiently to determine natural standard deviations. The final version of the model discards the energy removed by the drag; despite the theoretical arguments in favor of the effects of breaking waves, and the observations of (sporadic) turbulence, the inclusion of the drag in the form used here must be considered an artifact of the numerical modeling procedure to reduce the influence of the model top. We

thus in effect hypothesize that the waves propagate through the model's artificial lid, and are unavailable to influence events below.

As mentioned in the previous section, the model includes no explicit diffusion, either in the horizontal or in the vertical. Horizontal turbulence likely exists at all levels (e.g., Zimmerman and Keneshea, 1981), and vertical turbulent transfers are likely in the mesosphere (Allen et al., 1981). The exclusion of diffusion is based on the desire to present a model in which diffusion is not necessary for numerical stabilization, and does not influence model simulations in an unwarranted fashion. Subsequent versions of the model may incorporate realistic diffusion values if they can be accurately determined.

The time differencing is the same as that in I, except where it is modified in conjunction with the slopes scheme (see Russell and Lerner, 1981). The smoothing and conservation of integral properties in this model are the same as those in I.

d. Radiation

The radiation routines, both short wave and long wave, are essentially those used in I, except for the following differences.

1) For the short wave radiation, the optical thicknesses for CO_2, H_2O and O_2 were interpolated directly from numerical k-distribution tables as is the case for thermal radiation in I. (Solar radiation in I uses analytic formulas that were fitted to the k-distributions). This improved the accuracy in those cases where the analytic fit was imperfect, particularly in the upper stratosphere.

2) In the long wave radiation, the tabulated absorption coefficients were refitted to obtain a more accurate integration over zenith angle and closer agreement with 1D model results for stratospheric cooling rates. Both the 1D and 3D radiation codes use explicit integration over zenith angle; since zenith angle effects become more important in the stratosphere, there is some need to compensate for the coarser 3D resolution. This change is more important for improving the accuracy in the more rarified regions of the atmosphere.

3) In the long wave radiation, the 3D code merges the spectral and probability intervals of the k-distributions compared to using an explicit spectral integration scheme with typically 10 probability intervals per spectral band in the 1D model. We refined the parameterizations for merging the overlapping CO_2 and water vapor absorption to provide closer agreement with 1D model results for the downward directed thermal fluxes. This change basically improved the details of the surface energy balance, but is of lesser importance in the stratosphere.

One other change involved the way the temperatures are transmitted to the radiation scheme. The use of the slopes scheme in the vertical provides a first order approximation of the temperatures at the edges of the layers, in addition to the normally calculated value for the layer as a whole. As the radiation assumes a linear Planck function within a layer, a slope for σT^4 was least-squares fit to the linear T slope produced by the slopes scheme in the

dynamics subroutine. This then defined the temperature at the layer edges with more resolution than would have been the case otherwise.

The column average climatological ozone distribution as a function of latitude and month was taken from London et al. (1976). The vertical distribution is also a function of latitude and month, at altitudes below the 10mb level based on the distributions given by Dutsch et al. (1971, 1974) and at altitudes above 10mb from London et al. (1977). The resultant distribution is generally consistent with the more recent observations (McPeters, 1980; Wang et al., 1982), although they do not maintain the hemispheric asymmetry in upper stratospheric ozone (e.g., Maeda and Heath, 1973). The ozone distribution has not been altered to offset other radiation errors by tuning the equatorial stratospheric temperatures as has been done in other models; the philosophy is to present the model results unaltered so as to highlight uncertainties in modeling or theory. In addition, as noted previously, the ozone does not respond photochemically to changes in temperature. Although the ozone climatology includes longitudinal variations, in the model we used zonally averaged ozone amounts.

The water vapor distribution at altitudes of 18km and above was initialized at a value of 3×10^{-6} (kg H_2O/kg air), a value consistent with observations (WMO, 1981) although there is no increase with altitude prescribed. Due to the uniform distribution, after 15 months values throughout much of the upper stratosphere and mesosphere were close to the initial value. Thermal cooling would be slightly different if other values were used in the initialization.

In the lower stratosphere large-scale advection alters the initial water vapor distribution, due at least partially to unrealistic restrictions discussed below.

e. Convection and condensation

The only difference between the moist convection scheme outlined in I and the version employed here relates to the transition level between σ and pressure coordinates. Because of the complexity involved in the scheme, it is difficult to calculate the mass flux through this transition; thus in this model moist convection is not allowed to pass through the 100mb level. In addition, large-scale condensation is also not allowed above 100mb, again for the sake of simplicity. In earlier versions of the model, which were completely in σ coordinates, moist convection and condensation were allowed to occur at all altitudes, and the mass flux through 100mb, and condensation from 100-50mb, was small but not zero. The restrictions imposed here thus produce errors in the moisture profile. There is nothing about these schemes that inherently prohibit their use in σ and pressure coordinates, and these restrictions should be removed in future model integrations.

Dry convection is allowed at all levels.

f. Other model physics

The rest of the model physics is the same as that discussed in I. This includes cloud calculations, ground physics, and surface air quantities. The model computes clouds at all levels, temperature and moisture at two levels

within the ground, snow cover, and surface air temperature, wind and moisture for flux and diagnostic purposes. The version used in this model specifies the sea surface temperature and ocean and land ice cover (see I for more details).

3. Model Simulations

The model described above was integrated for 15 months, starting from climatological initial conditions for December 1. The boundary conditions affected by the seasonal cycle (e.g. sun, sea surface temperatures) were varied daily, and a diurnal cycle was included. The results presented here will be for the last 12 months of the simulation. The results for February of year 2 were similar although not identical to those for February of year 1, implying that the three month adjustment was sufficient for most quantities. In the troposphere, even with specified sea surface temperatures, there are longer time constants in the system (such as ground moisture and ground temperature in the second layer) for which three months are not sufficient. As the tropospheric simulations were discussed in detail in I, we will concentrate on the results for the stratosphere, except where results in the troposphere differ from those in the 9 layer model, or are important for understanding the stratospheric simulation and were not previously presented.

Comparison will be made with observations for a number of different quantities. This presents several problems. The observations often differ substantially from one another, either due to the use of different techniques or to the use of different years of data. Especially in the Northern Hemisphere winter, the inclusion of years with stratospheric warmings produces zonal averages which vary widely from those compiled for years without major warmings. The uncertainty in the meaning of a "typical" winter also may apply to the model: the model winter used for this comparison did not feature a major warming and there is no way to know what the interannual variability in the model will be without further integrations. We will thus try to compare the model results with those for typical non-warming winters, although the collected climatologies combine both types of winters.

For many quantities, especially in the Southern Hemisphere, we are limited to one or perhaps two years of analysis at most. These comparisons can thus not be thought of as definitive.

a. Temperature

The model simulations will be shown in a variety of formats, for both January and July.

1) ZONAL MEAN TEMPERATURE VERSUS ALTITUDE

Fig. 2 displays the results for January and July of the zonally averaged temperature as a function of latitude and pressure. Realistic features include temperature decreasing with increased altitude in the lower stratosphere, increasing above to the stratopause, then decreasing in the mesosphere. The summer stratosphere and troposphere are warmer than the winter ones, while the reverse is true in the mesosphere. A more detailed analysis is given below.

ORIGINAL PAGE IS
OF POOR QUALITY

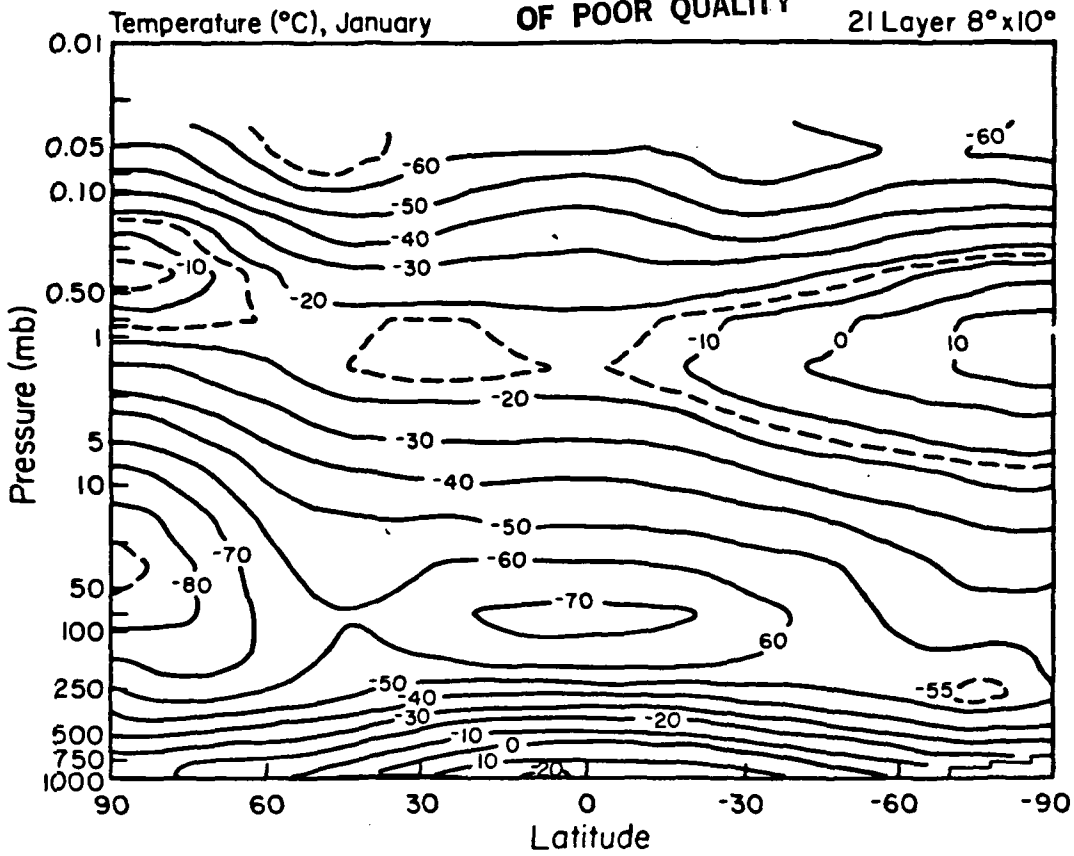

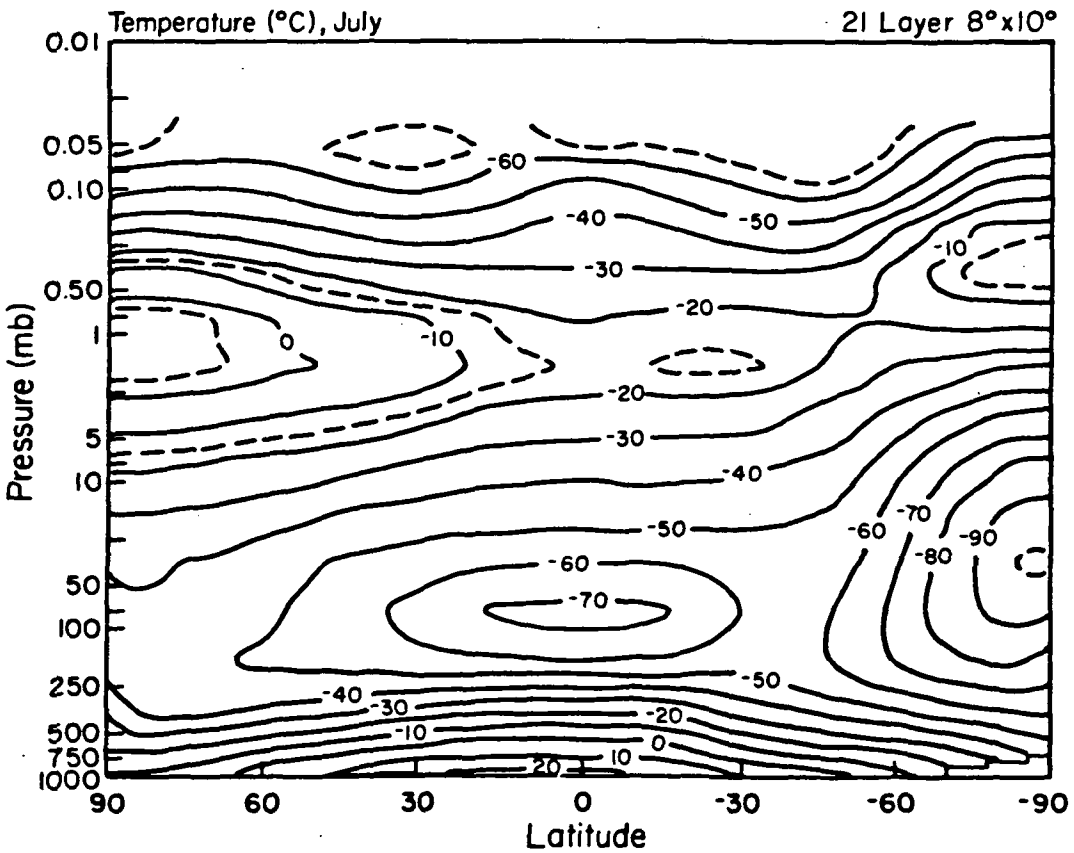

Fig. 2. Latitude-height profile of zonal mean temperature for (a) January and (b) July. Dashed lines indicate in-between contour values.

JANUARY: The tropical tropopause temperature of -74°C compares favorably with the value of -76°C reported by Geller et al. (1983) for the years 1978-1981. This is an important parameter if the region is acting as a cold trap for water vapor entering the stratosphere. It is also in agreement with the reports of Newell et al. (1969), but is somewhat warmer than the -80°C given by Oort and Rasmusson (1971). As pointed out by Newell (1972) the variation of this temperature is probably related to changes in the vertical motion associated with the Hadley circulation (whose estimates are also quite variable, as noted in I, and which may be subject to large year-to-year variations). Variations of several degrees also occur in this region due to the quasi-biennial oscillation and volcanic aerosols (e.g., Angell and Korshover, 1964; Quiroz, 1983), as well as the solar cycle (Quiroz, 1979). (The model value may also be affected by the vertical layering, as temperature changes rapidly with altitude).

The temperature gradient in the model's lower stratosphere properly reverses from the equator to 55°N, but the values north of about 60°N are too cold by 5-10°C. One possible contributing factor involves the water vapor, which as noted in Section 2e was not allowed to condense above 100mb. Thus in January the specific humidity poleward of 50°N was six times too large at 73mb, three times too large at 34mb, and two times too large at 16mb compared with observations of 3-4 ppmv (see the compilation of observations in the WMO report, 1981). Using Standard Atmosphere temperatures for a one time-step integration, this water vapor produced cooling rates which ranged from two times too large at 73mb, to 15% excessive at 16mb. A two month experiment was conducted to determine the effect the proper water vapor would have on the model's temperatures. Starting with the initial conditions for December 1, December and the final January were rerun with the water vapor fixed at the observed value. The monthly average temperatures in January were 2-3° warmer in the high latitude lower stratosphere, and seven degrees warmer in the middle stratosphere, while the cooling rate for the month was still reduced by some 33% at 73mb. It thus seems likely that the excessive water vapor, which would have been reduced if condensation had been allowed (as average relative humidities were well above 100%), was greatly if not entirely responsible for the cold temperatures in the model simulation. Another potential contributing factor, sensible heat transports, will be discussed in Section 3e.

The excessive water vapor peaks at the 150 and 73mb layers, and then decreases to observed values by 7mb. At 30mb high latitude winter temperatures are still slightly too cold compared to climatological averages (e.g., Geller et al., 1983) but are actually in good agreement with "cold" January observations, such as in January of 1981 (Labitzke and Goretzki, 1982). At the 10mb level the temperature throughout the Northern Hemisphere is in good agreement with a typical "cold" January (Labitzke, 1981), and it remains so through the 1.6mb (45km) level (Geller et al., 1983; Groves, 1971).

In the region extending from 50-60km at low latitudes, temperatures once again are colder than observed, by 15-20°C. As this region is not strongly affected by dynamic transports, the problem was thought to involve the radiation calculations. A comparison was made between the CO_2 cooling rates calculated in this model, and those reported by Apruzese et al. (1982). With the radiation scheme employed here the cooling rate from CO_2 increased from near 6°C day^{-1} at 45km to 9-10° day^{-1} at 50-56km for the U.S. Standard Atmos-phere (1962) temperature profile. In the several models reported by Apruzese et al. (1982)

the cooling rates were significantly lower from 50-56km, ranging from 7-8°C day^{-1}. While the lack of agreement in itself would not prove there is excessive cooling in this radiation scheme, the fact that the temperatures are so low compared with observations makes it likely that the cooling above 45km is overestimated. The current k-distribution method was developed for the more massive lower atmosphere; work is in progress to improve the scheme for the region above 45km.

The relatively warm high latitude temperatures observed near 50km at high northern latitudes during this month result from warming pulsations which occur associated with the large amplitude wave number 1 in the model. This will be discussed in Sections 3d and 3f.

The Southern Hemisphere model values during this month appear to be in good agreement with available observations (Newell et al., 1969; Koshelkov, 1977) although they might be 5°C too cold in the polar upper troposphere. However, the successful simulation of the extratropical summer stratospheric temperatures at 50km, in contrast to the relatively cold equatorial temperatures at that altitude, raises the possibility of compensation due to excessive ozone heating at Southern polar latitudes. To investigate this the model ozone heating rates were compared with those calculated by several modelers for the 50km region. On January 1 the heating rate in the model varied from about 9°C day^{-1} at the equator to around 21°C day^{-1} at 90°S. This is in essential agreement with the results of Park and London (1974) from whom the ozone distribution above 10mb was derived. It disagrees with the results of Wang et al. (1982) which range from 8°C day^{-1} at the equator to only 13°C day^{-1} at 90°S. The latter authors note their differences with Park and London, and ascribe it to different ozone distributions. However, at these altitudes and locations the ozone distributions are very similar. The possibility of excess ozone heating in the model cannot be discounted or confirmed given the uncertainties which exist for heating rates in the upper stratosphere.

The temperatures calculated for January were insensitive to the value of the drag used. In a separate experiment the drag was reduced by a factor of 4 from that used in the standard run. Zonally averaged temperatures did not vary by more than 2°C at any location at any altitude after a one month integration.

JULY: Results for this month can be compared with the observations compiled by Oort and Rasmussen (1971) and Taljaard et al. (1969) for the troposphere, and by Groves (1971), Koshelkov (1977), and Labitzke (1980) for the stratosphere and lower mesosphere. The results shown by Hartmann (1976a) for July through September of 1973 in the Southern Hemisphere can be used to provide a check from the surface through the lower mesosphere.

The simulation shown in Fig. 2 is in excellent agreement with the observations up to the 0.1mb level (65km) with the exception of the cold tropical temperatures from 50-60km, the same problem noted in January. Successfully reproduced features include the very cold Southern Hemisphere polar temperatures in the lower stratosphere, the lower stratosphere temperature gradient reversal from the equator to 43°S, the temperature gradient reversal throughout the Northern Hemisphere lower stratosphere, and the magnitude of the polar temperatures in both hemispheres in the upper stratosphere and lower

mesosphere. The region above 0.1mb is influenced by the incorporated drag, as well as the model top, and thus the temperatures are not sufficiently cold in the Northern Hemisphere polar region.

The lower stratospheric water vapor is not as excessive in polar regions as it was in January, due either to the extremely cold upper troposphere temperatures or simply the length of the run up to July as opposed to the following January. However, relative humidities are still greatly in excess of 100%, and there would likely be an influence on the temperature if the moisture were allowed to condense.

2) LATITUDINAL MEAN TEMPERATURE VERSUS MONTH

Shown in Fig. 3 are the temperatures as a function of latitude and month for the 1.6mb layer (45km) representative of the upper stratosphere and the 34mb layer (23km) representative of the lower - to mid-stratosphere. These levels were picked to allow for comparison with satellite derived radiances centered on the 2mb and 30mb levels (e.g., Labitzke, 1974, 1980, 1981; Labitzke and Barnett, 1973; Ghazi, 1976; McGregor and Chapman, 1979). The 30mb temperatures are also obtained by radiosonde data and analyses are available (e.g., Labitzke and Goretzki, 1982; Naujokat, 1981), while at 45km additional observations come from rocketsondes (Groves, 1971; Koshelkov, 1977).

In the model Northern Hemisphere, the upper stratosphere temperatures are coldest in December, warming somewhat in January, then cooling again in February, before the onset of the spring warming in March. The summertime temperatures show a peak around the solstice in June. In the lower stratosphere, high latitude northern temperatures remain cold throughout the winter. The relatively warmer January at 1.6mb results from warming pulses which occur during the month (Section 3f). These pulses do not occur with the same amplitude in the lower stratosphere, so it resembles the "cold" January observations. These features are in complete agreement with the generally occurring patterns noted in the references given above, although the 30mb polar temperatures are too cold by up to 10°C (Naujokat, 1981).

In the tropical upper stratosphere a semiannual variation is apparent with coldest temperatures around the solstices. This is also in agreement with observations (Labitzke and Barnett, 1973) and has been correlated with temperature changes at high latitudes in the respective winter hemispheres (Fritz and Soules, 1970; van Loon et al., 1972). As shown in Section 3f, this correlation occurs in the model as well.

In the Southern Hemisphere temperatures are actually coldest in late fall in the upper stratosphere, and there is gradual warming during the winter. In the lower stratosphere the coldest temperatures do occur in midwinter. Both features are in accord with observations (Labitzke and Barnett, 1973; Labitzke, 1974).

Comparing the two hemispheres, in the upper stratosphere during midwinter (January versus July), the Southern Hemisphere temperatures are about 9°C colder than corresponding Northern Hemisphere temperatures. In the later part of the winter (February versus August) the situation has reversed, with the Southern Hemisphere now being 10°C warmer than the Northern Hemisphere poleward of 60° latitude. The warming pulses in the Northern Hemisphere in midwinter

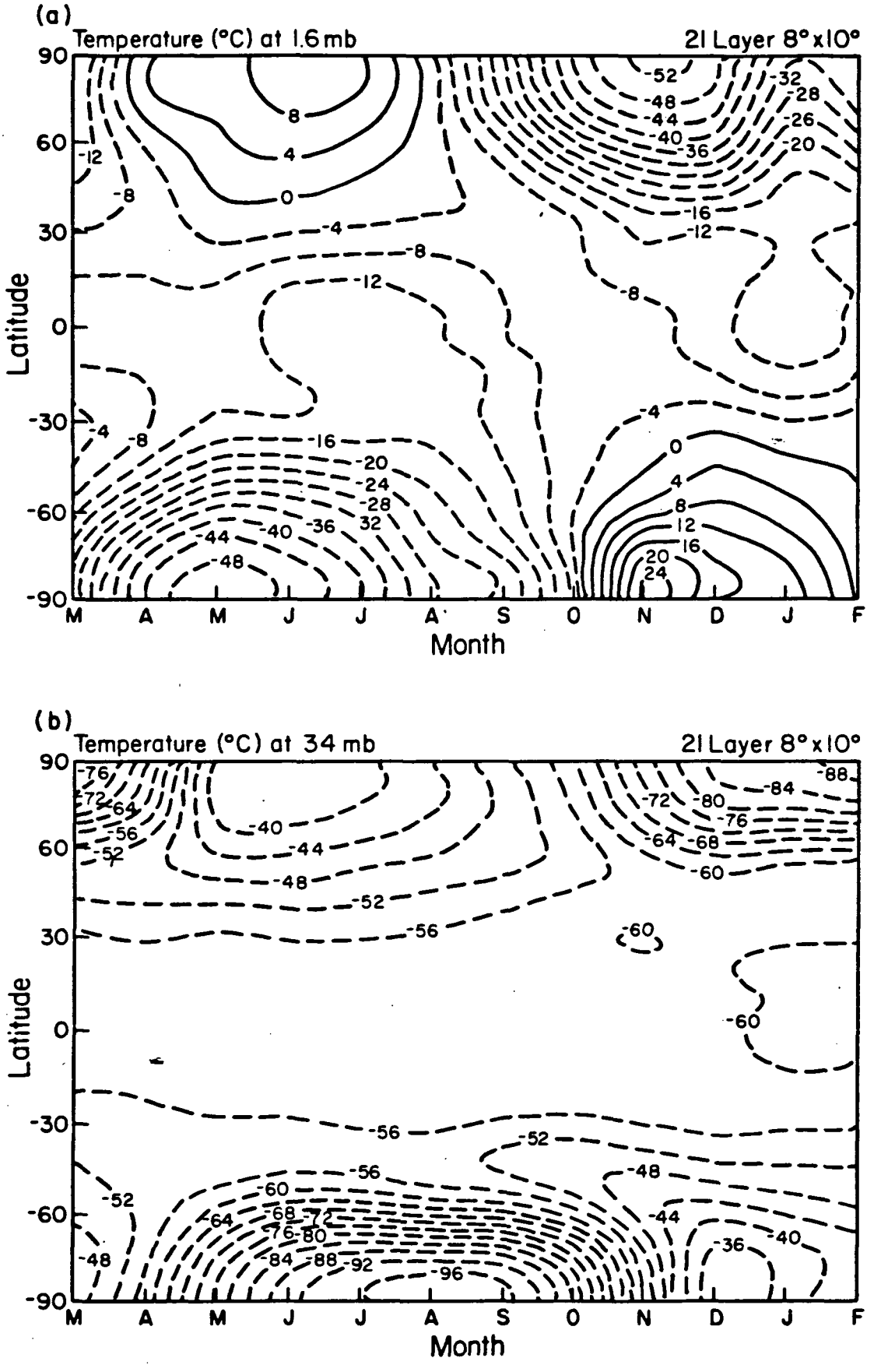

Fig. 3. Zonal mean temperature versus month for (a) 1.6mb level and (b) 34mb level. Dashed contours indicate negative numbers.

are followed by intensified cooling in late winter, in contrast to the gradual warming scenario which prevails in the Southern Hemisphere. The magnitudes, locations and timing of these differences are all in agreement with satellite observations (Labitzke, 1974).

The summer temperatures in the upper stratosphere at this level are warmer in the Southern Hemisphere in both model and reality, a fact which has been related to the shorter distance of the Earth from the Sun during Southern Hemisphere summer. In the model there is a difference in solar radiation heating rates of 0.5-1°C day^{-1} between the two hemispheres during summer. The magnitude of the temperature difference is in general agreement with observations (Labitzke, 1974; McGregor and Chapman, 1979).

The Southern Hemisphere high latitude temperatures in the model's upper stratosphere are warmest in November; this type of spring "overshooting", sometimes rapid, has been seen in the Northern Hemisphere (e.g., Nordberg et al., 1965; Johnson and Gelman, 1968). Theon et al. (1972) pointed out that the time of the temperature maximum in the Northern Hemisphere generally varies with latitude, occurring in spring at mid-latitudes, and in midsummer at the highest latitudes. This effect does occur in the model Northern Hemisphere and appears as a phase shift between the warm equinoctial conditions in the tropics and the warm solstice at the North Pole. In the model Southern Hemisphere conditions are warmest at the solstice from 27°-67°S, and the November overshooting is limited to the highest latitudes. The cause of this warming in the model remains to be investigated, as does its interannual variability.

In the lower stratosphere, the dominant hemispheric differences are at high latitudes, where the Southern Hemisphere is colder in winter and warmer in summer, in agreement with what is observed (Labitzke, 1974; McGregor and Chapman, 1979). The colder winters are thought to be due to the reduced planetary wave activity in the Southern Hemisphere, with the warmer summers again resulting at least partially from the shorter Earth-Sun distance. Both effects occur in the model (especially for standing waves - see Section 3d).

3) LATITUDE-LONGITUDE TEMPERATURE MAPS

The temperatures at various levels in the atmosphere are shown in Figs. 4 and 5 for January and July. The top panels in each figure give the results for the surface, and for the mid-troposphere (mean temperature for the 700-500mb layer, ~4.3km). The tropospheric results have been discussed in I, and will not be commented on further here except to note that they are in good agreement with observations. Results for the lower stratosphere (mean temperature for 100mb-30mb layers, ~20km) and mid-stratosphere (10mb-3.4mb, ~35km) are given in the middle panels. The bottom panels show the results for the upper stratosphere (3.4mb-0.7mb, ~45km) and lower mesosphere (0.7mb-0.16mb, ~55km).

JANUARY: The lower stratosphere temperature distribution features a warm region centered around the International Dateline in the Northern Hemisphere with a cold polar region centered around the Greenwich Meridian. Comparison with climatological 100mb maps (Crutcher and Meserve, 1970) and 30mb maps (Labitzke, 1977, 1980; Labitzke and Goretzki, 1982) indicates that the

ORIGINAL PAGE IS
OF POOR QUALITY

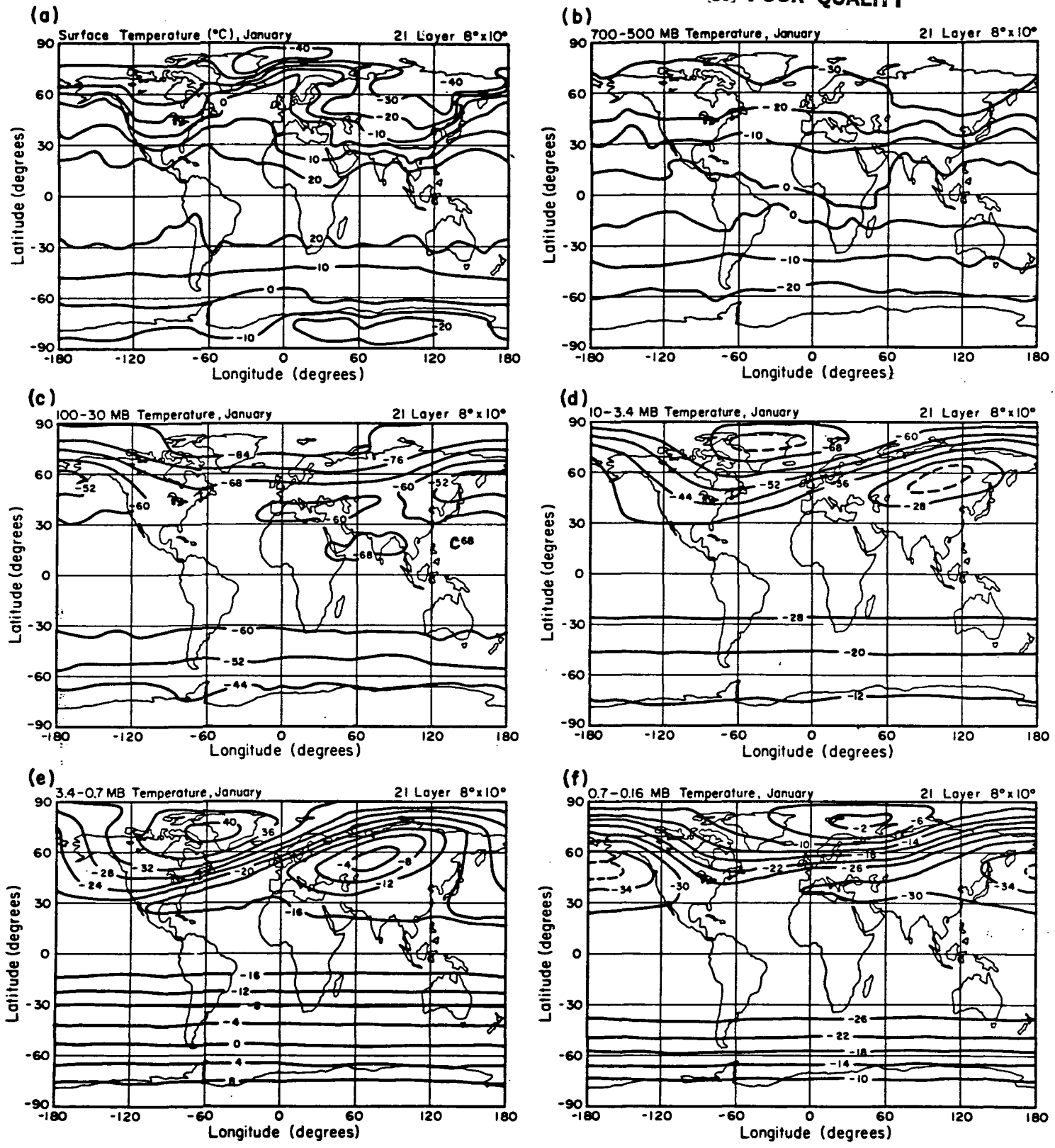

Fig. 4. Global distribution of temperature in January for (a) surface; (b) 700-500mb; (c) 100-30mb; (d) 10-3.4mb; (e) 3.4-0.7mb; (f) 0.7-0.16mb. Dashed lines indicate in-between contour values.

ORIGINAL PAGE IS
OF POOR QUALITY

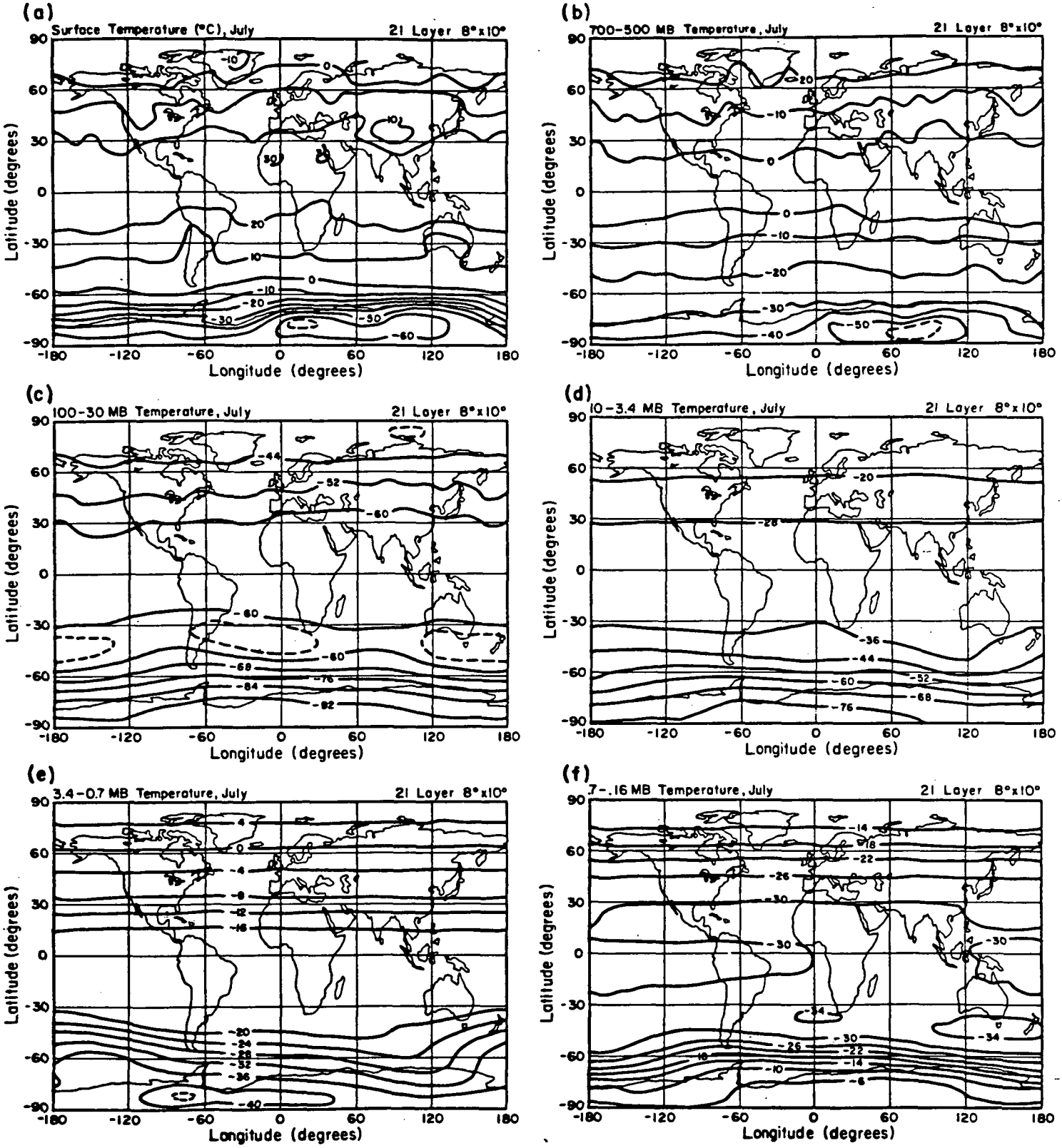

Fig. 5. Same as Fig. 4 for July.

simulation is in good agreement with observations. The polar temperatures are slightly too cold, as discussed earlier, but the difference is small at 30mb compared to "cold" January temperatures (e.g., 1981 as shown by Labitzke and Goretzki, 1982).

In the middle stratosphere the axis of the warm and cold regions has sloped to the west, to a position in agreement with observations (e.g., the observations shown by Manabe and Mahlman, 1976; McGregor and Chapman, 1979; Austen et al., 1977). The amplitude of the essentially wave 1 feature in the model upper stratosphere is greater than usually observed, as will be discussed in Section 3d. In the lower mesosphere the warm region is approaching the pole, as occurred in the observation of this altitude shown by Austen et al. (1977). This reversal of the latitudinal temperature gradient helps close off the stratospheric jet (from the thermal wind relationship), as will be shown in section 3b.

In the Southern Hemisphere during this month the temperatures are warmest near the pole throughout the stratosphere and lower mesosphere with a symmetric distribution (circular around the pole in polar stereographic coordinates; see Taljaard et al., 1969 who show that this is true even at 100mb).

JULY: The monthly average Southern Hemisphere winter has a much more symmetric temperature pattern than did the Northern Hemisphere, as is expected from the reduced standing long wave energy (Section 3d). The warm ridge that becomes evident by the upper stratosphere is located just to the west of the Dateline, in apparent agreement with the observations of McGregor and Chapman (1979) (but not with those shown by Labitzke, 1977 for June). The temperature gradient near the pole begins to reverse at heights of 45-50km, and is completely reversed in the lower mesosphere, acting to close off the stratospheric jet. This appears to be an observed feature above 1mb (Labitzke, 1980).

In the Northern Hemisphere the warm polar temperatures and the concentric appearance of the isotherms is in accordance with observations (e.g., Crutcher and Meserve, 1970; Manabe and Mahlman, 1976; Labitzke, 1980).

4) TEMPERATURE, LONGITUDE VERSUS ALTITUDE, 51°N

Shown in Fig. 6 is a longitude versus altitude plot of temperature at 51°N for January and July. In January the warm regions start near the surface from what is essentially a wave 2 feature at 10°W and 150°W, slope to the west with increasing altitude and become essentially a wave 1 feature in the stratosphere. The warm ridge is located at about 150°E at 30mb and shifts westward to near 60°E at 1.6mb (43km), and to 60°W by 70km. These results are in good agreement with those shown by Labitzke (1980, 1981) for temperatures, or, in the upper stratosphere and mesosphere, radiances.

The results for July show the absence of any long wave features above the tropopause, as expected due to the presence of east winds prohibiting wave propagation (Sections 3d, 3e).

ORIGINAL PAGE IS
OF POOR QUALITY

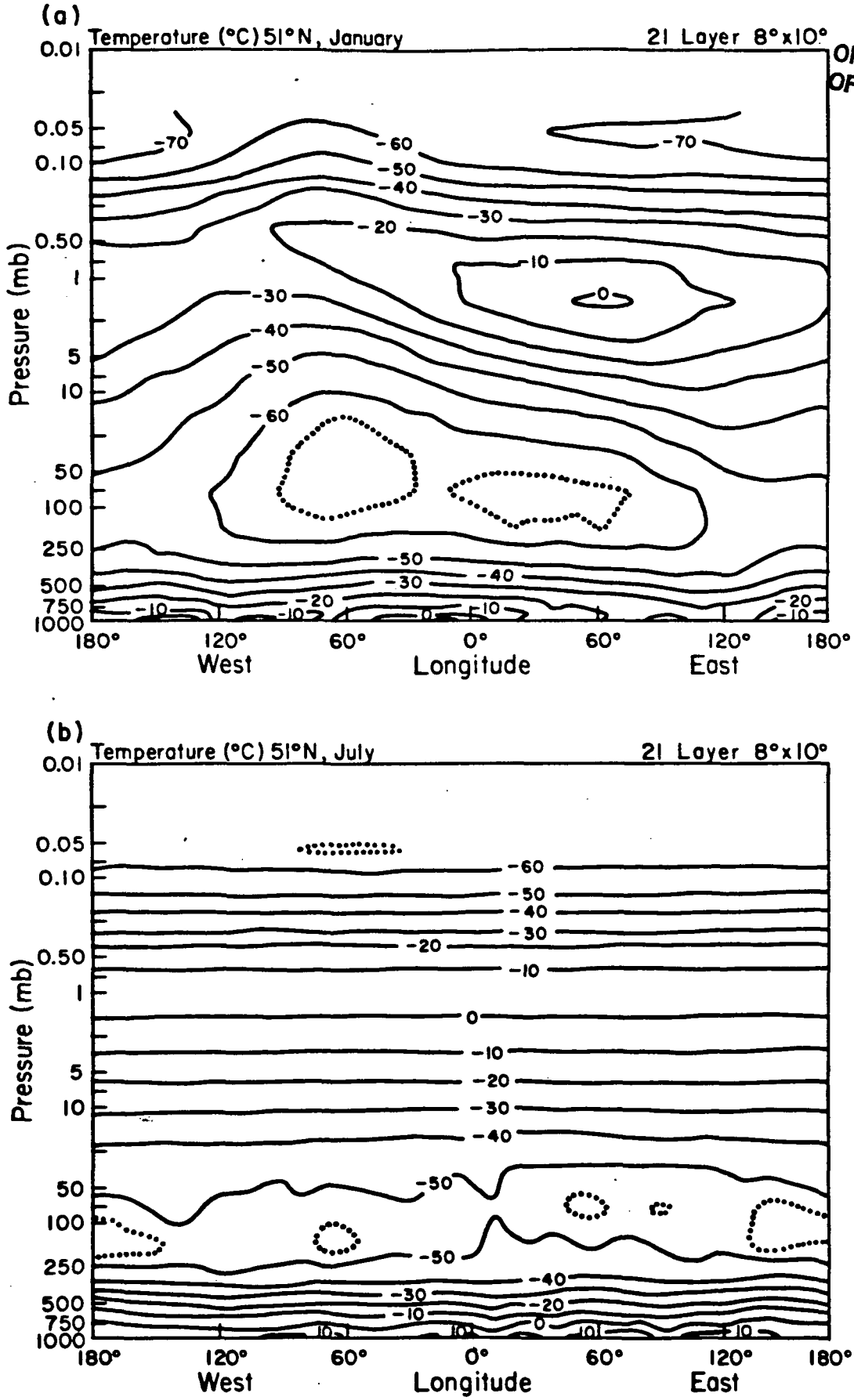

Fig. 6. Longitude-height profile of temperature at 51°N in (a) January and (b) July. Dotted lines indicate in-between contour values.

b. Wind

1) ZONAL MEAN WIND VERSUS ALTITUDE

Shown in Fig. 7 are the results for January and July of the zonally averaged zonal wind versus pressure.

JANUARY: The Northern Hemisphere shows the two prominent jets, tropospheric and stratospheric. The tropospheric jet is slightly weaker than observed (in I it was shown that it improves in intensity when the horizontal resolution is improved). The stratospheric jet appears realistic (e.g., Newell, 1968) although once again large variations are encountered in observations due to the occurrence of stratospheric warming events with light west winds. It will be shown below that the value of the jet is actually slightly larger in December and February, since January underwent warming pulses in the stratosphere. When the drag in the top three levels was reduced by a factor of four the stratospheric jet increased by 5-10ms^{-1}.

The vertical shear to the north and above the tropospheric jet is too weak in the model, a feature common to models with topography (Tenenbaum, 1982). This is consistent with the cold polar lower stratosphere discussed above. In his analysis Tenenbaum concluded that this deficiency affected wave 3, allowing it to propagate too easily into the stratosphere, and thus reducing the tropospheric wave 3 energy below its observed value. As will be shown in Section 3d, the effect may occur in this model as well.

Observations of winds in the extratropical mesosphere often give values of 70 ms^{-1} near 75km (Newell, 1968; Groves, 1969), although there are many observations of significantly smaller velocities (e.g., Gregory et al., 1981). The model value at that altitude in January is 45 ms^{-1} at upper mid-latitudes. While the observations will be affected by whether or not warmings have occurred, it is possible that the drag incorporated in the model, which is responsible for the decrease of wind speed above the stratospheric jet, might be too large.

The low latitude easterlies in January cross over into the Northern Hemisphere. In Section 3e it will be shown that this is related to angular momentum divergence caused by the long waves in the winter hemisphere, as postulated (Hirota, 1980). South of the equator the low latitude east winds appear realistic up to about 45km, but then become excessive. The geostrophic wind shear is very sensitive to the temperature gradient near the equator. For example, a 1°C temperature gradient between 12° and 4° latitude at 1.6mb will produce a wind shear of about 11 ms^{-1} up to 0.7mb; thus if the gradient increases to 3°C, the wind shear will be 33 ms^{-1} (which is similar to what occurs at low latitudes in the model). Given the potential problems with the radiation at 50km and above, the excessive temperature gradient right near the equator is not surprising. A similar problem was encountered by Crane et al. (1980) in their two dimensional model.

The direction of the zonal winds in the tropical lower stratosphere depends upon the phase of the quasibiennial oscillation. Given the length of this integration it is impossible to tell whether the model will experience such an oscillation. During the model run the winds in this region were

ORIGINAL PAGE IS
OF POOR QUALITY

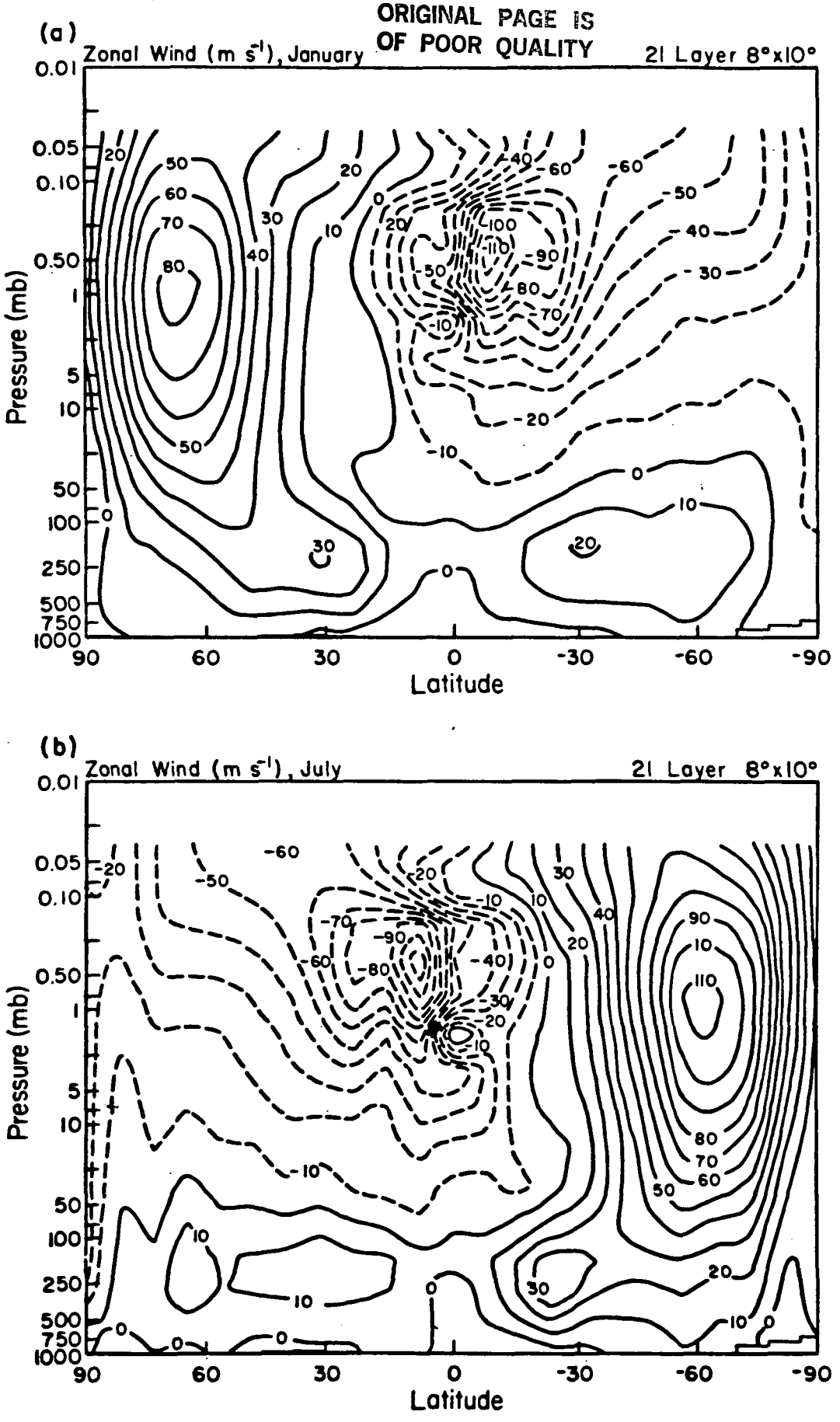

Fig. 7. Latitude-height profile of zonal mean zonal wind for (a) January and (b) July. West winds are shown by solid contours, east winds by dashed contours.

generally easterly although a region of west winds at the equator descended from 73mb to 150mb during the course of the run.

The Southern Hemisphere simulation, with tropospheric westerlies and stratospheric east winds appears realistic, although the subtropical tropospheric jet stream may be too weak (Labitzke, 1980, Fig. 5).

JULY: The July simulation correctly reproduces the summer stratospheric east winds and the winter stratospheric jet. Note the stronger magnitude of the Southern Hemisphere jet compared to that of Northern Hemisphere winter in the stratosphere; the values are in agreement with observations (McGregor and Chapman, 1979). Once again the tropospheric jet streams may be slightly too weak, and the east winds to the north of the equator are excessive above 50km. Again note the region of decreased east winds, this time manifesting as actual west winds, at 1.6mb, now just to the south of the equator. The mesospheric east winds in the Northern Hemisphere, which are also affected by the magnitude of the drag, are not too strong compared to observations (Groves, 1969).

MERIDIONAL WIND: Fig. 8 shows the meridional wind for January and July. It is difficult to compare these results with observations in the stratosphere; meridional winds in summer are weak as the circulation is symmetric around the pole, while in winter the wind field is dominated by large scale waves, and it would be necessary to properly incorporate observations from all longitudes to get a meaningful average. In addition, tidal variations near the stratopause are probably larger than the prevailing wind, so rocket observations, often taken near noon, introduce a spurious tidal component. The model tended to produce equatorward flow in the winter hemisphere at latitudes poleward of about 50° throughout the stratosphere. This appears to be in general agreement with the analysis of Crane et al. (1980) for December, 1976.

In the mesosphere the circulation from the summer pole to the winter pole is in agreement with observations (Groves, 1969) and model results (Holton and Wehrbein, 1980), although it is perhaps at a slightly lower altitude. This circulation is an artifact of the drag included in the top three levels, as it will act on both east and west winds to produce summer to winter pole flow. The magnitude of the flow is excessive for this altitude, reaching 10 ms^{-1} in the upper layer, while the (admittedly uncertain) observations give only a few ms^{-1}. At 90km, however, values of 10-15 ms have been found (Nastrom et al., 1982). In the lower mesosphere below the layers with drag the circulation produces south winds from 20°S to 40°N, and north winds elsewhere - this is in agreement with observations (Groves, 1969).

INERTIAL INSTABILITY: The meridional wind in the tropical stratosphere shows what appears to be inertial instability. The evidence is as follows: the meridional wind oscillations in the vertical appear clearly in both the months shown in Fig. 8 in the hemisphere in which the criterion for inertial instability (f-dU/dy less than zero - Northern Hemisphere; greater than zero in the Southern Hemisphere) is exceeded - Northern Hemisphere in January, Southern Hemisphere in July. As noted above, the east winds are found across the equator in the winter hemisphere, in both observations and the model, due to the influence of planetary wave momentum divergence at low latitudes of the winter hemisphere. The inertial instability extends only up to the latitude at which the above criterion is actually met: dU/dy is of order 2-4 x 10^{-5} s^{-1} a

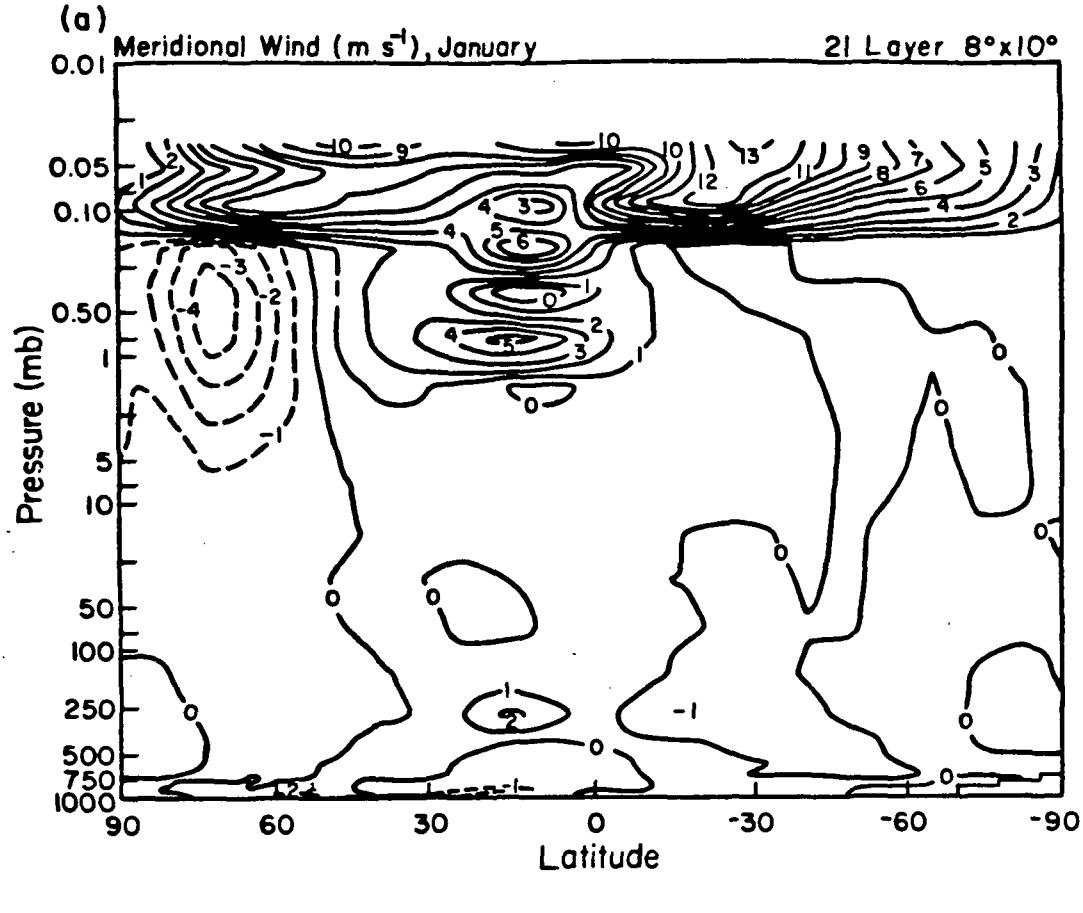

ORIGINAL PAGE IS
OF POOR QUALITY

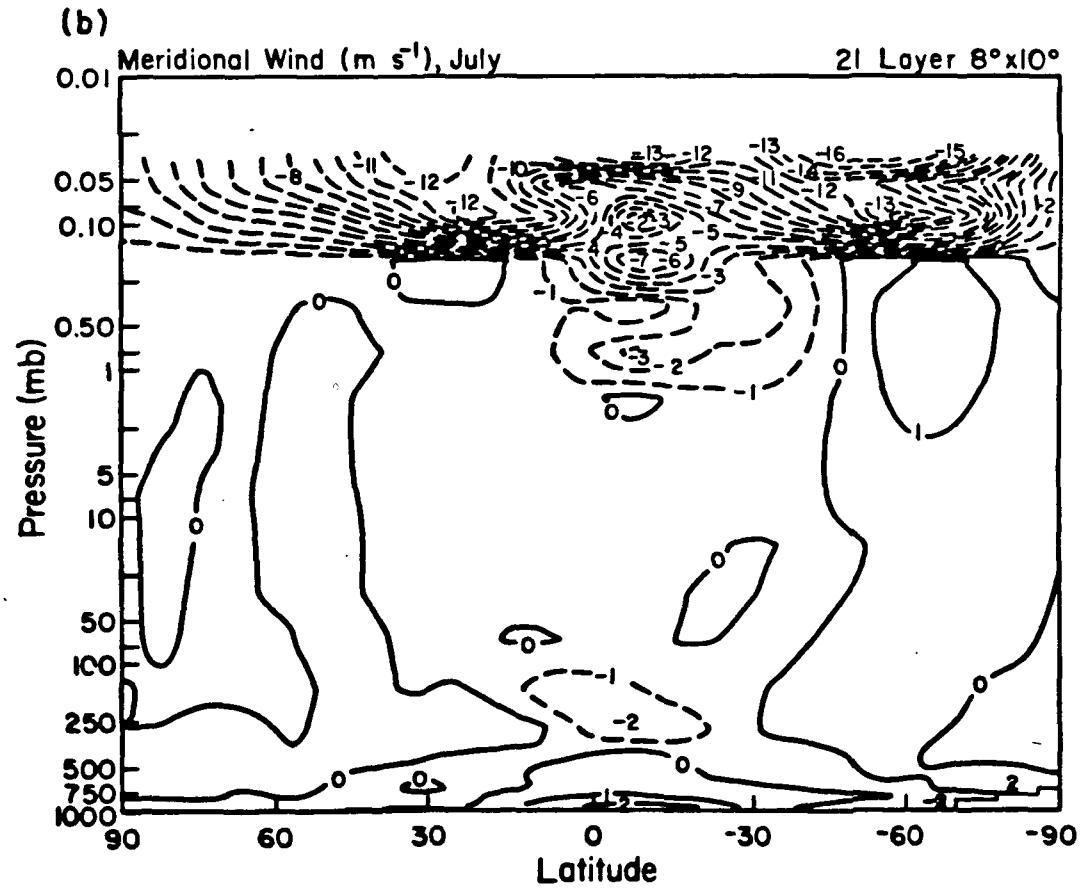

Fig. 8. Latitude-height profile of zonal mean meridional wind for (a) January and (b) July. South winds are shown by solid contours, north winds by dashed contours. Off-contour numbers on the graph indicate values in specific locations.

1.6mb in the model, and it drops below the value of the Coriolis parameter at about 20° latitude. During the equinoxes when cross equatorial shear is largely absent, these oscillations are either completely gone or substantially reduced. The oscillations are apparent in all the fields of interest, including the vertical velocity and thus the stream function, and eddy transports (Section 3e).

This oscillation appears to be similar to that obtained by Hunt (1981) in a general circulation model experiment. According to the analysis of Dunkerton (1981), cross-equatorial shears on the order of 1.5 day^{-1} should have vertical wavelengths on the order of 1km, and thus not be resolvable in models with coarser vertical resolution. The shears in this model were on the order of 2.3 day^{-1}, which is consistent with the greater vertical resolution used (5km), although shears about three times as large would be necessary to be quantitatively consistent with Dunkerton's analysis. The coarse resolution, both vertical and horizontal, may well exaggerate the magnitude of this effect in the model.

The vertical velocity perturbations induced by this instability, on the monthly average, are on the order of 5×10^{-7} mb s^{-1}. If this were to go entirely into local heating it could produce heating rates of 2°C day^{-1} at 1.6mb, which is certainly significant. The temperature profile does not show obvious perturbations in this region (Fig. 2), but what the effect of any heating is on the latitudinal temperature gradient and thus the zonal wind shear remains unknown.

The zonal wind field also shows perturbations (Fig. 7). These are located at or near the equator, in the region which has been characterized as associated with inertial instability. The zonal wind perturbation even switches hemispheres with the inertial instability, and is thus likely associated with it. However, the magnitude of the zonal wind oscillation is very large, with peak to peak values of 50 ms^{-1}, centered on the equator at 1.6mb. This is an order of magnitude larger than the meridional wind oscillation, and much larger than the oscillation shown by Hunt (1981) in the zonal wind. It might be associated with heating gradients induced by the vertical velocity perturbations. It is associated with local regions of angular momentum convergence and divergence and might be related to the effect of the instability on propagating Kelvin waves. Kelvin waves are discussed further in Section 3d.

2) LATITUDINAL MEAN ZONAL WIND VERSUS MONTH

Fig. 9 shows the variation of the zonal wind at 1.6mb and 34mb as a function of latitude and month. In the Northern Hemisphere, the upper stratosphere picture indicates that west winds dominate during the winter, peaking in February and being slightly weaker in January than the other winter months. The model's warming pulses in January, similar to those often observed in the real stratosphere during particular winter's, were responsible for the weakening in January. In the lower stratosphere there is a more progressive increase of west winds with time, again peaking in February. Summer easterlies appear at both levels, stronger in the upper stratosphere. This simulation is in agreement with observations at Northern Hemisphere extratropical latitudes (e.g., Richards, 1967; Groves, 1971) except for the winds in the lower stratosphere winter being excessive by about 10 ms^{-1}, as discussed earlier.

ORIGINAL PAGE IS
OF POOR QUALITY

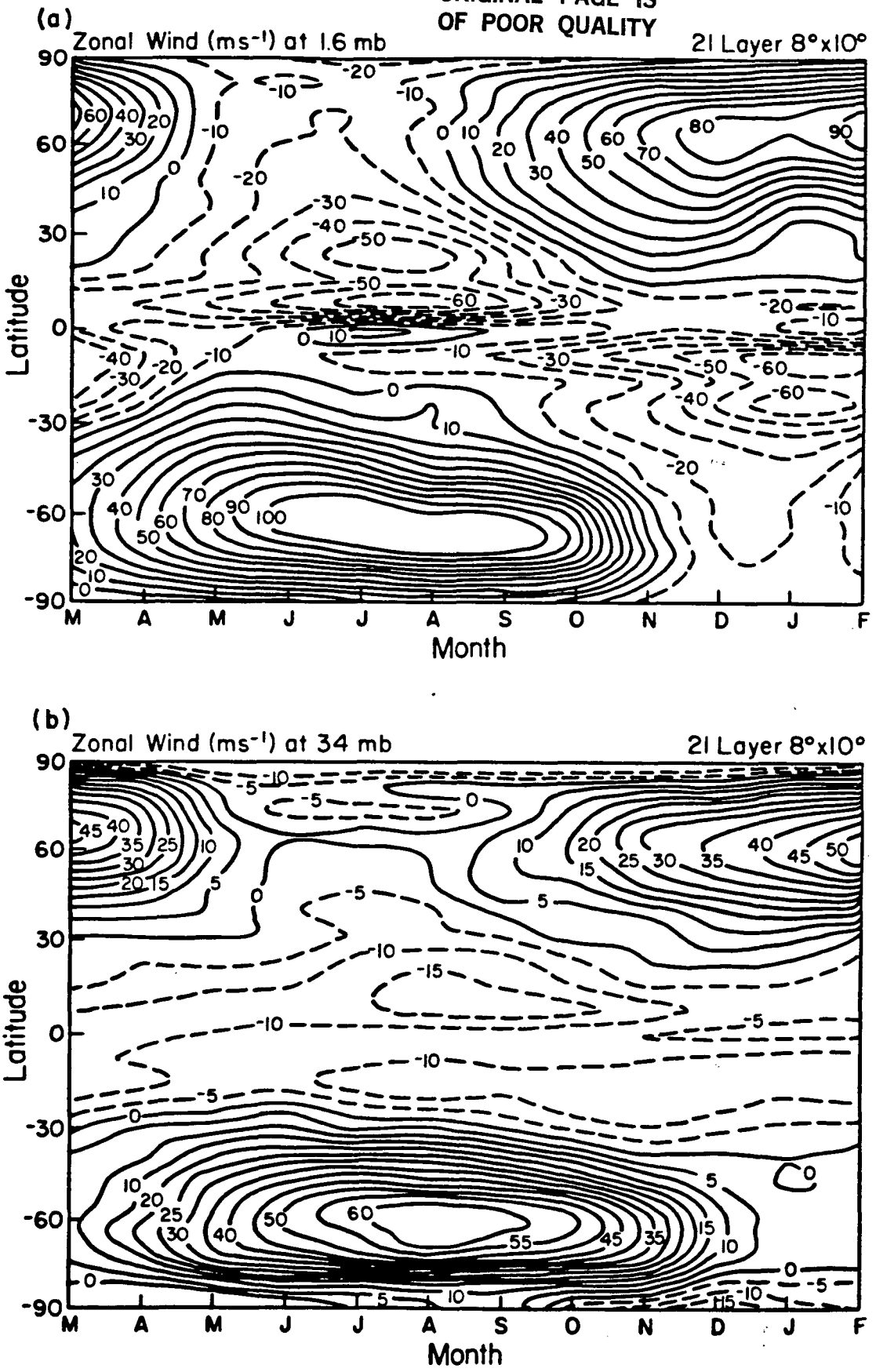

Fig. 9. Zonal mean zonal wind versus month for (a) 1.6mb level and (b) 34mb level. Solid contours indicate west winds.

(The east winds at both poles at both levels are a numerical artifact which results from using the Coriolis force and metric term at the pole).

In the Southern Hemisphere the seasonal variation is similar, except that the winter west winds are stronger than was the case during Northern Hemisphere winter. This is an observed feature (McGregor and Chapman, 1979 for the geostrophic wind field) and results partly from the lack of major warmings to interrupt the west wind field during winter. The lower stratosphere west winds are not excessive, as the cold polar stratosphere was properly simulated.

SEMIANNUAL WIND: The tropical upper stratosphere is dominated by a semiannual wind oscillation (e.g., Belmont et. al., 1974). Due to the zonal wind perturbation associated (in some sense) with the inertial oscillation, the 1.6mb level shown in Fig. 9 is not representative of the tropical upper stratosphere for this parameter. The oscillation which is present during the solstices produces light east or west winds at this level, in contrast to the observed flow (and flow at other levels) which shows maximum east winds during these seasons. If one averages the wind at the equator between 3.4mb and 0.17mb (38-60km) one obtains the variation shown in Fig. 10. East winds now do peak during the solstices, but the west wind phase is weaker than observed (Reed, 1966) (and in fact the April/May winds show only a diminution of east wind intensity). If the west wind phase is due to the momentum transport by propagating Kelvin waves (Hirota, 1980) this implies that either the Kelvin wave generation is too weak, or the waves are not reaching the upper stratosphere. This is discussed further in Section 3d.

3) ZONAL WIND, LONGITUDE VERSUS ALTITUDE, 51°N

Fig. 11 shows the variation of the zonal wind versus longitude at 51°N in January and July. The winter picture shows dramatically the dominant wave 1 feature in the stratosphere, with increasing wave number in the troposphere. At this latitude the strongest tropospheric winds occur in the eastern Asian region (Lau, 1978) as simulated by the model, and slope westward with height to become associated with the west wind maximum at upper stratospheric levels. As will be shown, the phase of wave 1 appears proper, although the amplitude in the upper stratosphere is probably excessive.

In July, the stratospheric westerlies are replaced by east winds, there is little wave propagation, and the stratospheric wind field shows little longitudinal variation.

c. Geopotential height

Figs. 12 and 13 show the geopotential height fields for various levels in the troposphere and stratosphere for January and July, as well as the sea level pressure.

JANUARY: The model produces realistic subpolar lows in both hemispheres, although the low centered at 30°E near Antarctica may be too weak (Taljaard et al., 1969). There is also a tendency for the subtropical highs to be displaced poleward of their observed positions. As shown in I, both of these deficiencies are removed by using greater horizontal resolution; in addition, as also shown in I there is much year to year variability in sea level pres-sure in the model, so it is improper to fully evaluate this

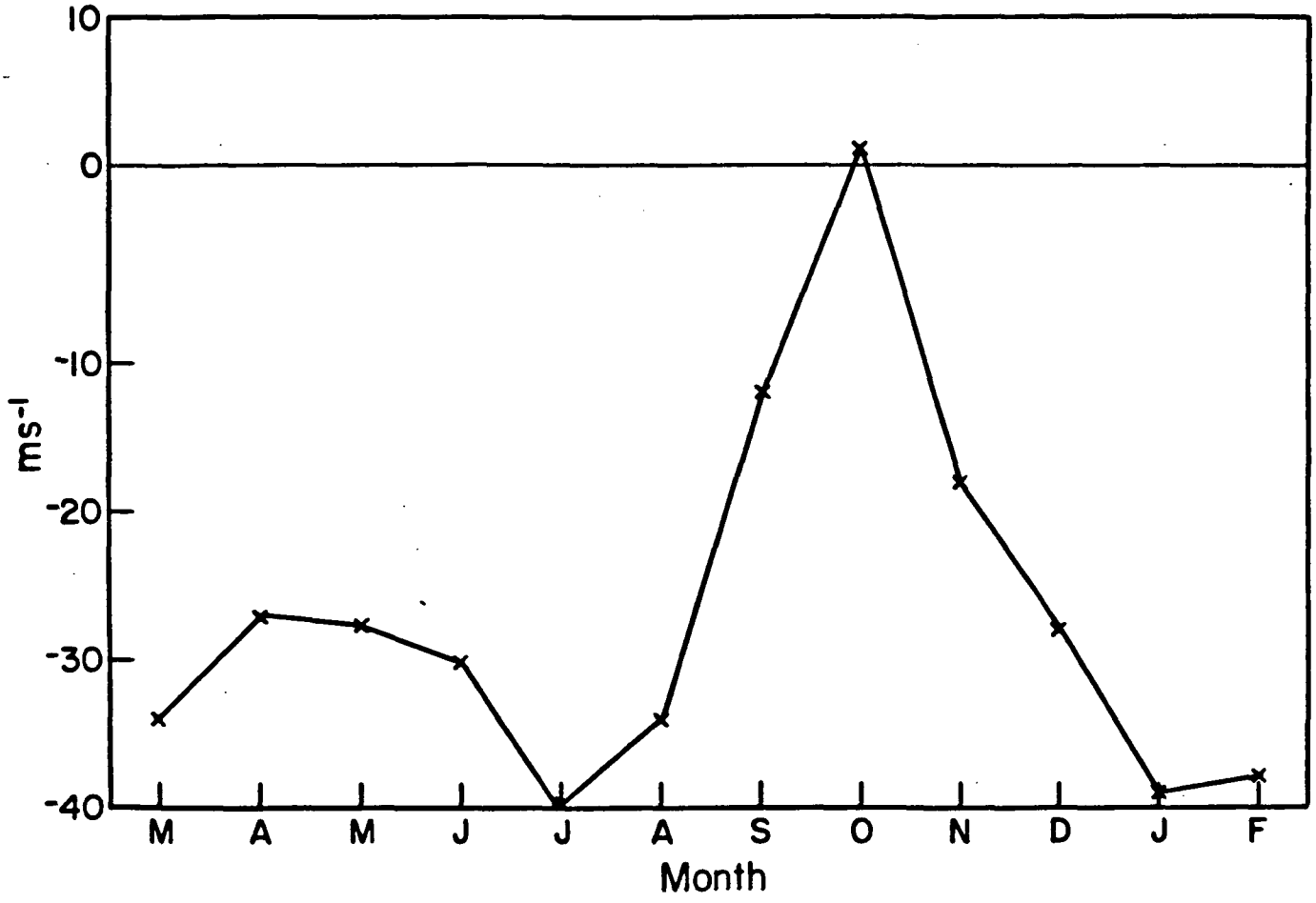

Fig. 10. Zonal mean equatorial wind averaged from 3.4mb-0.17mb versus month.

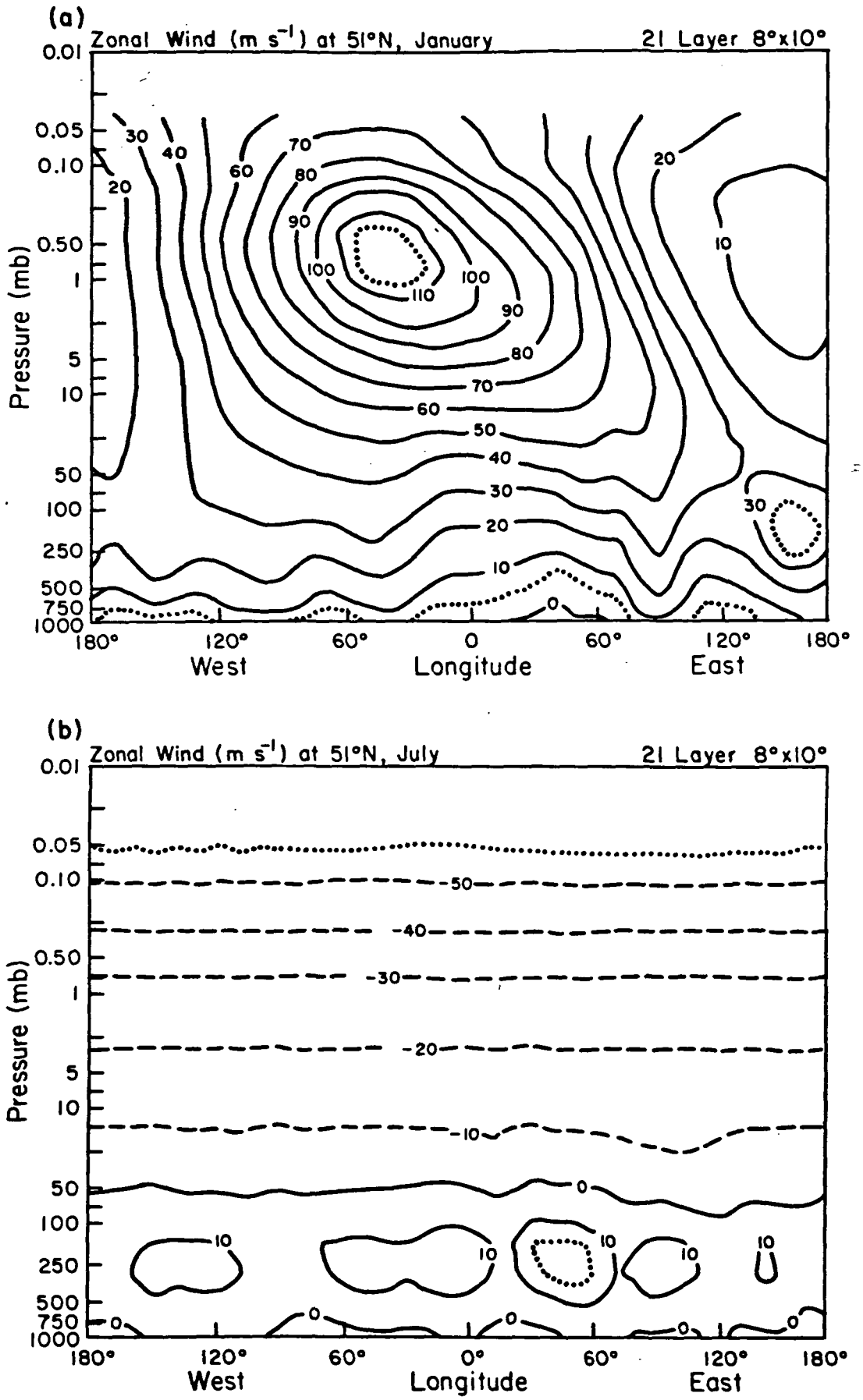

Fig. 11. Longitude-height profile of zonal wind at 51°N in (a) January and (b) July. Dashed contours indicate east winds, dotted contours indicate in-between contour values.

ORIGINAL PAGE IS
OF POOR QUALITY

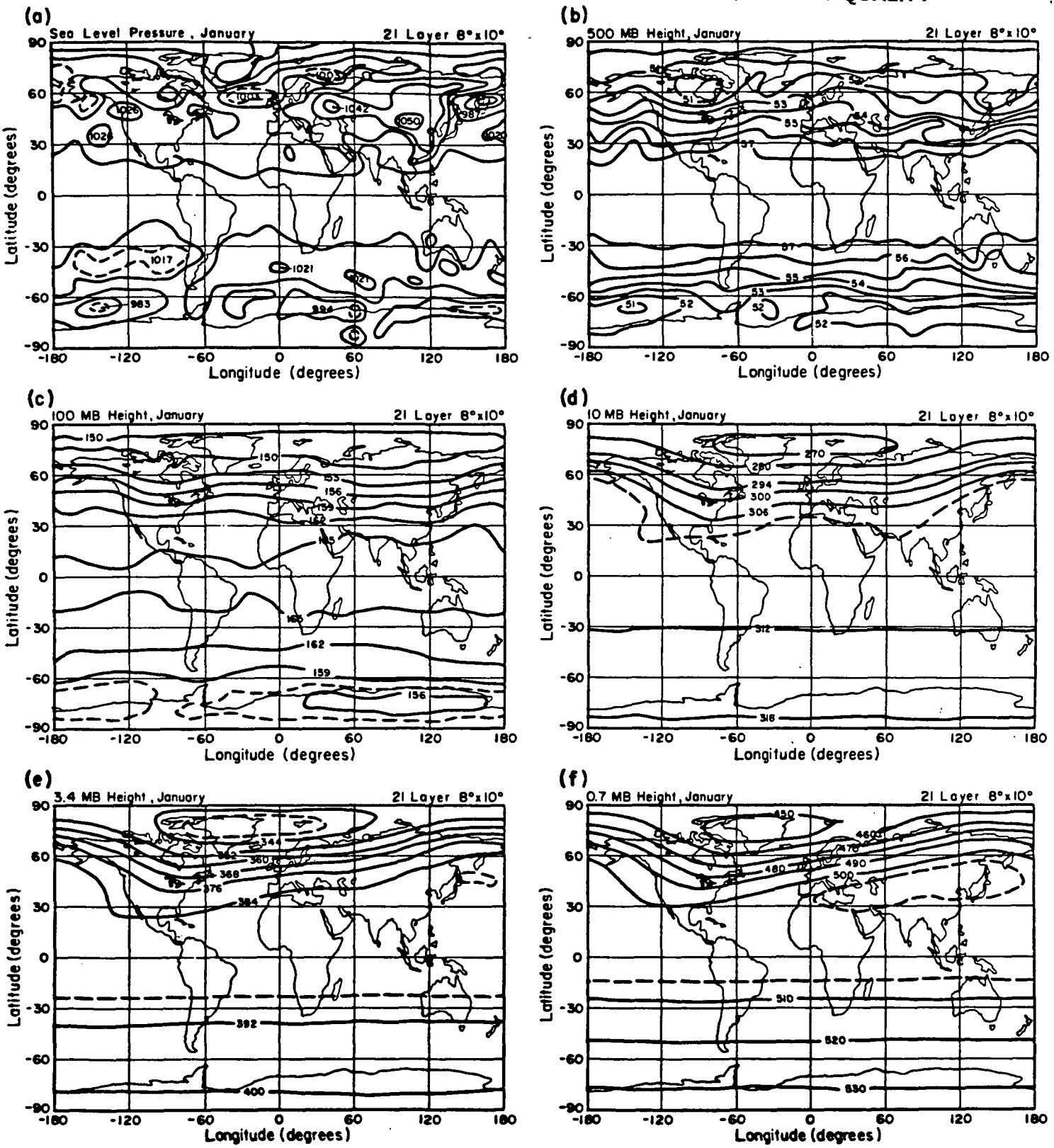

Fig. 12. Global distribution in January of (a) sea level pressure, and geopotential height fields at (b) 500mb; (c) 100mb; (d) 10mb; (e) 3.4mb; (f) 0.7mb. Sea level pressure is in mb with contours every 10mb; all others in hectometers (100m). Dashed lines represent in-between contour values.

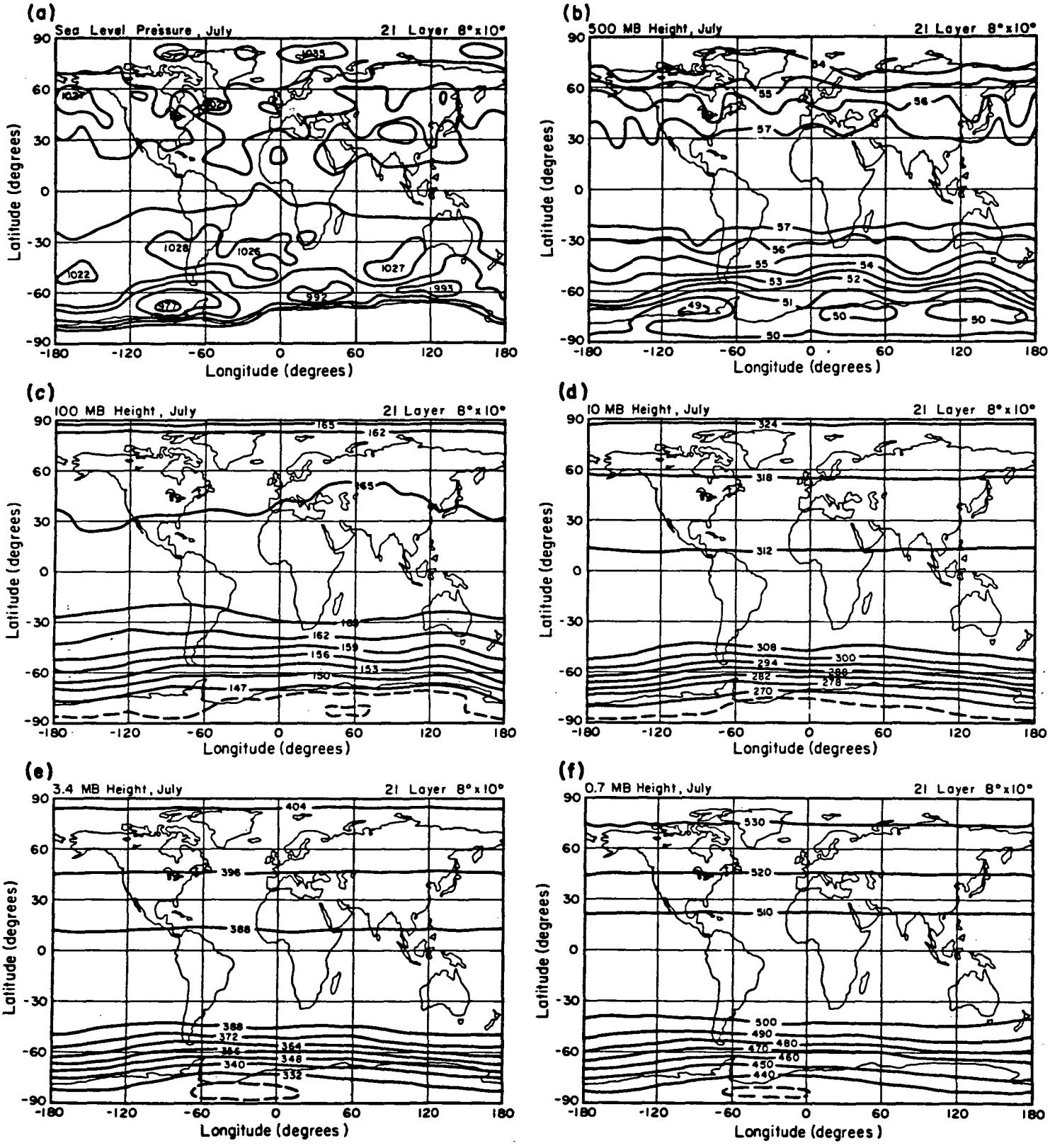

ORIGINAL PAGE IS
OF POOR QUALITY

Fig. 13. Same as Fig. 12 for July.

parameter on the basis of a one year simulation. At 500mb the Northern Hemisphere simulation looks reasonable both in phase and amplitude (compared with Crutcher and Meserve, 1970) except that the short wave feature centered in the model at 60°E in mid-latitudes may be slightly too far east. The comment on interannual variability applies at this level as well, and this particular feature has large observed variability (Lau and Oort, 1981). In the Southern Hemisphere the lack of a strong standing wave pattern, along with uncertain observations, makes comparison difficult, although the trough/ridge feature shown over Australia appears accurate (Taljaard et al., 1969). The tropospheric simulation is important as it establishes the position and amplitude of the standing waves which propagate into the stratosphere.

By 100mb in the Northern Hemisphere the observations show troughs centered over North America, Europe and Japan, with ridges in the Atlantic and Pacific. The model reproduces these features although the European trough is again too far east and probably too weak. As we will show in the next section this represents an underestimate of wave 3 energy in the troposphere. In the Southern Hemisphere the polar low is correctly positioned in the eastern hemisphere.

At 10mb the Aleutian High is properly positioned and at approximately the correct height (e.g., c.f. Lin, 1982), while the polar low is about 1km too low, due to the cold lower stratosphere temperatures. Climatological observations for the Southern Hemisphere for this month are difficult to obtain; the symmetric circulation around the pole is apparently correct (Cunnold et al., 1975), due to the inability of tropospheric waves to propagate vertically in an east wind regime, while the computed height of the polar anticyclone is slightly greater than that computed by Manabe and Mahlman (1976).

At higher levels, the Aleutian High amplifies and shifts slightly to the west. Perusal of the weekly synoptic analyses at these levels (Staff, Upper Air Branch, 1967-1971) shows that this is a realistic feature; the comparison between the mode wave 1 amplitude and that of the observations will be given in section 3d. In the Southern Hemisphere the circulation remains symmetric into the lower mesosphere.

JULY: Fig. 13 shows the geopotential height surfaces for this month. The subpolar lows in the Southern Hemisphere are of approximately the right magnitude, although their position shows some variance with climatology (Taljaard et al., 1969). The subtropical highs in both hemispheres are too far poleward. At 500mb the Northern Hemisphere has shorter wave features, as is expected for the season, but the subtropical highs are not well formed. In the Southern Hemisphere the weak troughs adjacent to the continents appear to be consistent with observations. By 100mb the model shows high pressure right near the poles: as mentioned in Section 3b this is affected by the numerical formulation at the poles. Northern Hemisphere observations (Crutcher and Meserve, 1970) show weak low pressure near the pole. The major deficiency is again the lack of well formed subtropical highs. In the Southern Hemisphere the simulation seems realistic, with the polar low displaced towards the Australian sector.

At 10mb the Northern Hemisphere circulation is properly symmetric about the pole (Staff, Upper Air Branch, 1967, 1969) and it remains so into the

lower mesosphere. In the Southern Hemisphere the winter circulation is also fairly symmetric, around the polar low, indicative of the dominant wave number zero pattern in the standing geopotential field (e.g., Labitzke, 1977). The long wave amplitudes in both hemispheres will be examined in Section 3d.

d. Eddy energy

1) EDDY KINETIC ENERGY

Fig. 14 shows the eddy kinetic energy as a function of latitude and pressure for January and July. The distribution in the Northern Hemisphere troposphere is realistic in both seasons except that in January the eddy energy is somewhat excessive at low levels, while in July it is slightly deficient in the upper troposphere. In the Southern Hemisphere values appear realistic in both seasons. This is essentially the same conclusion given in I, to which reference should be made for details of the comparison with observations.

In the equatorial tropopause region in July a local excess of eddy energy appears. This is essentially a wave 1 standing feature, which derives its energy from potential energy, generated by latent heat release. It is not at all evident in June, and is greatly diminished in August; nor does it exist in the five year average shown in I. This feature may be caused by an inertial instability as wind shears of the right sign do exist, but indications are not as clear as for the oscillation near the stratopause.

The eddy energy (per unit mass) increases with altitude in the winter hemisphere, much more so in the Northern than Southern Hemisphere. The summer hemispheres show little eddy energy in the stratosphere. These are all reasonably realistic features; it is difficult to compare with observations which are not usually given in this form in the stratosphere. A better comparison will be possible in the sections below.

Evident in both months is a local eddy energy maximum in the stratopause region near the equator, possibly associated with the inertial instability.

2) ENERGY CONVERSIONS AND BUDGET

How is the energy generated in the stratosphere? Figs. 15 and 16 show the energy diagrams for the troposphere and several regions in the stratosphere and lower mesosphere during January and July. These differ from the usual presentation of such diagrams in two ways. First, the wide arrows entering or leaving the zonal and eddy kinetic energy boxes represent the effect of the full pressure gradient force term, including both the convergence of geopotential flux and the baroclinic conversion from potential to kinetic energy; a decomposition of the two terms with better vertical resolution will be shown below. Second, due to the nature of the diagnostic routine, the transformation from zonal available potential energy to eddy available potential energy could not be calculated.

In both months the winter hemisphere has more zonal and eddy kinetic energy up through 0.48mb than the summer hemisphere. The Northern Hemisphere has greater eddy energy, both kinetic and potential in winter than does the Southern Hemisphere, while the reverse is true for the zonal potential and

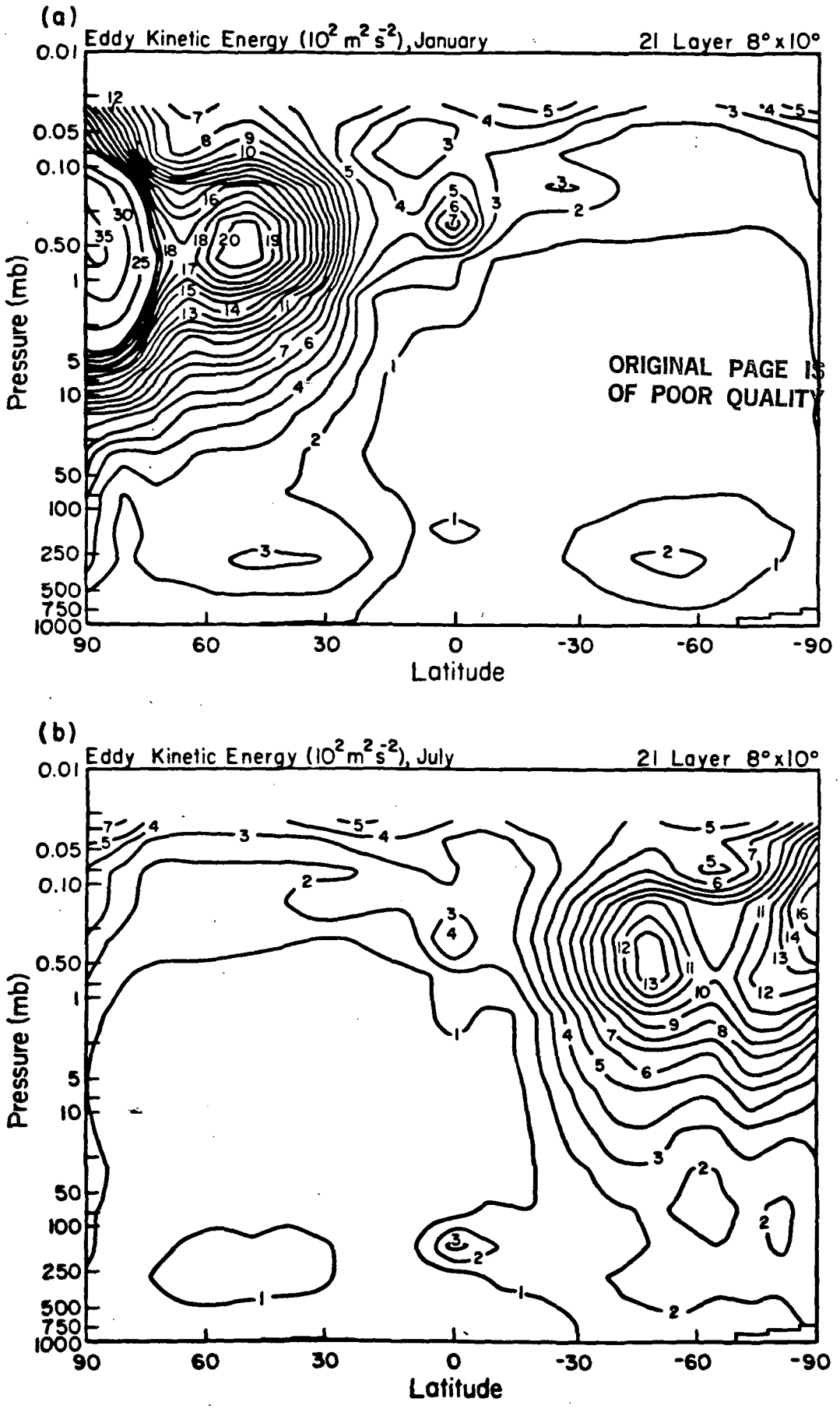

Fig. 14. Latitude-height profile of eddy kinetic energy (per unit mass) for (a) January and (b) July.

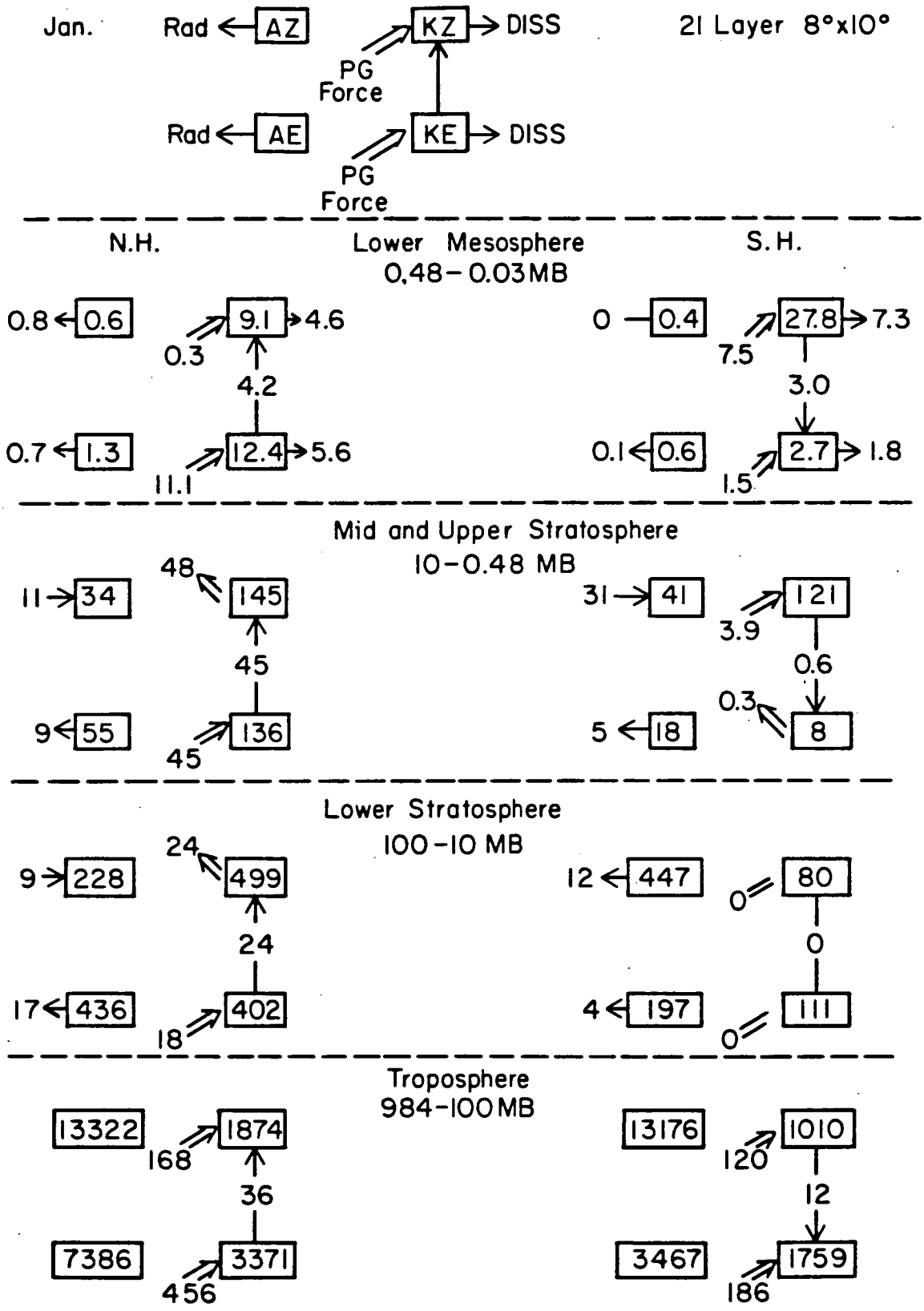

Fig. 15. Energy budget for January in various regions of the atmosphere. Schematic shown at top, with zonal available potential energy (AZ), eddy available potential energy (AE), zonal kinetic energy (KZ) and eddy kinetic energy (KE), in units of 10^{17}J. Transformations shown include KZ to KE, radiative generation or dissipation of AZ and AE, dissipation of KZ and KE, and effect of pressure gradient force (broad arrow) on KZ and KE (see text) in units of 10^{12}W. The various effects on A and K in the troposphere are not shown - see I for more details. Northern Hemisphere on left.

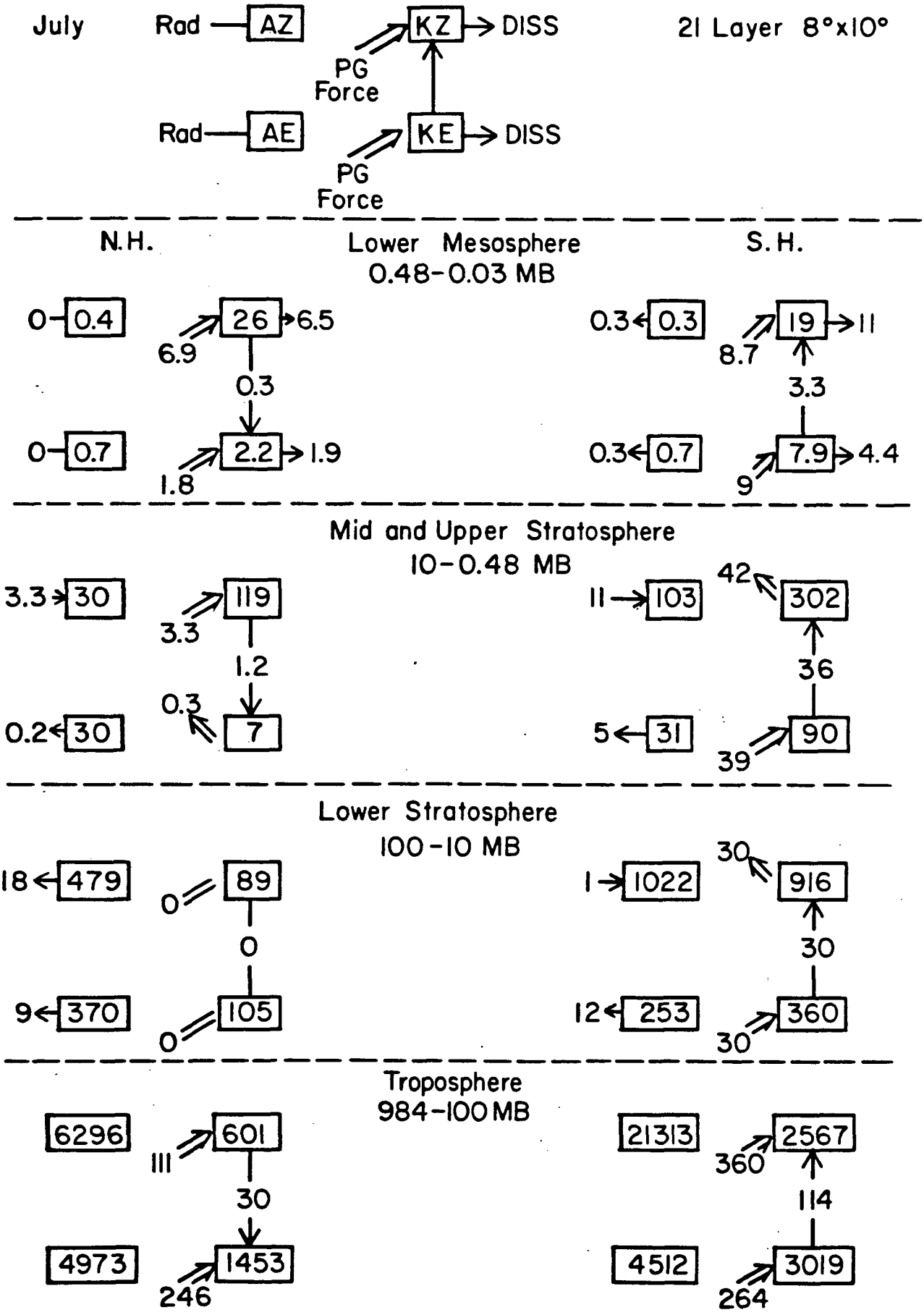

Fig. 16. Same as Fig. 15 for July.

kinetic energy. The Southern Hemisphere is dominated by a very cold polar low, while the Northern Hemisphere has large standing waves in winter. Both potential and kinetic energy decrease with altitude along with the mass of the atmosphere.

The magnitudes of the zonal and eddy potential and kinetic energies are in rough agreement with observations for specific months (generally ±50% - Dopplick 1971, Hartmann, 1976b) although comparisons are difficult since neither study included tropical areas, which, area weighted, occupy one-third of the globe.

The tropospheric energy cycle indicates that eddy kinetic energy is being generated by the pressure gradient term. The magnitudes of the transformation agree well with observations (e.g., Oort, 1964) as noted in I. In both winter stratospheres the energy cycles also show that the pressure gradient term is generating eddy kinetic energy, which in these regions is completely transferred into zonal kinetic energy, and then completely transferred out, into zonal potential energy or as a vertical flux. This is indicative of an energy cycle driven by waves propagating through the region, rather than in-situ processes. (See Plumb, 1983 for an alternate version of the energy cycle, which clarifies this point). Radiative fluxes destroy eddy available potential energy and generate zonal available potential energy. The energy transformations are again in rough agreement with observations (Dopplick, 1971; Hartmann, 1976b).

The summer stratospheres show, in general, smaller energies (except for the zonal available potential energy in January), and negligible energy transformations or fluxes.

The mesospheric energy cycle is strongly influenced by the large kinetic energy dissipation which occurs in the model at those levels. To the extent that this dissipation also arises in the real atmosphere, it must be replaced by processes such as generation from the pressure gradient force, as in the model.

The decomposition of the pressure gradient force into the eddy generation term $\overline{(-\omega'\alpha')}$ and the eddy convergence term $\left(-\partial/\partial p\ \overline{(\omega'\phi')} - \overline{\nabla' \cdot \nabla\phi'}\right)$ is shown in Fig. 17 for both months and hemispheres. In the troposphere energy is generated baroclinically between about 300mb and 900mb, accompanied by transport out of this region (thus a net divergence), both upward and downward. The upward flux propagates into the stratosphere (especially in the winter hemisphere extratropics) and its convergence provides the kinetic energy source indicated in Figs. 15 and 16. The convergence term thus dominates the eddy kinetic energy generation term in the model winter stratosphere, in agreement with observations (Newell and Richards, 1969; Miller, 1970; Dopplick, 1971; Hartmann, 1976b). As the energy is, to a good extent, propagating vertically straight through the region (to the extent that the noninteraction theorem conditions are obeyed) the energy simply cycles into eddy kinetic energy, then to zonal kinetic energy, and then out, as shown in Figs. 15 and 16.

The eddy conversion term is generally opposite in character to the convergence term, not only on the hemispheric average but also at each

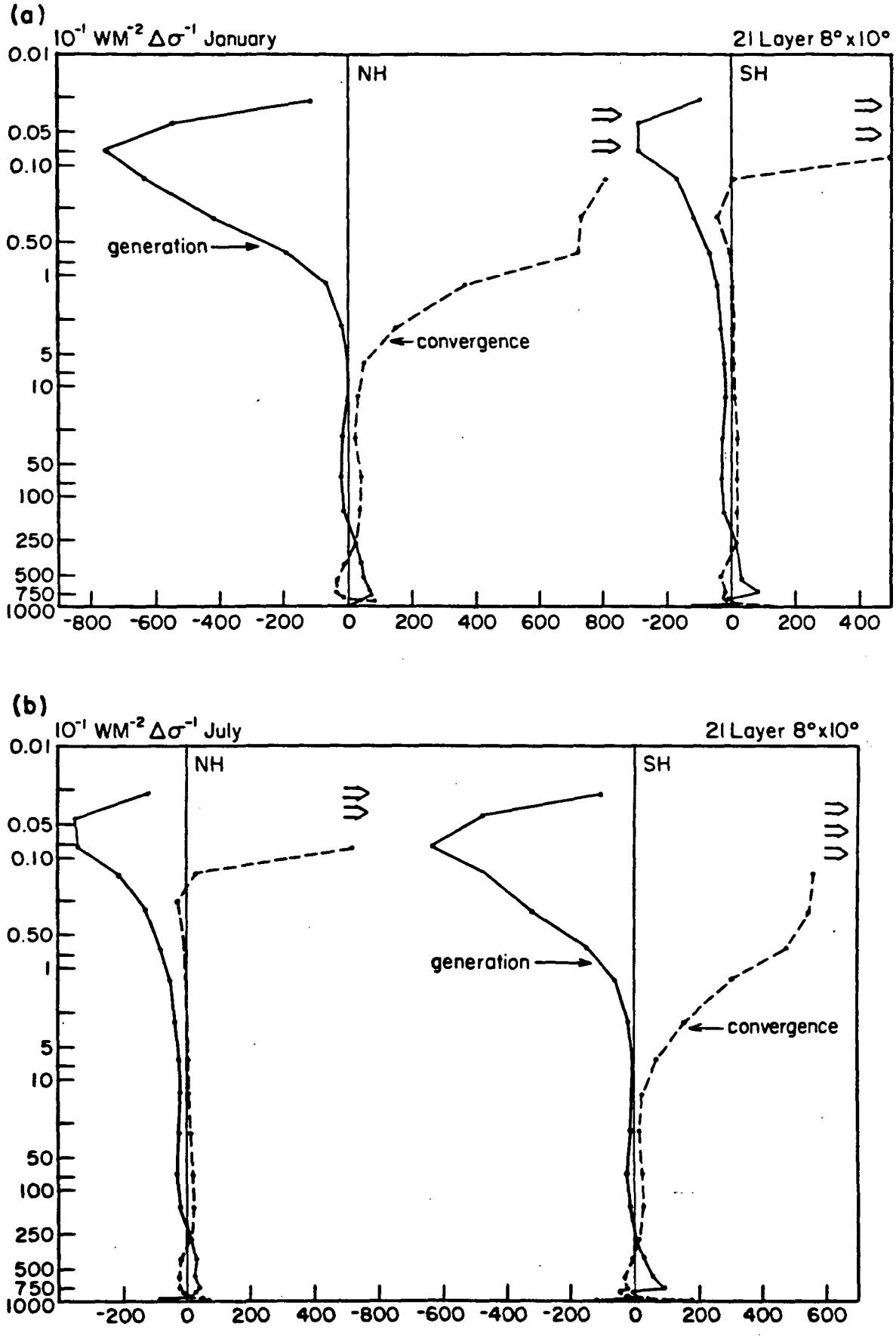

Fig. 17. Eddy generation $\overline{(-\omega'\alpha')}$ and convergence $(-\partial/\partial p\ \overline{(\omega'\phi')} - \overline{v' \cdot \nabla\phi'})$ per unit σ as a function of altitude in the Northern and Southern Hemispheres for (a) January and (b) July.

latitude and altitude. The latitude-height pictures of conversion and convergence from the model (not shown) look extremely similar to those shown by Manabe and Mahlman (1976) from their GCM. As shown in Fig. 17 the generation term is slightly negative throughout the stratosphere; for steady waves in an adiabatic atmosphere both the vertical energy propagation and the baroclinic conversion should be positive when the northward transport of sensible heat by the eddies is downgradient (thus in a region where west winds are increasing with altitude) (Hartmann, 1976b). As we will show in Section 3e, the model eddies do transport heat northward in the stratosphere where there is positive shear, and yet the baroclinic conversion is slightly negative. This is also the result found in both models and some observations (Manabe and Mahlman, 1976, Fig. 9.4; Kasahara and Sasamori, 1974; Manabe and Hunt, 1968; Oort, 1964) although not by Dopplick (1971) or Hartmann (1976b). A possible reason for the discrepancy is that the conditions are not adiabatic, and the phase relation between the temperatures and heights are not necessarily those of a steady or freely propagating wave. For example, if one adds a dissipation term to equation (6) in Hartmann (1976b), and uses the dissipation time constant associated with Newtonian cooling indicated by Dickinson (1973), one finds that at 16mb the ratio between dissipation and the model's northward transport of sensible heat by eddies is equal to 2.6 at 51°N in January. Thus the sensible heat transport is not balanced primarily by vertical motion, as is the case for a free wave propagating in an adiabatic atmosphere, but is dissipated effectively by radiative damping.

The model stratosphere, and presumably the real stratosphere, is made up of waves propagating with greater or less difficulty, depending upon dissipation, reflection or other phenomena (such as critical layers). For a vertically propagating wave, for which the vertical velocity and geopotential fields are in phase, if the temperature wave lags the height wave by more than 1/4 wavelength it will result in a negative generation of eddy energy (as the warm air will be closer to the descending motion in the trough). However, the wave will continue to transport heat northward until the temperature wave lags the height wave by 1/2 wavelength (as, until that lag, the positive meridional wind will still occur in the warm sector). If one compares Fig. 4 and Fig. 12 one can see that the standing temperature wave lags the standing height wave by approximately 1/4 wavelength (90° for wave 1), indicative of little baroclinic energy generation but maximum northward sensible heat transport for vertically propagating waves. The monthly average negative energy generation indicates that the average phase lag for all waves is slightly greater than 1/4 wavelength in the model stratosphere. An example of the day to day variation in this phase lag will be given in Section 3f.

At levels above 2mb, the shear reverses, the northward heat transport is now associated with a substantial negative generation term, and the eddy convergence increases as wave dissipation becomes more effective. Despite the slightly negative generation term in the model stratosphere, compared to the slightly positive value found by Hartmann (1976b), the results in Fig. 17 look very similar to Hartmann's analysis of observations.

3) SPECTRA AND LONG WAVE AMPLITUDES AND PHASES

The spectra of the eddy kinetic energy averaged over various layers in the model are shown for January and July in Figs. 18 and 19. In both months the ratio of the short wave to long wave energy decreases as expected with

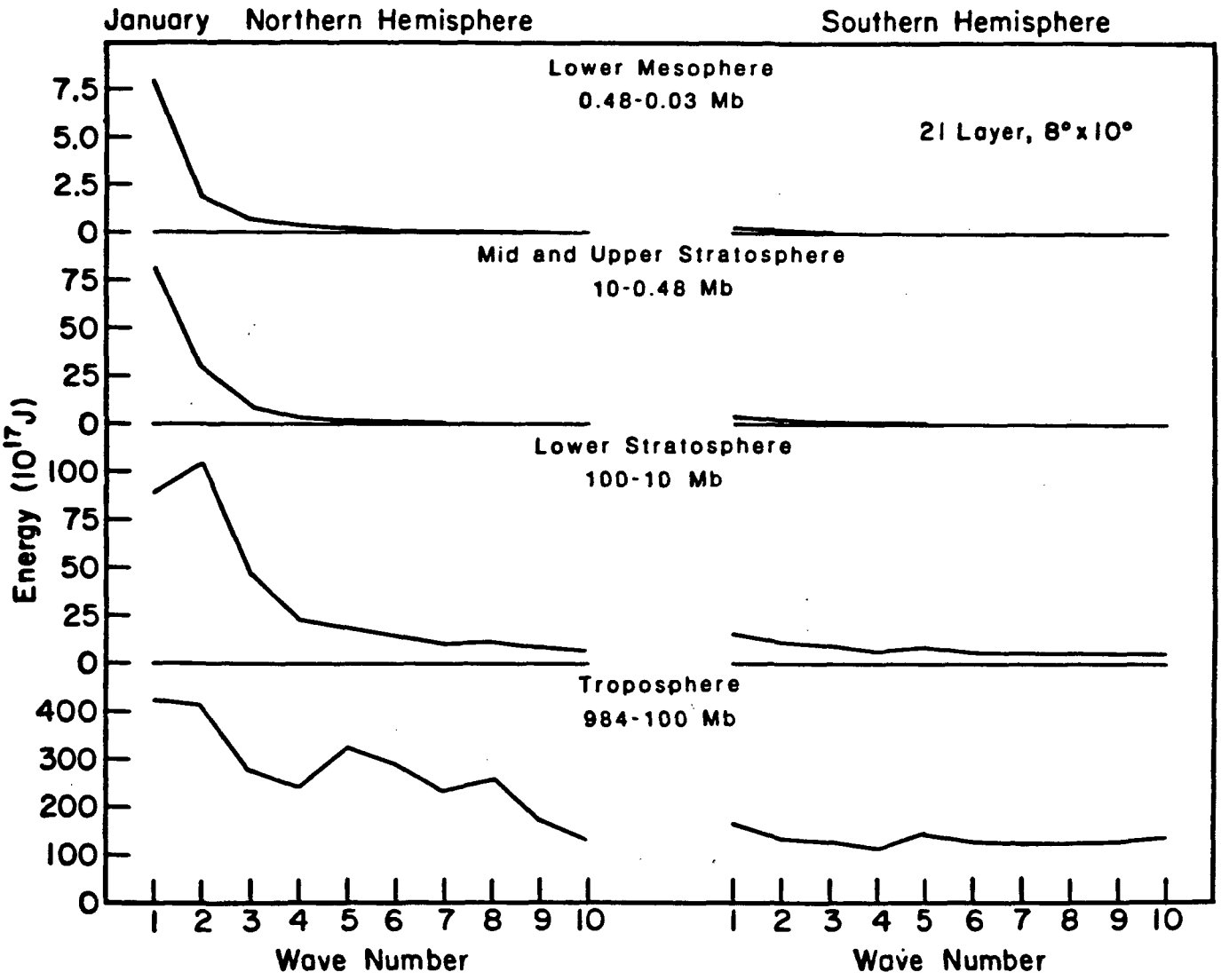

Fig. 18. Eddy kinetic energy (10^{17}J) as a function of wavenumber in January for various regions of the atmosphere. Northern Hemisphere on left. Note the change of scale with elevation.

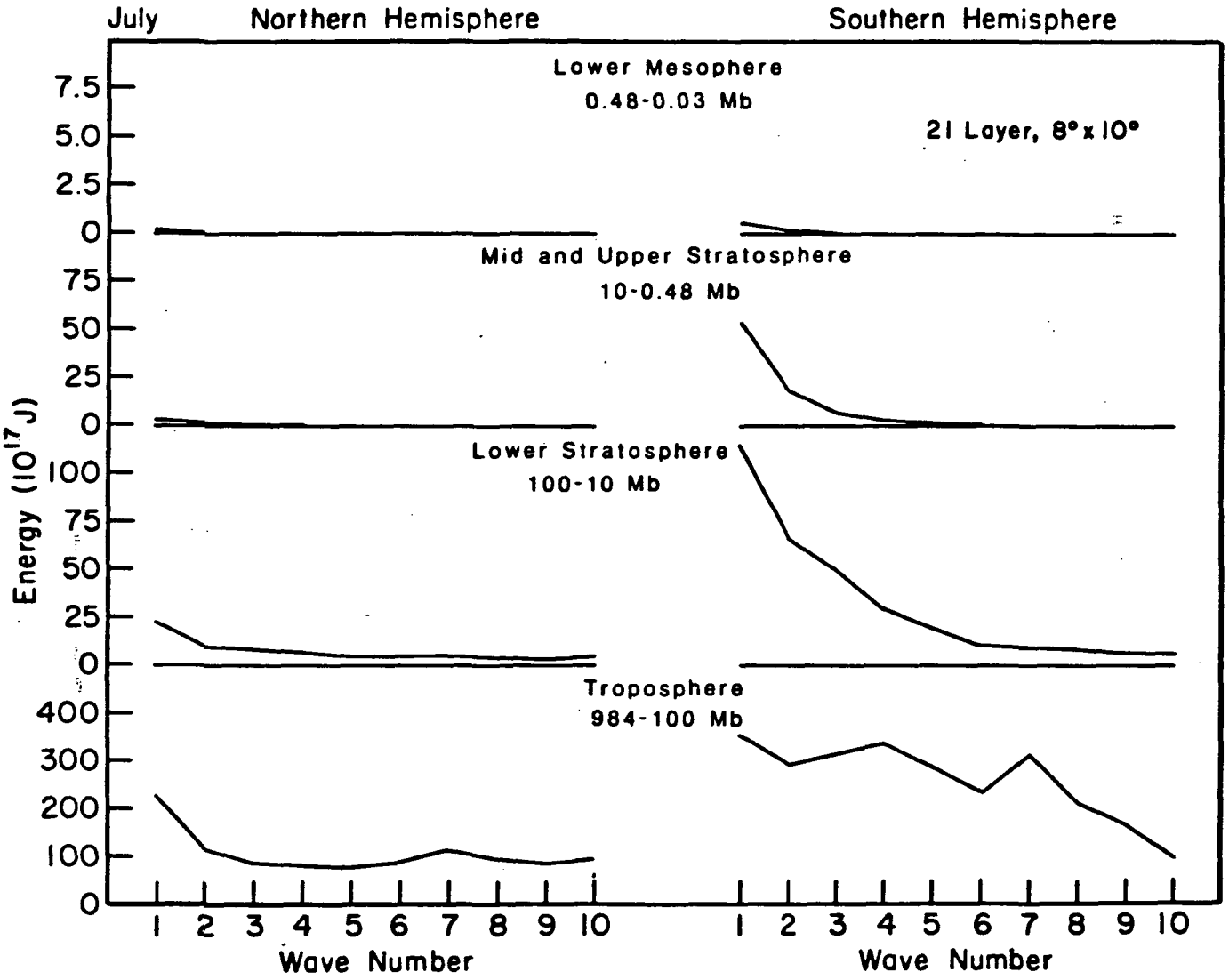

Fig. 19. Same as Fig. 18 for July.

increasing elevation until the model has primarily wave 1 with some wave 2 energy at the highest levels during winter. In summer there is little wave energy above the lower stratosphere. In the Northern Hemisphere winter wave 1 energy appears to pass through the lower stratosphere relatively unaffected, and accumulate at higher levels, as indicated for all waves in Fig. 17. In contrast, wave 2 energy (or activity) propagates in a more limited fashion between the same regions (it is reflected more easily). During July both wave 1 and wave 2 show little energy throughout the stratosphere. In the mesosphere, wave energy is affected by the parameterized drag.

The magnitudes and general shape of the spectrum for January in the Northern Hemisphere troposphere compare extremely well with the observed spectrum shown by Chen (1982) for the winter of 1976-77; the only deficiency is that the energy dip shown in the figure for wave numbers 3 and 4 was not observed during that winter. The January simulation which was part of the three month spin-up also had deficient energy in these wave numbers, but the alternate January run with corrected water vapor had 30% more wave number 3 energy.

The somewhat smaller spectral slope seen through the medium scale wave numbers during Southern Hemisphere winter in the troposphere is hard to verify, although the relative importance of the medium scale waves during Southern Hemisphere summer has been documented (Randal and Stanford, 1983), and also appears in the model. Both van Loon and Jenne (1972) and Trenberth (1980) show that standing waves 1-3 account for most of the standing wave energy at 500mb - this is true in the model as well, as waves 1-3 in the Southern Hemisphere troposphere during July represented 60% of the standing wave energy. However, in the model the standing waves accounted for only 23% of the total eddy energy, and the spectrum shown in Fig. 19 fails to reveal the long wave dominance when transient energy is also considered. In the Northern Hemisphere troposphere during winter, standing wave energy accounted for 40% of the total eddy energy.

More definitive comparisons can be made by looking at the stationary long wave geopotential amplitudes and phases - these are shown in Figs. 20 and 21 for January and July for wave numbers 1-3.

JANUARY: The Northern Hemisphere wave number 1 amplitude reaches very large values in the upper stratosphere then starts decreasing; the decrease begins below the region of the parameterized drag (which occurs above 0.1mb and is not shown in these figures), and appears to be caused by transfer of energy into zonal kinetic energy and radiative damping. The phase of wave 1 slopes westward with height, fairly rapidly in the troposphere and lower stratosphere, and then more slowly above 10mb. The rapid phase progression is indicative of a relatively freely propagating wave, as noted in the discussion of the spectral diagnostic (Fig. 18), while the slower variation implies less wave transmission. Wave 2 reaches a more modest amplitude maximized at a lower elevation (10mb), and its phase variation implies little propagation above that height, as did the spectral analysis. Wave 3 grows to a smaller amplitude maximum in the upper stratosphere, and the spectral analysis shows that this is associated with substantially reduced energy; its phase variation indicates little propagation above the lower stratosphere. The relative amplitudes and phase variations among these three waves are in accordance with

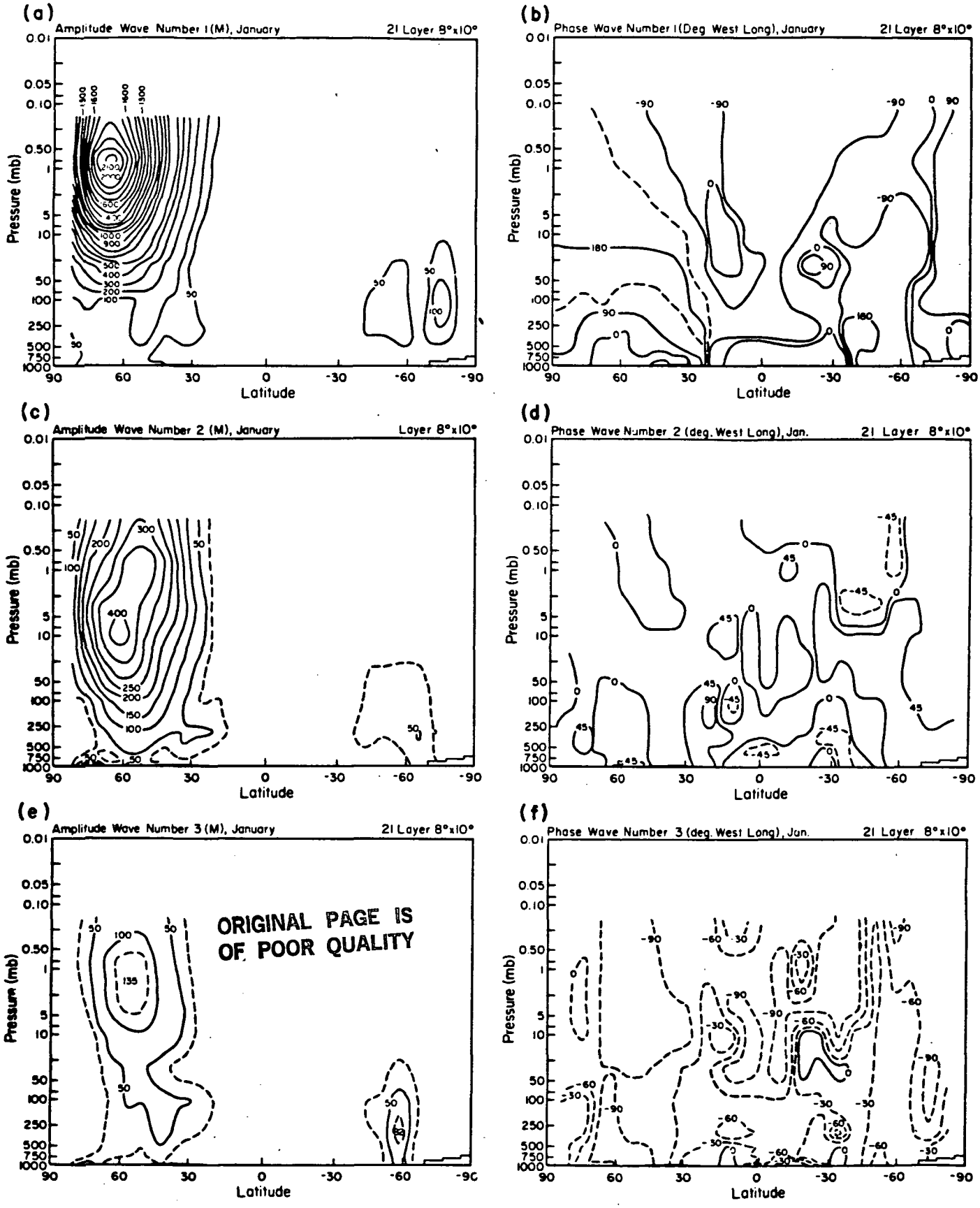

Fig. 20. Latitude-height profile of the amplitude (m) and phase (location of ridge, measured west of Greenwich) in January for wave numbers 1, 2, and 3 (from top to bottom). For the phase of wave number 1 and all wave amplitudes, dashed lines indicate in-between contour values; for the phase of waves 2 and 3 they indicate degrees east longitude.

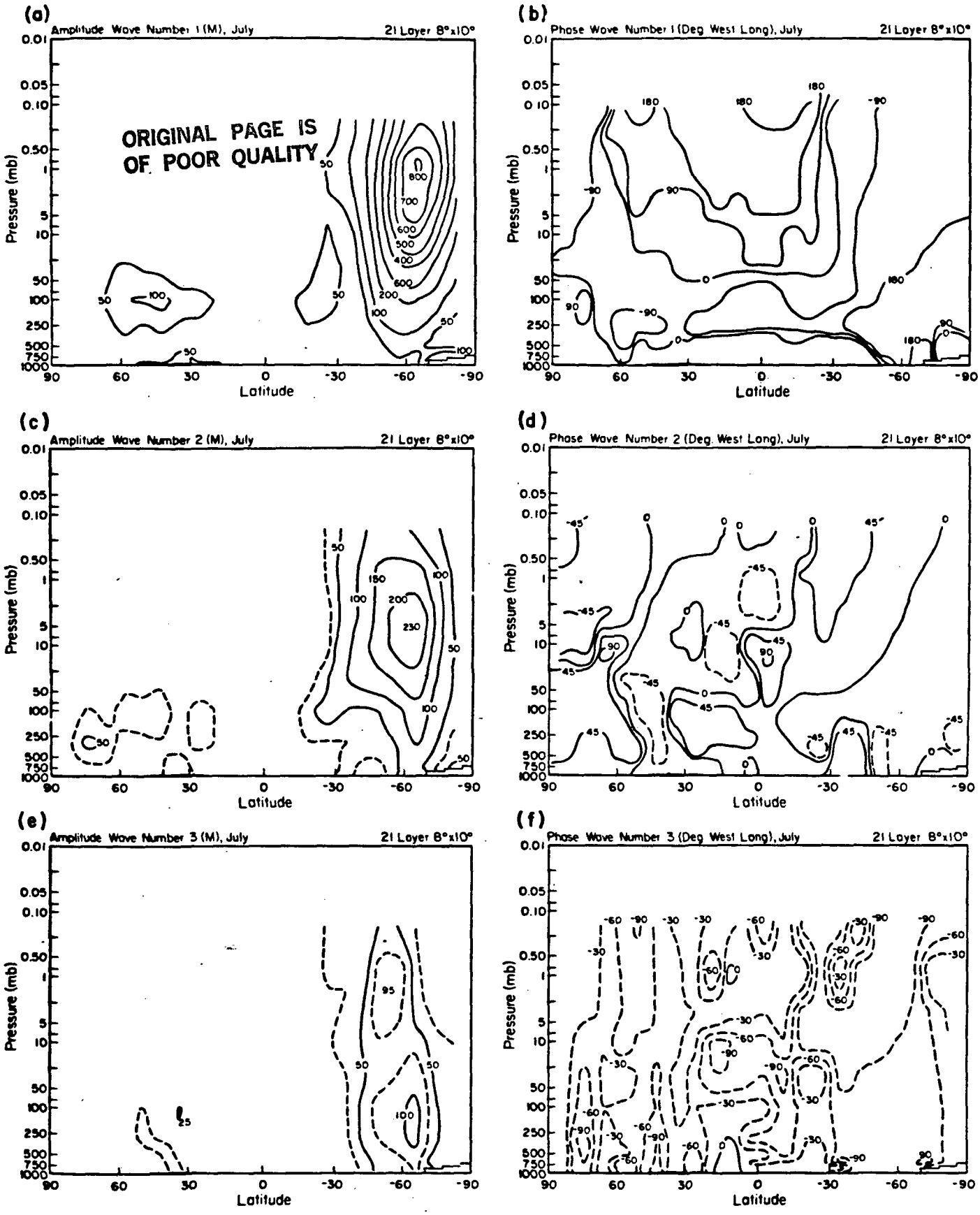

Fig. 21. Same as Fig. 20 for July.

expectation given the increased susceptibility to west wind reflection encountered by waves with increasing wavenumber (Charney and Drazin, 1961).

There are numerous observational data analyses with which to compare the model results. As stratospheric dynamics rely heavily on long wave generation in the troposphere we will discuss the tropospheric simulations in some detail. The Northern Hemisphere January wave 1 amplitude of 100m in the mid-troposphere at 50°N, rising to 130m in the upper troposphere is in agreement with observations (Muench, 1965; van Loon et al., 1973; Defant et al., 1979; Reiter and Westholff, 1981; Geller et al., 1983). The phase variation, such that the wave starts near 50°E at 50°N near the surface, tilts westward so that the ridge is near the Greenwich meridian by 500mb, and near 100°W by 100mb, is also in agreement with these observations. At 50°N wave number 2 amplitude is about 40% deficient in the mid-troposphere, although its value of 180m at 100mb is in agreement with observations. The phase variation at this latitude, starting at 60°E near the surface, tilting to near 30°E by 500mb and near 10°E by 100mb is slightly greater (by about 10°) than that indicated by most of the observations, consistent with the more rapid growth experienced by the wave in the model. Wave number 3 is about 50% deficient in amplitude throughout the troposphere, as indicated in the spectral analysis, although its slope, starting near 0° at the surface, and sloping just slightly to reach 30°W by 100mb is correct. Thus the model provides proper amplitude wave 1 and wave 2 forcing to the lower stratosphere, which is highly important as they are the predominant factors in driving stratospheric dynamics. The wave 3 amplitude, however, is deficient by a factor of 2; this should have little effect on the mid and upper stratosphere due to the difficulty this wave experiences in propagating into the stratosphere. (However, as shown below wave 3 amplitudes at higher levels in the stratosphere appear realistic. This lends some credence to the conclusion of Tenenbaum (1982) that wave 3 in the troposphere is underestimated in models because too much energy propagates into the statosphere due to the lack of sufficient negative shear above the jet stream level - and thus incorrect refractive index. Uncertainty in the effect of photochemical dissipation, as is discussed below, prevents any firm conclusion). Wave 3 amplitudes are 33% larger in the mid-troposphere in the alternate January with corrected stratospheric water vapor, which again raises the question of model, and natural, variability.

At 10mb the model has the following amplitude and phase (at 65°N, the location of maximum amplitude): wave 1 - 1000m, 170°E; wave 2 - 400m, 175°E; wave 3 (at 51°N) -90m, 100°E. Comparison with observations (van Loon et al., 1973; Barnett, 1980; Quiroz, 1980; Geller et al., 1983) shows that the amplitudes are all in agreement with observations, although both wave 1 and wave 2 amplitudes reach those values only in given years (1965, 1977, 1978 - van Loon et al., 1973; Quiroz, 1980). The phases are all in good agreement. By 1mb, observations (Barnett, 1980; Smith, 1983; Geller et al., 1983) show amplitudes for wave 1 equal to, and for wave 2 less than those at 10mb, while the model shows wave 1 amplitude having doubled, and wave 2 remaining relatively constant. Even considering the uncertainties in the observations (both Green, 1972 and Hirota and Barnett, 1977 report large amplitude standing waves in the mesosphere) it is likely the model overestimates the long wave amplitudes, for wave 1 and possibly 2, by 50% or more at 1mb. Wave 1 energy at this altitude in the model is lost primarily through interaction with the mean flow (KE to KZ) and secondarily through radiative damping. However, the radiative damping provides a violation of the

noninteraction theorem, and thus may indirectly allow a portion of the energy transfer to the mean flow to occur. As noted in Sections 2b and 2d, the model does not incorporate photochemical damping associated with the temperature dependence of the ozone reactions. Ghazi et al. (1979) have estimated that inclusion of this damping increases the total damping in the upper stratosphere by about a factor of two. Whether this would be sufficient to reduce the wave amplitudes to values more in line with published observations is uncertain. Wave 3, which was underestimated at 100mb, reaches an amplitude of about 130m between 1 and 2mb, in agreement with observations (Geller et al., 1983), and thus appears to be of realistic amplitude throughout most of the stratosphere. Of course its amplitude might also be reduced, at least in the upper stratosphere, were photochemical damping to be included. Diffusion would also reduce the amplitudes of all the waves. The phase variation of all three waves between 10mb and 1mb are in agreement with observations, wave 1 shifting slowly westward to 160°E by 1mb at 65°N, while waves 2 and 3 show little variation with altitude. As the phases of the waves are correct throughout the stratosphere, the waves appear to be propagating in a realistic fashion.

In the Southern Hemisphere mid-troposphere during January, the model's values for wave 1 amplitude of 50-70m are slightly less than the observed 80m (van Loon and Jenne, 1972; Trenberth, 1980) at 50-60°S while the phase, near 180° longitude, is some 30° west of the observed phase. For wave 2 the amplitude of 20-30m in mid-latitudes appears realistic (Trenberth, 1980), while the phase is about 20° too far west; the higher amplitude of 50m at 67°S has not been reported. The wave 3 amplitude of over 60m is more than twice that observed, while the phase of about 30°E from 50-60°S is appropriate. In both the model and observations (van Loon and Jenne, 1972) wave 1 shifts westward with height at high latitudes up to about 30mb, and then the phase becomes stationary, implying that upward propagation effectively ends at that level (due to the appearance of the summer east winds as in Fig. 7a). The amplitude maximum of 140m at 100mb is greater than that reported (from one year of observations in van Loon and Jenne, 1972). Wave 3 shows little phase variation with altitude and thus little propagation in either the model or observations. If the observations are accurate and representative, the model seems to overestimate the standing wave amplitude of wave 3 in the Southern Hemisphere troposphere, and wave 1 in the lower stratosphere, while maintaining an approximately accurate phase. The Southern Hemisphere summer stratosphere has very small wave amplitudes, as is observed.

JULY: The results for the different wavenumbers are shown in Fig. 21. In the Southern Hemisphere winter the tropospheric amplitudes for waves 1-3 all reach 100m, increasing to 800m for wave 1 by 0.7mb, to 250m for wave 2 at 3.4mb, and with a slow but general decrease with altitude for wave 3. In the Northern Hemisphere mid-stratosphere, more than half of the eddy energy associated with wave 1 is in the standing waves, and slightly less than half for wave 2. In the Southern Hemisphere, only about 1/4 of each is in the standing wave component - this agrees with observations, especially for wave 2 (Hartmann, 1976a) (and as noted earlier, is true for the Southern Hemisphere troposphere as well). This makes comparison with observations difficult above about 30mb for the standing waves, since analysis of continuous time series are necessary to remove the traveling component. Below 30mb the model amplitudes are in good agreement for wave 1 (compared to van Loon and Jenne, 1972), while waves 2 and 3 may be up to a factor of two too large in the mid-troposphere

(van Loon and Jenne, 1972; Trenberth, 1980). The phase of wave 1 appears to be 40° too far west, while the phase of wave 3 appears 40° too far east. In the Northern Hemisphere the amplitudes agree well with observations (van Loon et al., 1973; Defant et al., 1979; Reiter and Westhoff, 1981) with small amplitudes of about 20m for waves 2 and 3 in the mid-troposphere, and amplitudes for wave 1 of about 100m in the upper troposphere. The phases show strong variations with latitude and altitude, a commonplace occurrence for small amplitude waves, and evident in observations (Defant et al., 1979). In the stratosphere, the amplitudes remain quite small in the east wind regime. Note that the winter-summer difference in amplitude of the long waves at 500mb is substantially less in the Southern Hemisphere, in agreement with the observations of Trenberth (1980).

To summarize these comparisons: in both winter hemispheres wave 1 appears to be well simulated in the troposphere and lower stratosphere, while waves 2 and 3 show some deviation from observations in the mid-troposphere. Given that the wave 1 forcing appears realistic, it should be possible to evaluate why both the model and observations show smaller wave 1 amplitudes in the Southern Hemisphere mid and upper stratosphere than is found in the Northern Hemisphere during winter. As shown in Fig. 20 and 21 there is little difference at 100 mb. Above 100mb, however, wave 1 propagates better in the Northern Hemisphere. A complete discussion of wave propagation will be given in Section 3e.

KELVIN WAVES (?): One other aspect of the wave spectrum relates to the discussion in Section 3b, subsection 2, and Fig. 10 which shows the semiannual zonal wind variation between 3.4 and 0.17mb at the equator. It has been hypothesized (Hirota, 1980) that the westerly phase of this variation is caused by the upward propagation of Kelvin waves, which provide westerly momentum when they are damped in the tropical stratosphere. Kelvin waves travel eastward, have long wavelengths, with zonal wind but no meridional wind oscillations. They should propagate best into the upper stratosphere when the zonal winds are easterly (during the solstices), and thus provide the momentum source for the change to west winds (during the equinoxes).

Fig. 22 shows the time power spectrum of the zonal wind for eastward traveling components of wave number 1 near the equator averaged for the months around the solstices and equinoxes when the model tropical stratosphere winds were most easterly (July, August, January and February) and most westerly (April, May, September, October). The wave number one component was determined by Fourier analysis, and the time power spectrum was obtained using the maximum entropy method (e.g., Hayashi, 1977) with order 10 regression (which was found to give the best results for artificially generated waves during a 30 day period). The results are shown for the upper troposphere and several levels in the stratosphere. As the winds did not obtain the proper west wind strength during the equinoxes it might be presumed that the model results will not be as informative as would otherwise have been possible, but certain similarities between the model simulations and theory are apparent. At 300mb and 50mb the energy at the solstices is only very slightly greater than that at the equinoxes; the east winds in the lower stratosphere in the tropics are also only slightly stronger during the solstices (Fig. 9b). By 10mb there is significantly more energy during the solstices, and this holds true at 1mb. As altitude increases the power shifts to shorter periods, peaking in the 10-15 day period range by 10mb, with significant energy at 5-10

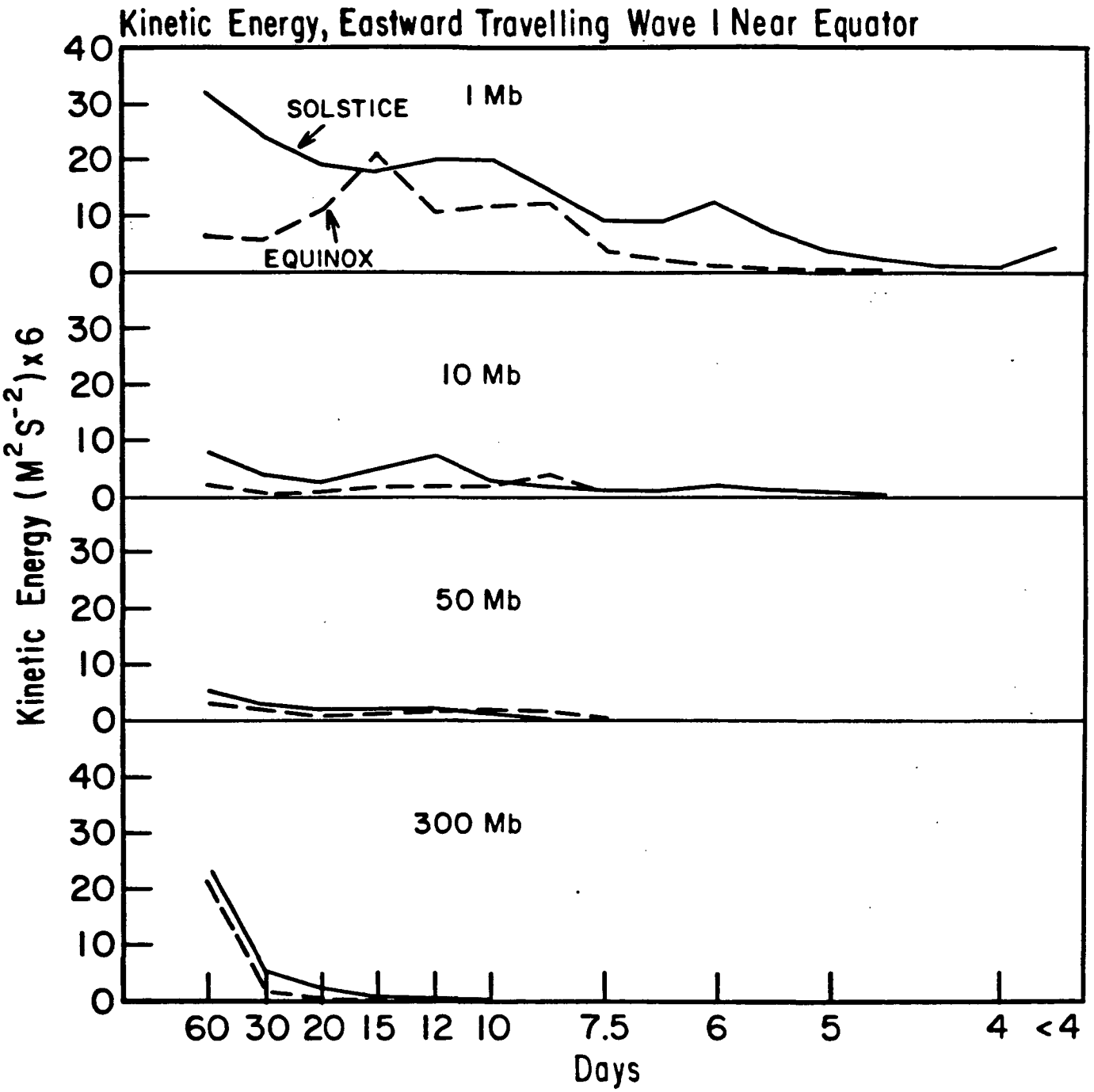

Fig. 22. Time power spectrum (per unit mass) of the zonal wind for eastward traveling components of wave number 1 near the equator. Results for the solstice (solid line) are for the months of January, February, July and August. Results for the equinox, dashed line, are for April, May, September and October.

days by 1mb. This is expected as the damping rate of Newtonian cooling increases with decreasing Doppler-shifted frequency (Holton, 1975). Observations show Kelvin waves with periods of 10-20 days in the lower stratosphere (e.g., Wallace and Kousky, 1968) and periods of 4-9 days in the stratopause region (Hirota, 1980). It can also be seen that the longest periods occur at the solstices, so the Doppler-shifted frequency has less variation from season to season (as observed by Hirota, 1980).

Besides the above mentioned characteristics, these waves have the necessary attribute that the meridional velocity fluctuations are an order of magnitude less than the zonal. To truly identify them as Kelvin waves requires analysis beyond the scope of this paper. The results shown provide "prima facie" evidence that Kelvin waves are propagating vertically and providing for angular momentum convergence (which is occurring due to vertical transports by eddies) in the model upper stratosphere. Transports will be discussed in Section 3e, as will the influence on the equatorial mean flow of Rossby wave propagation from mid-latitudes, which is thought to be responsible for generating the east wind phase of the semiannual socillation.

e. Wave propagation and transports

1) HORIZONTAL EDDY TRANSPORTS

SENSIBLE HEAT: Fig. 23 shows the northward transport of sensible heat by eddies during January and July. The tropospheric values in the Northern Hemisphere during January agree well with observations (Oort and Rasmusson, 1971; Lau, 1979). (For further comparison with observations in the troposphere, see I). In the lower stratosphere, the values range from 15K m s^{-1} at 100mb to 45K m s^{-1} at 30mb. This is in agreement with the observations for January in this height range of Oort and Rasmusson (1971), Newell et al. (1969), Dopplick (1971), Lau (1979) and Crane et al. (1980); values shown by Geller et al. (1983) are almost a factor of two higher at 30mb. This is an important diagnostic, as the cold lower stratospheric temperatures in the model might be caused by a deficiency in sensible heat transport, in addition to the radiative impact of too much water vapor. Labitzke and Goretzki (1982) show that there is great variability from year to year at 30mb. The underestimate of wave number 3 at 100mb should not strongly impact the sensible heat transport, if the analysis of Kao and Sagendorff (1980) for the winter of 1964 is representative.

By 10mb the value has risen to 130K m s^{-1} in the model, in agreement with the observations of Geller et al. (1983) and slightly less than those reported by Dopplick (1971). The values then rise to a peak of almost 350K m s^{-1} at 1mb, about 50% greater than that reported by Geller et al. (1983). This excess sensible heat transport is consistent with the larger amplitude wave 1 produced by the model at that altitude.

In the Southern Hemisphere troposphere during this month the model values are slightly too small to appear in a contour, but they are in agreement with the value of 10K m s^{-1} reported by van Loon (1980). Values remain small in the Southern Hemisphere summer stratosphere, as the eddy energy is very small.

In July, the small Northern Hemisphere sensible heat transports in the troposphere are in agreement with the observations of Oort and Rasmusson (1971)

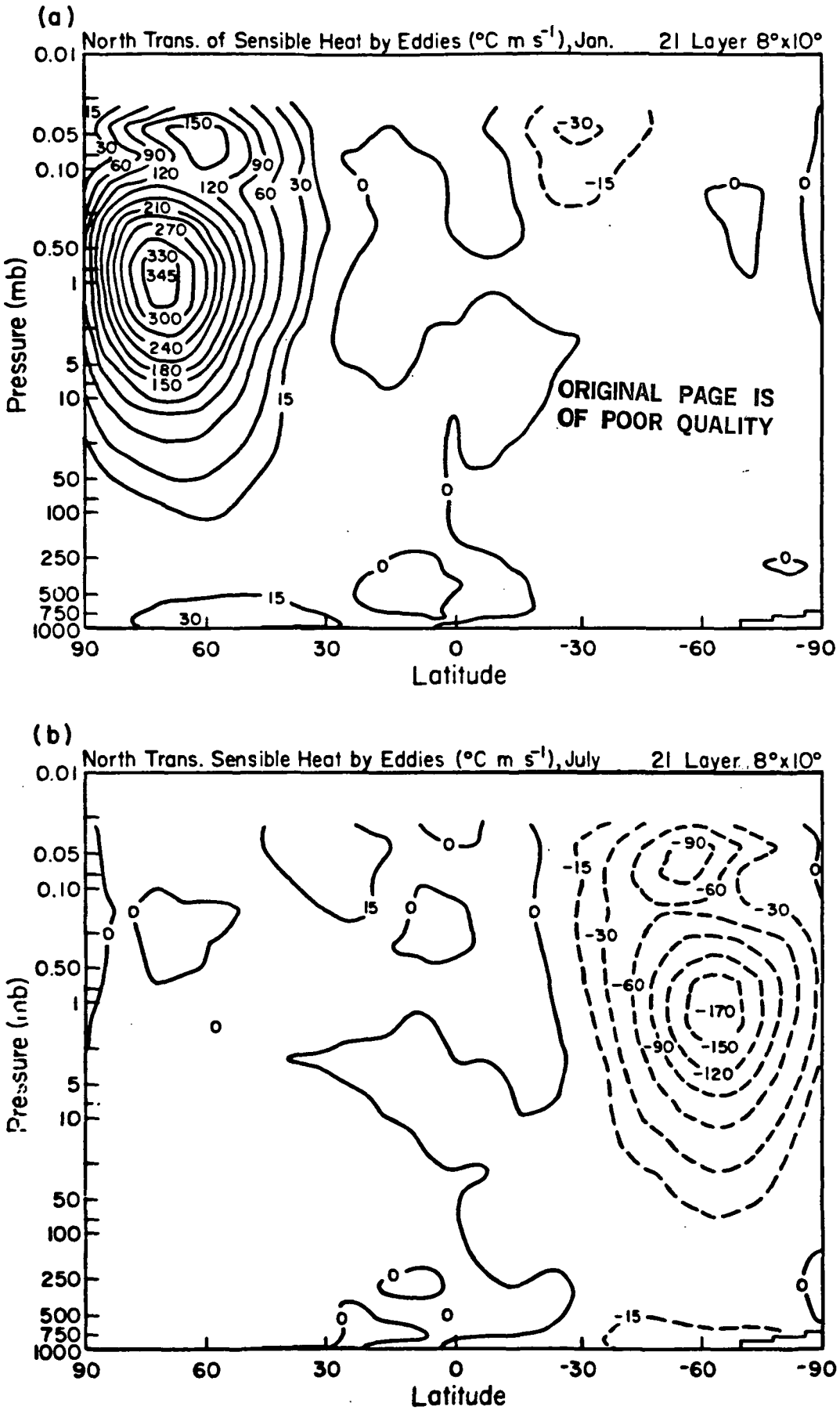

Fig. 23. Latitude-height profile of the northward transport of sensible heat by eddies for (a) January and (b) July.

of 5K m s^{-1}, while the small stratosphere values are again indicative of small summertime eddy energy.

In the Southern Hemisphere winter troposphere the values are in agreement with results shown by van Loon (1980). The model values rise to a peak near 1mb, with a value almost three times larger than that shown by Hartmann (1976a) for standing eddies. As noted earlier, the energy in the Southern Hemisphere winter stratosphere in the model is made up of 25% standing eddies and 75% transient eddies; the model transport associated with standing eddies is a little less than one-third the value shown in the figure, and thus in agreement with Hartmann. Thus the model's total poleward transport of sensible heat in the Southern Hemisphere winter stratopause region is dominated by the transient fluxes.

WESTERLY MOMENTUM: The northward transport of westerly momentum by eddies for January and July is shown in Fig. 24. During January in the Northern Hemisphere troposphere the model simulation is in good agreement with the observations of Oort and Rasmusson (1971) and Lau (1979). The values in the low and mid stratosphere are in agreement with observations reported by Crane et al. (1980) although they may be slightly low compared with the observations of Geller et al. (1983); as shown by Labitzke and Goretzki (1982) there is much year to year (and week to week) variation for January. It is not obvious from a comparison with observations that the model is underestimating the northward momentum transport in the region around 100mb, which would affect the zonal wind distribution above the tropospheric jet. In the upper stratosphere the model is in fairly good agreement (within about 20%) of the value reported by Geller et al. (1983) but it climbs to larger values, by almost a factor of two, in the lower mesosphere. This again is apparently due to the overestimate of the wave amplitudes at this height.

In the Southern Hemisphere troposphere, there is only a small variation in the momentum transport from summer to winter, in both the model and observations (Oort, 1982). At higher levels during July, the Southern Hemisphere transports can be compared with observations of standing eddy transports shown by Hartmann (1976a). Once again the standing eddy transports are in agreement with the observations, while representing only one-third of the total eddy momentum transport.

The July transports in the Northern Hemisphere are small, and may underestimate the transport in the upper troposphere by a factor of two (compared with Oort and Rasmusson, 1971; Oort, 1982). Note that the Northern Hemisphere tropospheric jet stream in July (Fig. 7) is also somewhat too weak.

2) VERTICAL PROPAGATION AND TRANSPORTS

GEOPOTENTIAL ENERGY: Shown in Fig. 25 is the vertical transport of geopotential energy by eddies for January and July. In January in both hemispheres the transport is downward from the middle troposphere to the surface, and upward from the mid-troposphere into the stratosphere. It thus indicates that the energy generated in the middle troposphere due to baroclinic conversions (see Fig. 17) is exported both upwards and downwards. The convergence of this flux is also shown in Fig. 17; this flux is often called the eddy pressure interaction term, or simply the boundary flux. The directions of transport are consistent with the results shown by Oort and

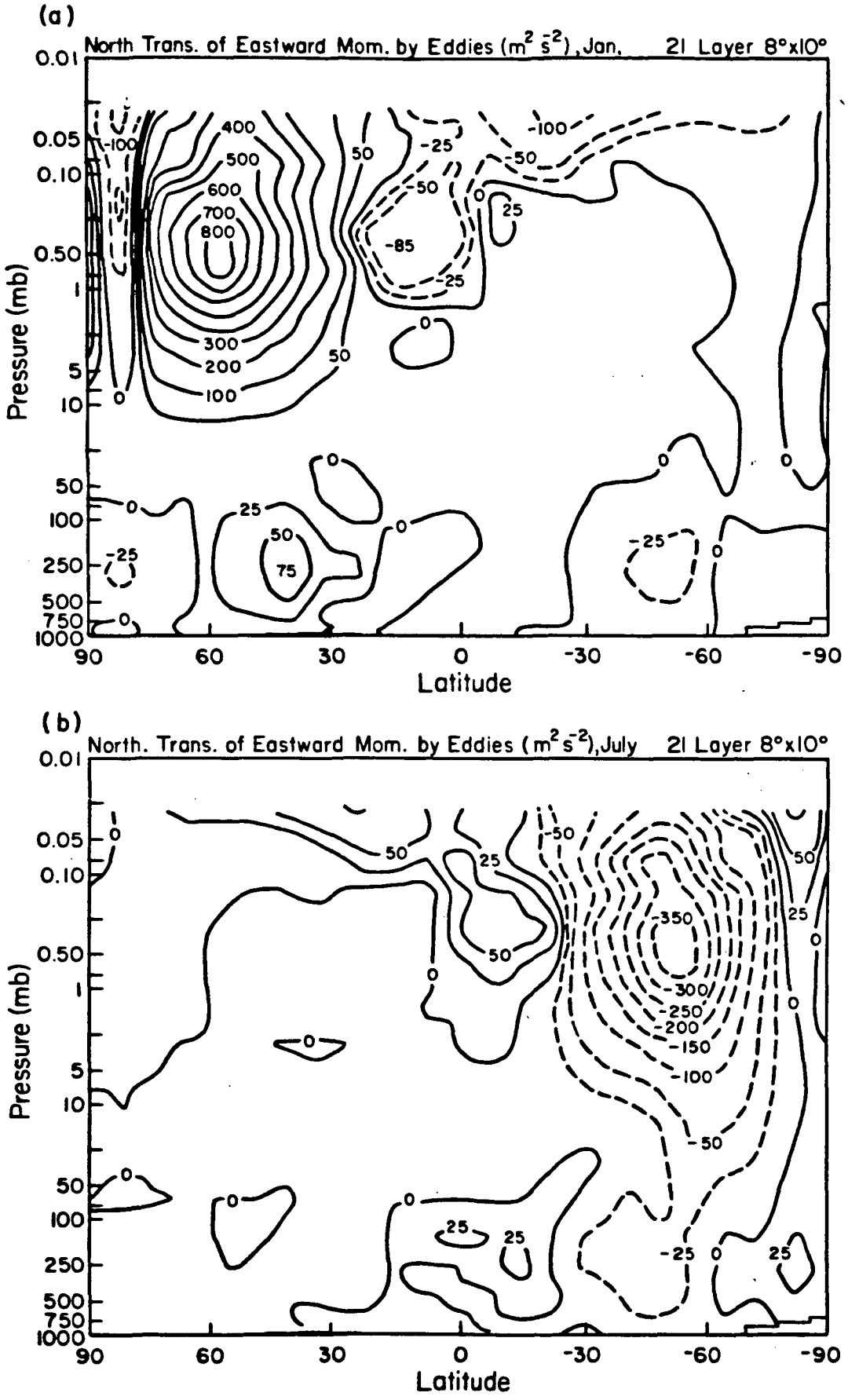

Fig. 24. Latitude-height profile of the northward transport of eastward momentum by eddies for (a) January and (b) July.

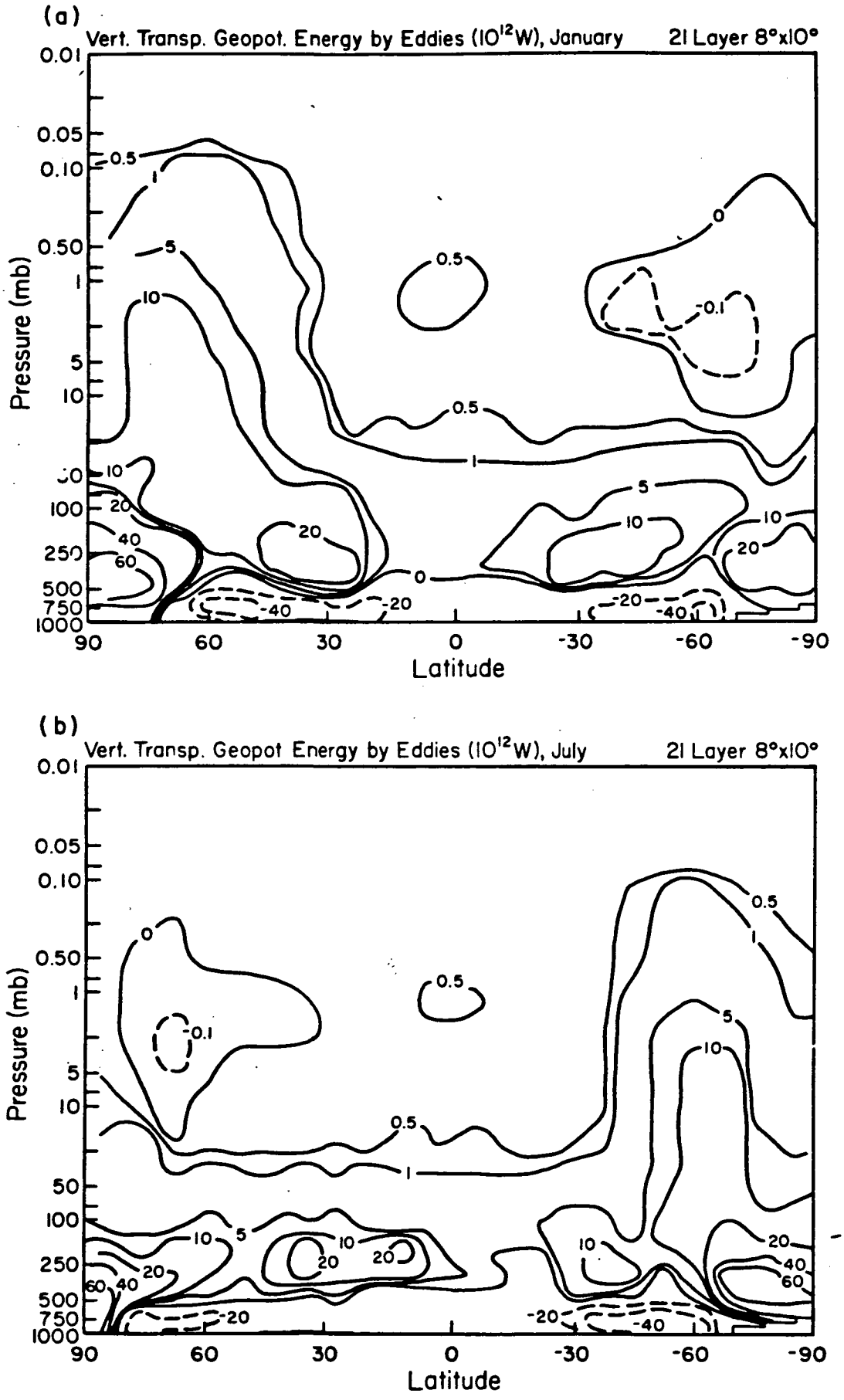

Fig. 25. Latitude-height profile of the vertical transport of geopotential energy by eddies for (a) January and (b) July.

Rasmussen (1971) for standing eddies, with the implied vertical transport shown by Kung (1966), and in essentially complete agreement in both magnitude and direction with the transport shown by Manabe and Mahlman (1976) for their model January.

The vertical transport through the 100mb level in the Northern Hemisphere is similar to that shown by Manabe and Mahlman (1976) for the total eddy transport in their model; it is 50% greater than the standing eddy flux computed by Newell and Richards (1969) and Oort and Rasmussen (1971), and 2 to 3 times greater than the standing eddy flux obtained by Dopplick (1971). The standing wave energy at this altitude in the model is one-third the total eddy energy, so the total eddy vertical transport is not unreasonable. Between 100mb and 10mb the model values are 30% excessive compared to the results shown by McNulty (1976) for standing wave fluxes. As shown in the figure there is only a gradual decrease of the vertical flux through the stratosphere indicating that waves are propagating relatively freely (especially wave 1) in the Northern Hemisphere. In the Southern Hemisphere there is a strong decrease in geopotential flux above 200mb, as will be discussed in greater detail below.

During July, in the Northern Hemisphere the vertical transport above 200mb decreases to very small values, in agreement with the relative change shown by Oort and Rasmussen (1971) for standing eddy transports. The vertical flux remains small throughout the summer hemisphere. In the Southern Hemisphere the vertical flux is about a factor of two larger, from all eddies, than the values shown by Hartmann (1976a) for standing eddies; the importance of transient eddies in the model's Southern Hemisphere stratosphere has already been mentioned.

Comparing the two winter hemispheres, it can be seen that the eddy vertical flux is similar at 21mb, but decreases above in the Southern Hemisphere relative to the Northern Hemisphere. This is shown in another format below.

ELIASSEN-PALM FLUX: Fig. 26 shows the Eliassen-Palm (EP) flux (Eliassen-Palm, 1961) for January and July, as well as the flux divergence. For presentation purposes constant length arrows are used in the troposphere; in addition, above 100mb the vertical component is multiplied by a factor of 250 relative to the horizontal, below 100mb by a factor of 7. The dominant terms in this flux are the eddy transport of sensible heat, which provides for an upward EP flux when the transport is poleward, and the eddy transport of westerly momentum, which provides an equatorward EP flux when the transport is northward. (The computation which produced these figures includes the additional, non-quasigeostrophic terms as well, a heat transport term multiplying the shear in the northward component, and the vertical eddy momentum flux in the vertical component). For steady waves under adiabatic and frictionless conditions these fluxes are equivalent to the northward and vertical geopotential energy fluxes normalized by the zonal wind, and thus represent the direction of the group velocity for propagating waves in regions where the group velocity is well defined (Palmer, 1982). It is immediately obvious from this figure, compared with Fig. 25, that the vertical EP flux, which is dominated by the poleward sensible heat transport shown in Fig. 23, is opposite in direction to the actual geopotential flux in the low and

ORIGINAL PAGE IS
OF POOR QUALITY

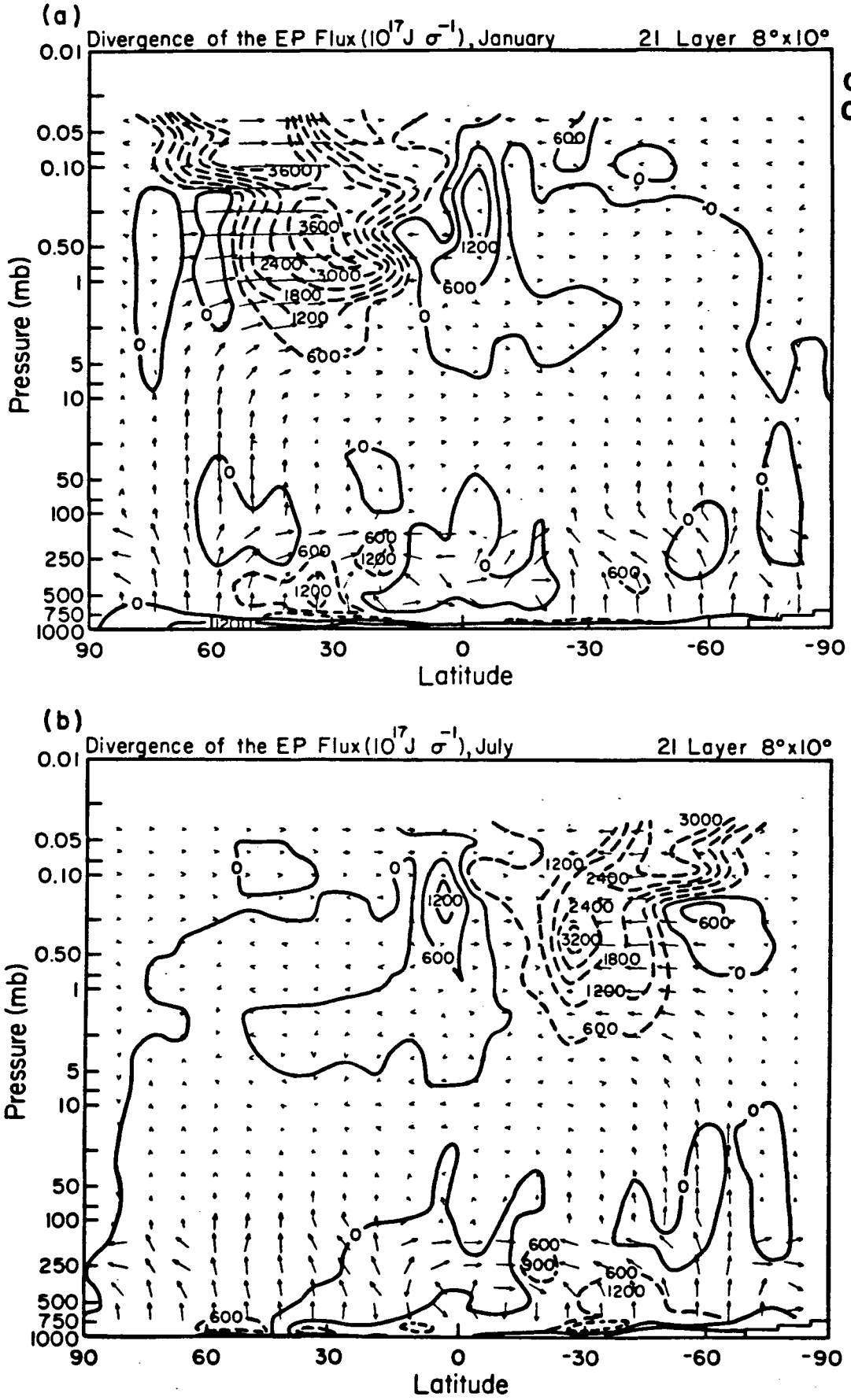

Fig. 26. Latitude-height profile of Eliassen-Palm flux and flux divergence for (a) January and (b) July. The vertical component of the flux has been multiplied by a factor of 250 relative to the horizontal above 100mb, and by a factor of 7 below 100mb for presentation purposes. Constant length arrows are used in the troposphere.

middle troposphere. A similar result can be seen in observations of stationary eddy transports (Oort and Rasmusson, 1971). In this region the assumptions of steady flow and adiabatic frictionless conditions are strongly violated; thus also is the relationship between poleward heat transport and vertical geopotential transport discussed, for example, by Hartmann (1976b). (This is a similar result to that given in Section 3d, subsection 2, for the relationship between northward heat transport and baroclinic eddy generation).

From the upper troposphere through the stratosphere the flux is aligned with the flux of geopotential energy (normalized by the zonal wind). It graphically indicates vertical propagation at mid and high latitudes, of greater magnitude in the winter hemispheres, consistent with the sensible heat transport shown in Fig. 23. In the winter hemispheres the flux is equatorward from mid-latitudes, with a tendency for poleward flux at the highest latitudes - this is consistent with the momentum transport relationship discussed above and shown in Fig. 24. In the low and mid-stratosphere the flux is from the winter hemisphere into the summer hemisphere, while the reverse appears true above about 2mb.

The flux directions can be compared with those shown by Edmon et al. (1980) and Karoly (1982) for all eddies in the troposphere, with observations of Sato (1980) and Geller et al. (1983) for troposphere and stratosphere, and with those of Smith (1983) in the stratosphere for wave 1. In the troposphere the directions are in complete agreement except that the summer subtropical fluxes in the Northern Hemisphere are not equatorward in the model (remember that the westerly momentum transport in this region during this month, as shown in Fig. 24, is underestimated, as is the strength of the summertime subtropical jet). The magnitudes are presumably realistic, (although it is hard to tell from the diagrams in the literature), because as discussed above, the sensible heat and momentum transports are generally in agreement with observations from the troposphere through the middle stratosphere.

REFRACTIVE INDEX: The characteristics of wave propagation are understood in the quasigeostrophic system in terms of the refractive index squared (as defined by Matsuno, 1970, and modified by Palmer, 1982). Waves will not propagate through (infinitely thick) regions of negative refractive index, which is caused either by a negative latitudinal gradient of quasi-geostrophic potential vorticity ($\overline{q}_y$), east winds or very strong west winds; the largest EP fluxes occur in regions of moderate positive values of the refractive index, curving toward the direction of increasing index in regions of large gradients (Smith, 1983).

Fig. 27 shows the refractive index-squared for wave number 1 for January and July, as modified by Palmer (values divided by $\sin^2 \theta$ where θ is the latitude). The value for wave 1 is shown since it provides the greatest portion of energy in the stratosphere; thus while an exact comparison with the total wave propagation shown by the EP flux diagrams is not possible, a qualitative relationship can be determined. The refractive index-squared is negative in the summer hemisphere stratospheres above about 30mb due to the east winds; the vertical EP flux (and the vertical transport of geopotential energy) decreases to very small values in the summer hemisphere above that altitude. At low latitudes the refractive index-squared becomes very large and negative (due to east winds and the latitudinal weighting), or occasionally

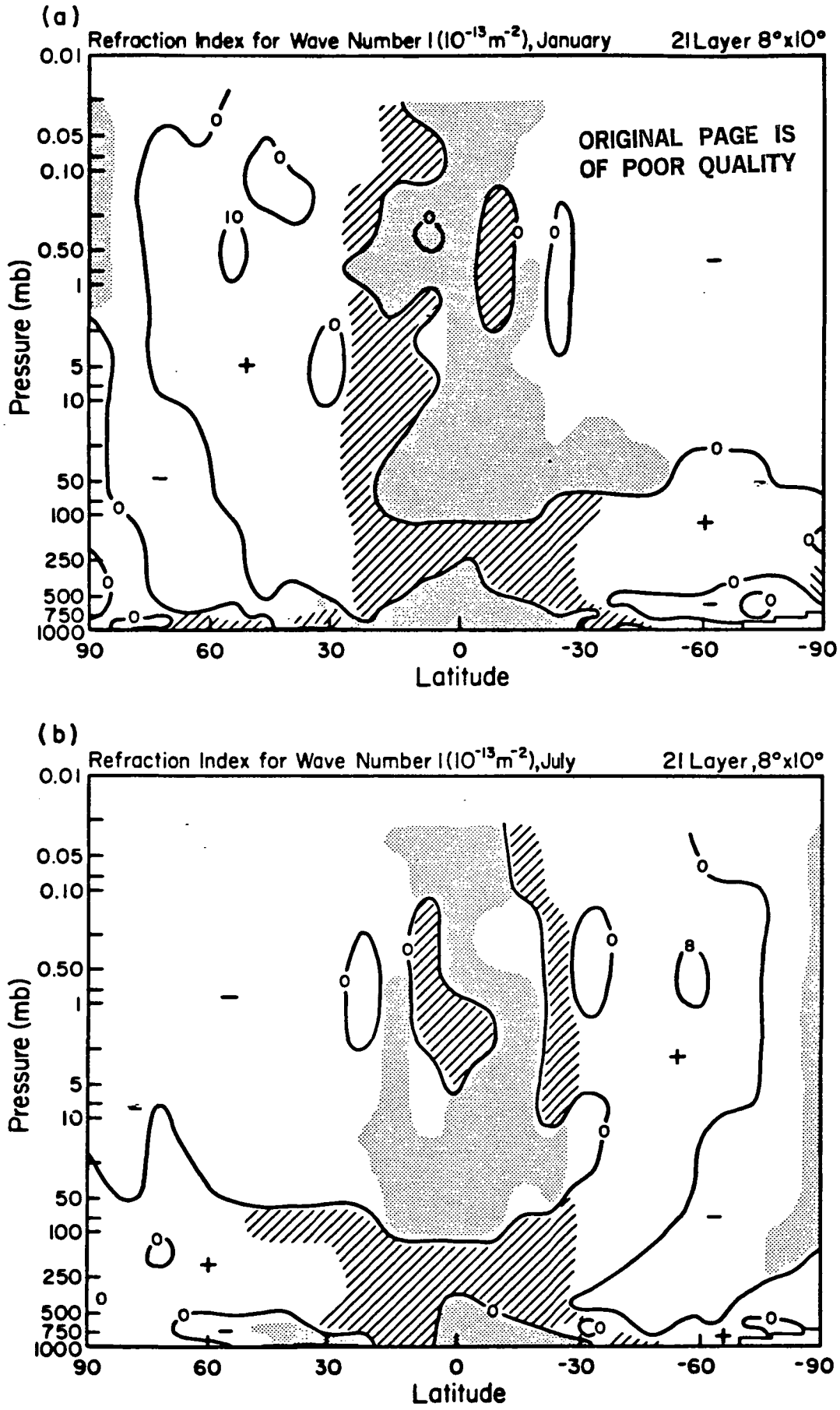

Fig. 27. Latitude-height profile of the modified refractive index-squared of wave number 1 for (a) January and (b) July. Regions with values greater than 100 are striped, with values <-100 are shaded.

very large and positive so the EP flux is basically horizontal. The EP flux is large in regions of positive refractive index-squared, and is guided into the core of the west winds (as shown in Fig. 7) due to the relatively large

value of $\overline{q}_y$ there (which in turn is due to the curvature of the latitudinal wind profile). This is all in accordance with expectations and observations, including the negative value of the refractive index-squared found at the highest latitudes in winter above 10mb (Smith, 1983).

However, there are some discrepancies: the diagnostic shows a region of negative refractive index-squared, due to a negative latitudinal gradient of quasi-geostrophic potential vorticity, in the mid to upper troposphere at upper mid-latitudes of the winter hemisphere. Some observations show negative

values of $\overline{q}_y$ in the mid-troposphere at these latitudes (Fullmer, 1982), although others give only positive values of the refraction index-squared (Lin, 1982; Karoly, 1982). As shown by the vertical EP flux, the waves do not appear to be making any special effort to avoid the region. Furthermore, observations (Lin, 1982) imply a minimum in the refractive index-squared directly above the tropospheric jet, which does not occur in the model, although one does occur around 10 mb. These negative values of q_y are caused by the failure of the model to decrease the latitudinal temperature gradient with increasing altitude in the lower polar stratosphere. This deficiency is equivalent to the inability of the model to provide a decrease in the zonal wind at mid-latitudes in the lower stratosphere, as discussed in Section 3b.

As shown by Fullmer (1982), $\overline{q}_y$ is very sensitive to changes in the zonal wind. It is curious, however, that the EP flux does not seem to be affected strongly by these deviations, which raises the question of the applicability of this quasi-geostrophic diagnostic to the general circulation model, at least insofar as details are concerned. The index is slightly larger in winter in the Northern Hemisphere above 20mb than in the Southern Hemisphere. As noted above, there is considerably less wave propagation in the Southern Hemisphere at these heights. The zonal winds are some 20 ms^{-1} stronger at these altitudes during winter in the Southern Hemisphere and this would act to limit vertical propagation all other things being equal.

DIVERGENCE OF EP FLUX: Also shown in Fig. 26 is the divergence of the EP flux; this is a measure of the eddy effect on the mean flow, being zero for steady waves in adiabatic frictionless flow with no critical level (Andrews and McIntyre, 1976). In the upper troposphere, the zero wind line, a critical line for stationary waves, occurs at low altitudes of the winter hemisphere; the EP convergence there acts to decelerate the zonal flow. The same effect is noted in the stratopause region, and this, at least in the model, verifies the contention of Dickinson (1969) and Hopkins (1975) that the east wind phase of the semiannual oscillation appears to be caused by absorption of planetary waves propagating from the winter hemisphere. Note that in Fig. 24 there is strong westerly momentum divergence in the subtropics of the winter hemisphere due to eddy transports. The large values of the EP flux divergence near the stratopause in the region of relatively large refractive index-squared may be because the group velocity is decreased in this region and the vertical scale of the waves decreases (relative to regions of moderate refractive index-squared), thus dissipation is larger (Smith, 1983). The convergences in the upper levels of the winter hemispheres are due to the effect of the

parameterized drag on the waves. In regions of EP flux divergence the waves are accelerating the mean flow - note the strong eddy induced westerly momentum convergences shown in these regions in Fig. 24. The regions of divergence in the west wind maximum, the region of convergence in the subtropical winter stratopause region, and also the region of convergence at the same altitude in the summer hemisphere subtropics have all been identified (Geller et al., 1983). The tropospheric convergence region in the winter subtropics is in agreement with observations (Karoly, 1982; Edmon et al., 1980; Geller et al., 1983) and the entire tropospheric pattern at mid-latitudes is qualitatively similar to the picture given by Edmon et al. (1980) for the time-averaged life cycle of baroclinic waves.

In the summer hemisphere stratospheres there is little in the way of EP flux divergence. This represents the fact that the eddies are not affecting the mean flow in these east wind regimes.

Experiments calculating the transport of passive tracers in the stratosphere (e.g., Hunt and Manabe, 1968) have indicated that the net transport is a small difference between transports in one direction due to eddies, and transports in the opposite direction by the mean meridional circulations. This is now recognized as an example of a type of non-interaction theorem (Mahlman et al., 1980), as the mean cells are also set up by the eddies. The cancellation will be incomplete to the extent that conditions similar to those for the noninteraction theorem are violated, i.e., in regions where the EP flux divergence is nonzero. While this holds true for passive tracers, it also applies to atmospheric parameters. In the regions of the free atmosphere in the model (those not strongly influenced by friction like that occurring in the lower troposphere or the upper three levels), winter hemispheric transports occur essentially in regions of nonzero EP flux divergence. In the region of EP flux divergence the total atmospheric horizontal transport (by eddies plus the mean circulation) of dry static energy (sensible heat plus geopotential energy), and of angular momentum is equatorward; in regions of EP flux convergence, the fluxes are poleward. In the summer hemispheres there is little divergence and little transport.

POTENTIAL VORTICITY: One additional vertical transport which is of interest is that of potential vorticity. Mixing between the troposphere and stratosphere demands that the higher values of potential vorticity in the stratosphere be brought down into the troposphere, and be dissipated by friction or nonadiabatic effects. The scale at which this transport occurs is not well known, and there is some question whether it can be adequately resolved in a coarse grid model. With potential vorticity written in pressure coordinates (Gidel and Shapiro, 1980), the vertical transport through the 100mb layer for January and July is shown in Fig. 28, for both eddies and the total (eddies plus the mean circulation). The locations of downward transport, strongest in mid-latitudes of the winter hemisphere, but also occurring in upper mid-latitudes of the summer hemisphere agree with the NCAR GCM results reported by Gidel and Shapiro (1980), and, for the Southern Hemisphere winter, the analysis of Hartmann (1977). The eddy transports are generally the same sign as the total transports, but in winter are not the dominant component. The validity of using a coarse grid model to investigate tropospheric-stratospheric transports can be tested by using the model to advect passive tracers and comparing with appropriate observations.

ORIGINAL PAGE IS
OF POOR QUALITY

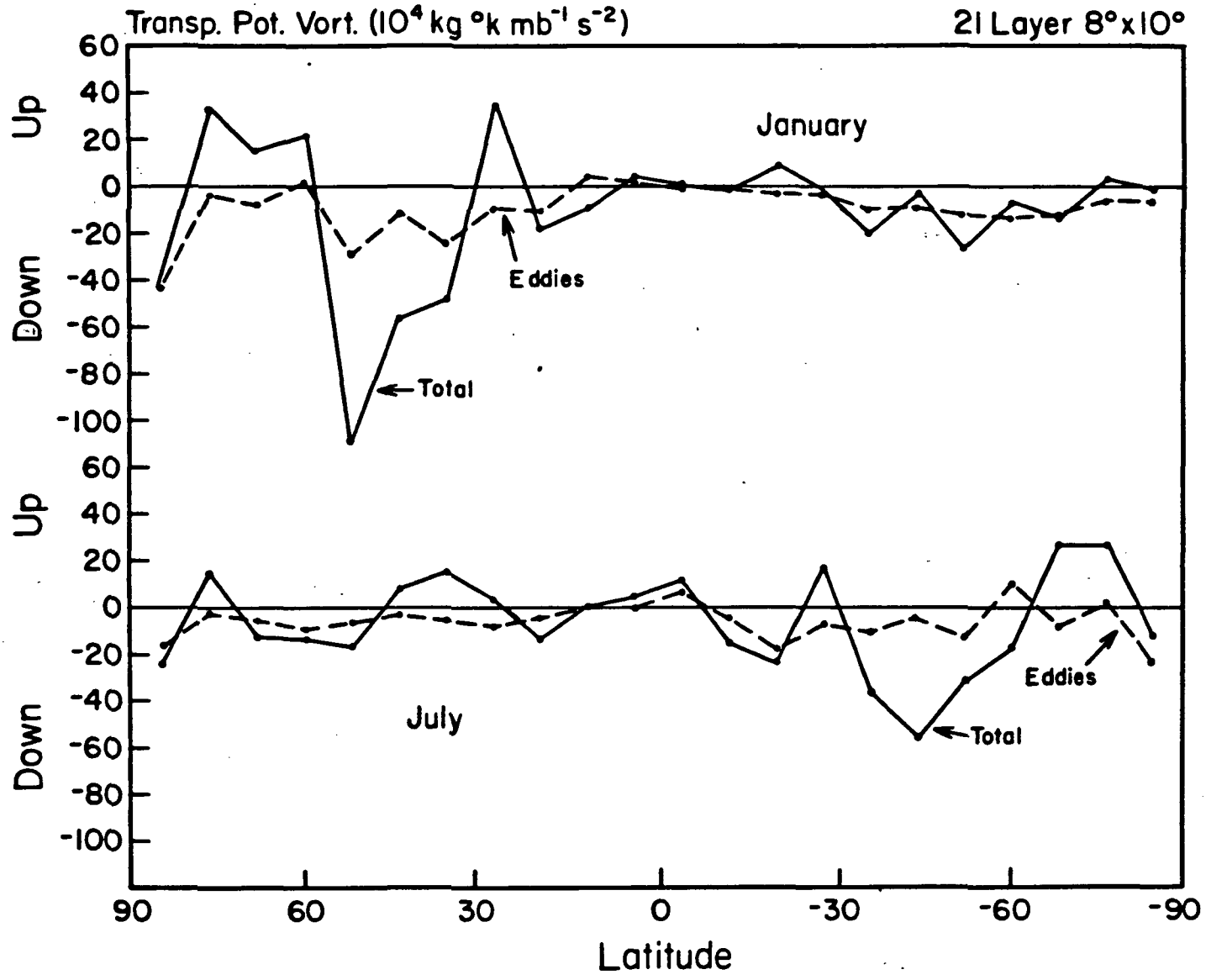

Fig. 28. Vertical transport of potential vorticity through the 100mb level by eddies and total for January (top) and July (bottom).

f. Time sequences

As noted previously, the Northern Hemisphere stratosphere underwent pulsing events during the winter, with warming amplitudes most noticeable during January. A sequence of events is shown in Fig. 29 at 0.75mb (45-50km in the Northern Hemisphere) starting on January 1, the 14th month of the simulation. The left hand side of each row shows the geopotential height map averaged over the day, while the right hand side shows the temperature pattern. Every fourth day is shown through day 13. Starting on January 1, the first maps indicate that the polar cyclone was situated over Greenland, with a ridge centered over the Mediterranean Sea. The warmest temperatures, +5°C, were located in a warm region just to the northwest of the high, while the coldest temperatures were found in the Aleutian area. Four days later the ridge had strengthened by 1km, and was now centered somewhat further east, and slightly north, at 50°N, 90°E. The polar cyclone had moved slightly westward. The warmest region had strengthened and moved far to the north, with 10°C located north of the ridge near the pole. By day 9 the ridge had weakened and moved eastward, to a position over the mid-Pacific, while the polar low had also moved eastward, to the side of the pole near the Greenwich meridian. Both the warm and cold regions showed little movement, although the warm region was weaker, now at 0°C. On day 13 the high is now again further west, near 120°E, and somewhat stronger, while the low is still east of Greenland. The warm region has moved south, and intensified strongly, now at 20°C, while the cold region has moved eastward to a position over the Canadian Maritimes, and is 5°C colder than it had been.

The movements described here in the upper stratosphere are typical of those seen at various levels in the stratosphere associated with major or minor warmings (e.g., Williams, 1968). There are several points to be made. There was no major warming, since the polar cyclone never retreated from its near pole position, and the latitudinal temperature gradient did not reverse (and further the definition of a major warming requires that this happen at 10mb). While wave 1 dominates the maps, the event is not restricted to standing or slowly moving wave 1 processes - note the warm and cold regions on day 13, at their greatest amplitudes, were separated by just 120° longitude at 60°N. The whole pattern of shifting locations for the ridge and trough could be analyzed in terms of travelling and standing waves. The time power spectrum for geopotential at 50°N and 1mb shows significant energy at 15-30 day periods for westward traveling waves. Finally, if one observes the temperatures near the equator at the approximate longitude of the warm region, it can be seen that when the region at high latitudes is warmest, the equatorial region is coldest. When the warm region is at 5°C, the equatorial temperature to the south is at -10°C (day 1); when it is at 10°C, the equatorial temperature is at -15°C (day 5); and when it is at 20°C, the equatorial temperature is at -20°C (day 13). This simultaneous negative correlation has been observed during warmings (e.g., Labitzke and Barnett, 1973), and has been associated with wave transports set up as planetary waves are absorbed (Matsuno, 1971); the mechanical forcing sets up a residual mean circulation (Plumb, 1982).

The appearance of these warming pulses as a function of time and altitude can be seen by looking at the zonal average temperature at 67°N from late December through January. This is shown in Fig. 30. The amplitude of the perturbation is reduced somewhat by using the zonal average, as can be seen in

ORIGINAL PAGE IS
OF POOR QUALITY

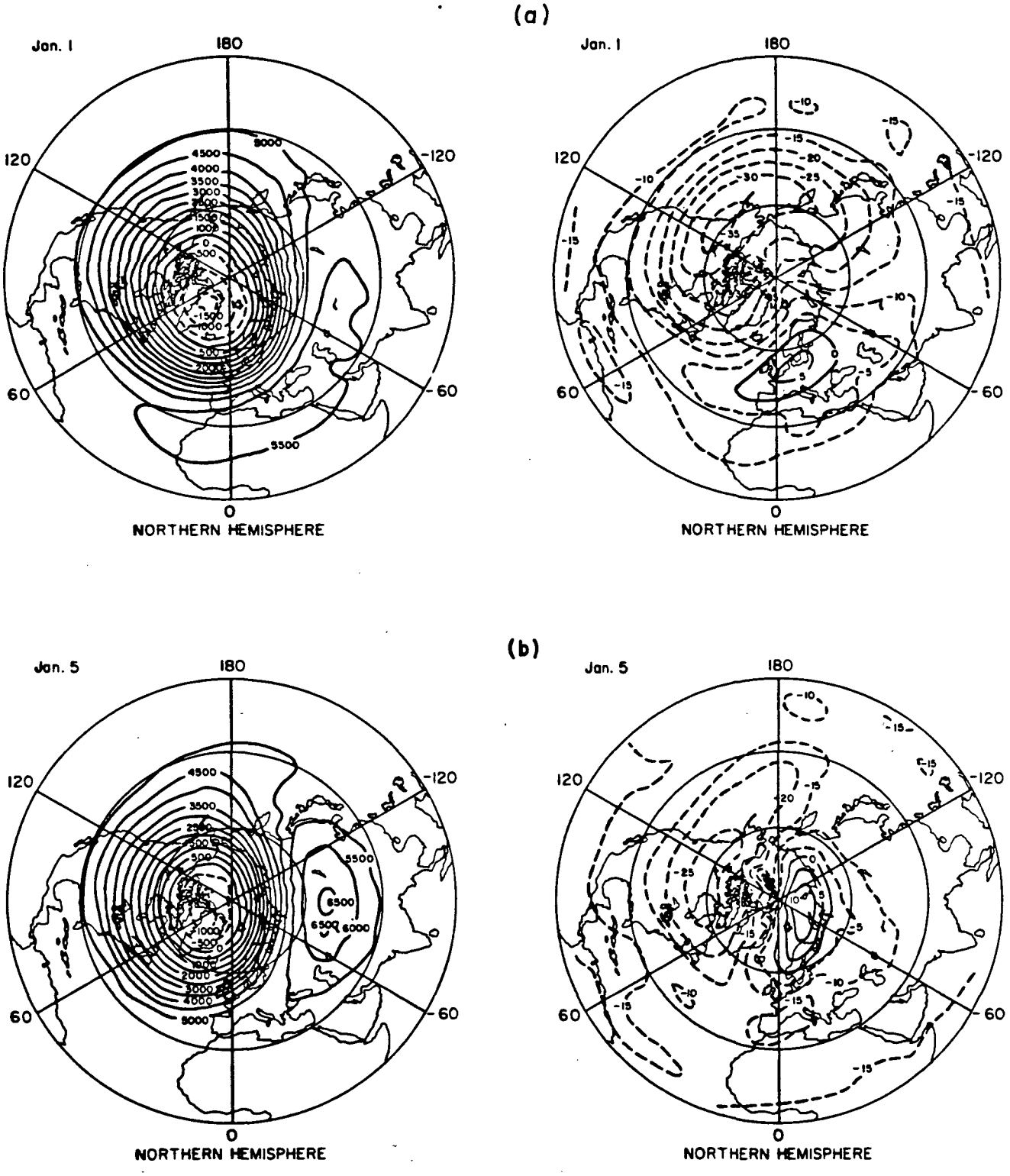

Fig. 29a. Northern Hemisphere geopotential heights (left) and temperatures (right) for the 0.75mb level for (a) January 1; (b) January 5. Height contours are in meters above or below 45 km.

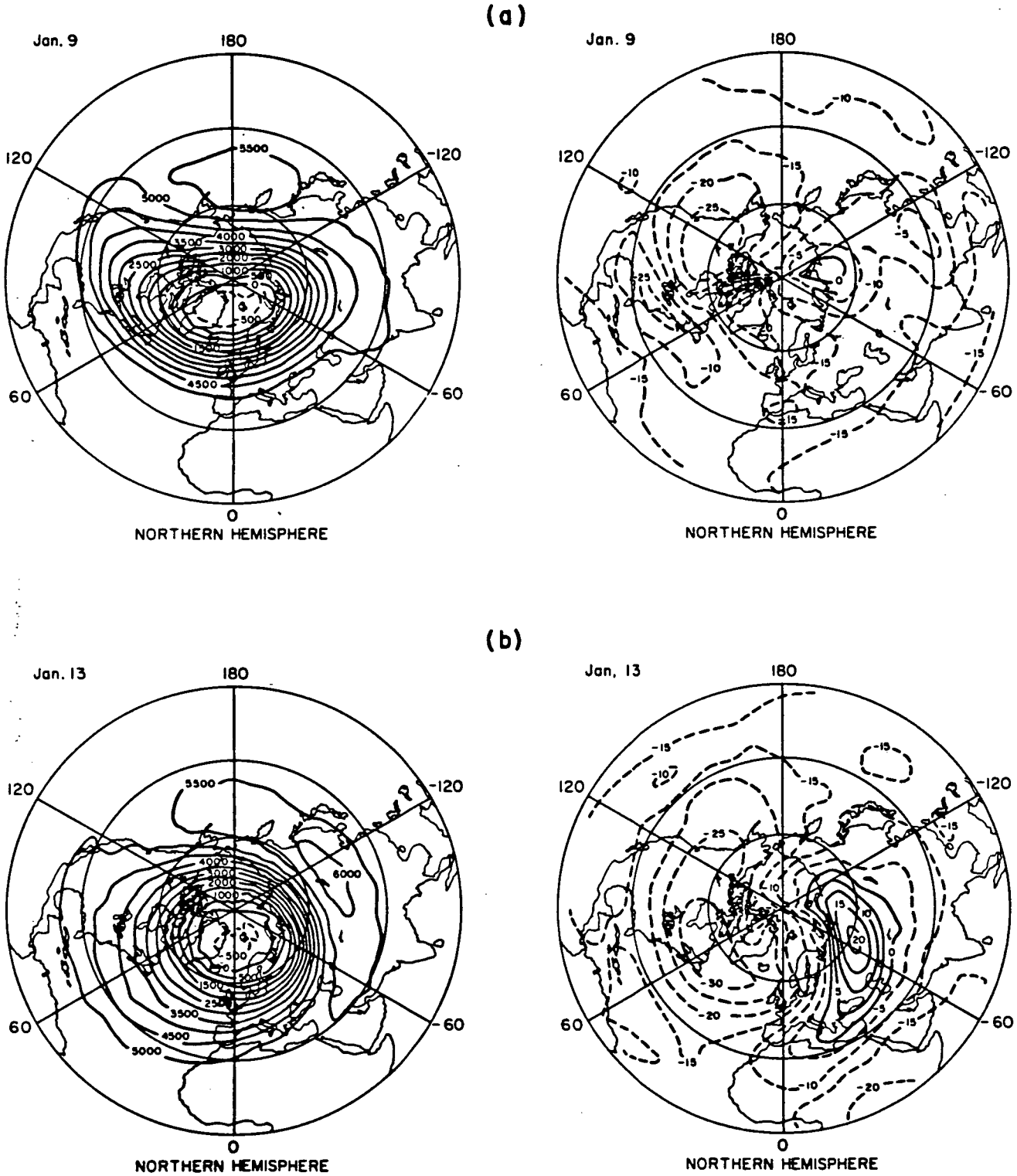

29b. Same as Fig. 29a for (c) January 9; (d) January 13.

ORIGINAL PAGE IS
OF POOR QUALITY

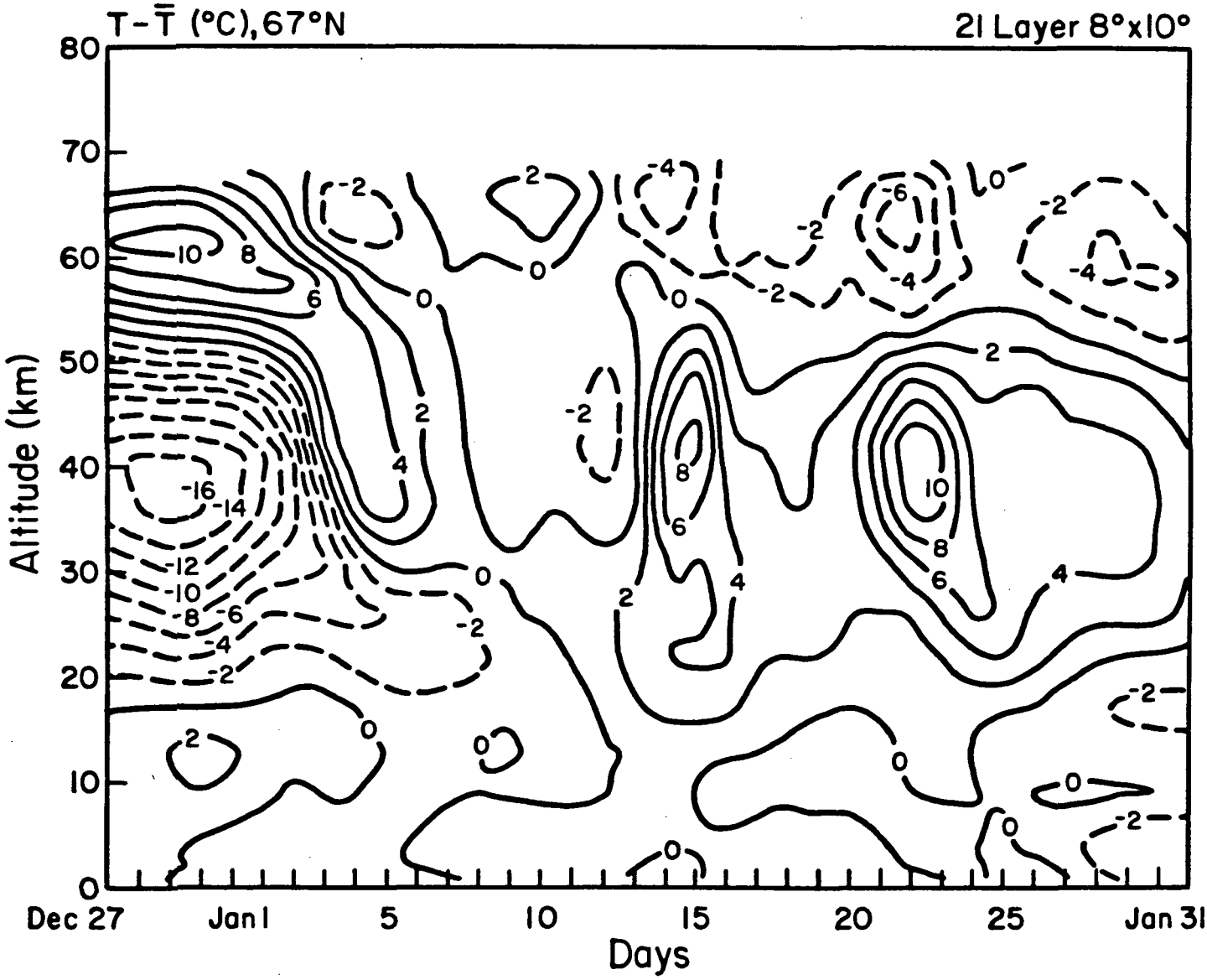

Fig. 30. Temperature deviation from the 35 day average at each pressure level as a function of day from December 27 through January 31 for the zonal mean temperature at 67°N.

Fig. 29. From the figure it appears as if the warming pulses originate at about 65km and propagate down to 45km in 4-5 days. Propagation to 25km occurs more quickly, in 1-3 days. In the stratosphere the perturbation reaches its largest amplitude around 42km and is hard to detect at levels below 20km. This type of downward propagation of warming events is a well-known phenomenon. It is possibly associated with vertically propagating transient waves initiating their effect at high altitudes, where the density is low and wave amplitude large, and altering the atmosphere so the effect is felt subsequently at successively lower levels (with or without the formation of critical levels -e.g., Matsuno, 1971). Note also that in association with the phase lag, the warming in the upper stratosphere occurs simultaneously with cooling in the mesosphere, also an observed feature (e.g., Scott, 1972) in agreement with Matsuno's model and the properties of the forced Hough functions (Plumb, 1982). The pulses in the model occur with a quasi-periodicity of 9-13 days, in agreement with observations of 1-3 week pulsations (Madden, 1975) (and the time power spectrum at 50°N), and may be thought of as indicating the presence of traveling wave modes which alternately constructively and destructively interfere with the quasi-stationary waves (Madden, 1975).

It is beyond the scope of this paper to analyze these events in great detail. The time sequence is presented here to indicate the model's fidelity to observations. It is important for modeling changes in the stratosphere associated with climate perturbations that the model be able to reproduce transient features as well as climatological averages, for they may lead to major or minor warmings which impact the transport of constituents such as ozone.

4. Discussion

The comparisons with observations shown in the previous section indicate that the model is capable of generating a realistic troposphere and stratosphere. The model produces generally realistic temperatures, heights, winds, long waves, energy fluxes and transports, as well as realistic latitudinal, longitudinal, seasonal and hemispheric variations of the above quantities. The comparison also shows the need for improvements in the following areas:

(1) The temperature in the Northern Hemisphere winter polar lower stratosphere is too cold by some 5-10°C. This appears to be mostly the result of the excessive water vapor which is allowed to accumulate in the region and increase long wave radiation losses. The obvious solution is to allow water vapor to condense above the 100mb level, a process which was not included in the current version of the model.

(2) As a result of these cold polar temperatures, or at least consistent with them, the winds in the lower stratosphere are too strong. The resulting latitudinal wind profile helps to produce an apparently unrealistic refraction index profile, although the effect of this on the long wave propagation is not overly apparent. If the problem results from the excessive water vapor cooling it should be alleviated by the correction suggested above.

(3) The apparent deficiency in wave 3 energy in the troposphere may be related to the unrealistic refractive index profile, as suggested by Tenenbaum

(1982). The magnitude of the underestimation is uncertain, however, since the alternate January has significantly more wave 3 energy. Wave 4 energy also appears to be deficient in the troposphere.

(4) Temperatures at 50km and above in equatorial regions are too cold. This is probably due to the inability of the current radiation scheme to properly simulate CO_2 long wave cooling above about 45km. The radiation scheme needs to be altered to remove this possible deficiency.

(5) The excessively cold tropical stratopause temperatures result in a low latitude temperature gradient which is too large, and, from the thermal wind relationship, this results in the model's simulation of east winds being about two times too strong in the tropical lower mesosphere.

(6) There is some evidence that the drag incorporated in the top three model levels is too strong in winter and could be reduced, so that the winter west winds would not decrease as rapidly with altitude above the stratospheric jet. The summer mesosphere winds, however, do not appear excessive.

(7) Planetary wave amplitudes in the upper stratosphere and lower mesosphere are too large. The model does not include photochemical damping associated with the temperature dependence of ozone reactions, which would likely reduce the amplitudes. A parameterized form of photochemical damping, (e.g., Fels et al., 1980) should be included.

(8) The possibility of including explicit diffusion should be reexamined. The model currently uses none; obviously the choice of appropriate diffusion coefficients could by itself alleviate some of the deficiencies noted above (for example the large planetary wave amplitudes in the upper stratosphere). The problem with using diffusion is that the uncertainty in the true magnitude of the diffusion coefficients provides leeway for using values which "tune" the model to the current climate, and thus limit the nature of the stratospheric reaction to climate changes.

(9) The model produces apparent inertial oscillations in the tropical upper stratosphere. While these may exist, the model simulation may be resolution dependent, with a coarse resolution magnifying the effects of the instability.

(10) This last point leads to the more general conclusion that model results may be affected by increasing the vertical and horizontal resolutions. The modeled processes in the lower stratosphere, and tropospheric-stratospheric exchange may well differ with higher resolution, and it is important to quantify these effects. The coarse resolution model employed here is useful for testing and model development, and to the extent that it simulates climatology it is an adequate model for understanding the current stratosphere, but its use in climate change experiments must ultimately be validated against higher resolution versions.

(11) Finally, the model needs to be run for at least several years to determine its true climatology and interannual variability.

ACKNOWLEDGMENTS

We thank A. Del Genio, W. Robinson, W. Rossow, and P. Stone for advice, J. Lerner for producing model plots, and L. DelValle and J. Mendoza for drafting the figures. The initial GCM model development was supported by the NASA Climate Program managed by Dr. R. Schiffer; supplementary funding was supplied by the ERBS/SAGE II Science Program through NASA Langley Research Center, and for the preparation of this paper by the NASA Upper Atmospheric Research Program managed by Drs. R. Watson and D. Butler.

REFERENCES

Allen, M., Y. Yung, and J. Waters, 1981: Vertical transport and photochemistry in the terrestrial mesosphere and lower thermosphere (50-120km). J. Geophys. Res., 86, 3617-3627.

Andrews, D., and McIntyre, 1976: Planetary waves in horizontal and vertical shear: the generalized Eliassen-Palm relation and the zonal mean acceleration. J. Atmos. Sci. 33, 2031-2048.

Angell, J. and J. Korshover, 1964: QbO variations in temperature, total O_3, and tropopause height. J. Atmos. Sci., 21, 470-492.

Apruzese, J., M. Schoeberl, and D. Strobel, 1982: Parameterization of IR cooling in a middle atmosphere dynamics model. 1. Effects on the zonally averaged circulation. J. Geophys. Res., 87, 8951-8966.

Arakawa, A., 1972: Design of the UCLA General Circulation Model. Tech. Rep. No. 7, Dept. Meteor., University of California, Los Angeles, 116 pp.

Austen, M., J. Barnett, P. Curtis, J. Houghton, C. Morgan, C. Rodgers, and E. Williamson, 1977: Satellite temperature measurements in the 40-90km region by the Pressure Modulator Radiometer, COSPAR Space Research XVII, 111-115.

Barnett, J., 1980: Satellite measurements of middle atmosphere temperature structure. Phil. Trans. Roy. Soc. Lond. A, 296, 41-57.

Belmont, A., D. Dartt, and G. Nastrom, 1974: Periodic variations in stratospheric zonal wind from 20-65km at 80°N to 70°S. Quart J. Roy. Met. Soc., 100, 203-211.

Charney, J., and P. Drazin, 1961: Propagation of planetary-scale disturbances from the lower into the upper atmosphere. J. Geophys. Res., 66, 83-109.

Chen, T.-C., 1982: A further study of spectral energetics in the winter atmosphere. Mon. Wea. Rev., 110, 947-961.

Craig, R. and W. Hering, 1959: The stratospheric warming of January-February 1957. J. Meteor., 16, 91-107.

Crane, A., J. Haigh, J. Pyle, and C. Rogers, 1980: Mean meridional circulation of the stratosphere and mesosphere. Pageoph., 118, 307-328.

Crutcher, H., and J. Meserve, 1970: Selected Level Heights, Temperatures and Dew Points for the Northern Hemisphere. NAVAIR 50-1C-52, 424pp. (U.S. Govt. Printing Office).

Cunnold, D., F. Alyea, N. Phillips, and R. Prinn, 1975: A three-dimensional dynamical-chemical model of atmospheric ozone. J. Atmos. Sci., 32, 170-194.

Defant, F., A. Osthaus, and P. Speth, 1979: The global energy budget of the atmosphere. Part II: The ten-year mean structure of the stationary large-scale wave disturbances of temperature and geopotential height for January and July (Northern Hemisphere). Contributions to Atmos. Phys., 52, 229-246.

Dickinson, R., 1969: Theory of planetary wave-zonal flow interaction. J. Atmos. Sci., 26, 73-81.

Dickinson, R., 1973: Method of parameterization for infrared cooling between altitudes of 30 and 70km. J. Geophys. Res., 78, 4451-4457.

Dopplick, T., 1971: The energetics of the lower stratosphere including radiative effects. Quart. J. Roy. Met. Soc., 97, 209-237.

Dunkerton, T., 1981: On the inertial stability of the equatorial middle atmosphere. J. Atmos. Sci., 38, 2354-2364.

Dutsch, H., 1971: Photochemistry of atmospheric ozone. Adv. Geophys., 15, 219-315.

Dutsch, H., 1974: The ozone distribution in the atmosphere. Can. J. Chem., 52, 1491-1504.

Edmon, H., B. Hoskins and M. McIntyre, 1980: Eliassen-Palm cross sections for the troposphere. J. Atmos. Sci., 37, 2600-2616.

Eliassen, A. and E. Palm, 1961: On the transfer of energy in stationary mountain waves. Geophys. Publ., 22, 1-23.

Fels, S., J. Mahlman, M. Schwarzkopf, and R. Sinclair, 1980: Stratospheric sensitivity to perturbations in ozone and carbon dioxide: radiative and dynamical response. J. Atmos. Sci., 37, 2265-2297.

Fritz, S., and S. Soules, 1970: Large-scale temperature changes in the stratosphere observed from Nimbus-3. J. Atmos. Sci., 27, 1091-1097.

Fullmer, J., 1982: Calculations of the quasi-geostrophic potential vorticity gradient from climatological data. J. Atmos. Sci., 39, 1873-1877.

Geller, M., Wu, M.-F., and M. Gelman, 1983: Troposphere-stratosphere (Surface - 55km) monthly winter general circulation statistics for the Northern Hemisphere - four year averages. J. Atmos. Sci., 40, 1334-1352.

Ghazi, A., 1976: Ozone and stratospheric temperatures. J. Geophys. Res., 81, 5365-5373.

Ghazi, A., V. Ramanathan, and R. Dickinson, 1979: Acceleration of upper stratospheric radiative damping: observational evidence. Geophys. Res. Res. Let., 6, 437-440.

Gidel, L., and M. Shapiro, 1980: Global circulation model estimates of the net vertical flux of ozone in the lower stratosphere and the implications for the tropospheric ozone budget. J. Geophys. Res., 85, 4049-4058.

Green, J., 1972: Large-scale motion in the upper stratosphere and mesosphere: an evaluation of data and theories. Phil. Trans. R. Soc. Lond., A271, 577-583.

Gregory, J., C. Meek and A. Manson, 1981: Mean zonal and meridional wind profiles for the mesosphere and lower thermosphere at 52°N, L=4.4, during solar maximum. Atm.-Ocean, 19, 24-34.

Groves, G., 1969: Wind models from 60 to 130km altitude for different months and latitudes. J. Brit. Inter. Soc., 22, 285-307.

Groves, G., 1971: Atmospheric structure and its variations in the region from 25 to 120km. AFCRL-71-0410, Env. Res. Pap. No. 368. Available from the U.S. Air Force, L. G. Hanscom Field, Bedford, Mass. Available from NTIS #N72-24459.

Hansen, J., G. Russell, D. Rind, P. Stone, A. Lacis, R. Ruedy and L. Travis, 1983: Efficient three-dimensional global models for climate studies: models I and II. Mon. Wea. Rev., 111, 609-662.

Hartmann, D., 1976a: The structure of the stratosphere in the Southern Hemisphere during late winter 1973 as observed by satellite. J. Atmos. Sci., 33, 1141-1154.

Hartmann, D., 1976b: The dynamical climatology of the stratosphere in the Southern Hemisphere during late winter 1973. J. Atmos. Sci., 33, 1789-1802.

Hartmann, D., 1977: Dynamic studies of the Southern Hemisphere stratosphere. COSPAR Space Research, XVII, 167-174.

Hayashi, Y., 1977: Space-time power spectral analysis using the maximum entropy method. J. Meteor. Soc. Japan, 55, 415-420.

Hines, C., 1974: A possible mechanism for the production of sun-weather correlations. J. Atmos. Sci., 31, 589-591.

Hirota, I., 1980: Observational evidence of the semiannual oscillation in the tropical middle atmosphere - a review. Pageoph., 118, 217-238.

Hirota, I. and J. Barnett, 1977: Planetary waves in the winter mesophere - preliminary analysis of Nimbus 6 PMR results. Quart. J. Roy. Met. Soc., 103, 487-498.

Holton, J., 1975: The dynamic meteorology of the stratosphere and mesosphere. Meteor. Monogr. 37, Amer. Meteor. Soc., 216pp.

Holten, J., 1983: The influence of gravity wave breaking on the general circulation of the middle atmosphere. J. Atmos. Sci., 40, 2497-2507.

Holton, J. and W. Wehrbein, 1980: A numerical model of the zonal mean circulation. Pageoph., 118, 284-306.

Hopkins, R., 1975: Evidence of polar-tropical coupling in upper stratospheric zonal wind anomalies. J. Atmos. Sci., 32, 712-719.

Hunt, B., 1981: The maintenance of the zonal mean state of the upper atmosphere as represented in a three-dimensional general circulation model extending to 100km. J. Atmos. Sci., 38, 3172-2186.

Hunt, B. and S. Manabe, 1968: Experiments with a stratospheric general circulation model. II. Large-scale diffusion of tracers in the stratosphere. Mon. Wea. Rev., 96, 503-539.

Johnson, K. and M. Gelman, 1968: Temperature and height variability in mid and upper stratosphere during 1964-1966 as determined from constant pressure charts. Mon. Wea. Rev., 96, 371-382.

Kao, S.-K., and J. Sagendorf, 1970: The large-scale meridional transport of sensible heat in wavenumber frequency space. Tellus, 22, 172-185.

Karoly, D., 1982: Eliassen-Palm cross sections for the Northern and Southern Hemispheres. J. Atmos. Sci., 39, 178-182.

Kasahara, A. and T. Sasamori, 1974: Simulation experiments with a 12-layer stratospheric global circulation model. II. Momentum balance and energetics in the stratosphere. J. Atmos. Sci., 31, 408-421.

Kirkwood, E. and J. Derome, 1977: Some effects of the upper boundary condition and vertical resolution on modelling forced stationary planetary waves. Mon. Wea. Rev., 105, 1239-1251.

Koshelkov, Y., 1977: Monthly mean temperatures, pressures and densities in the stratosphere of the Southern Hemisphere, 25-50km. COSPAR Space Research, XVII, 123-130.

Kung, E., 1966: Kinetic energy generation and dissipation in the large-scale atmospheric circulation. Mon. Wea. Rev., 94, 67-82.

Labitzke, K., 1974: The temperature in the upper stratosphere: difference between hemispheres. J. Geophys. Res., 79, 2171-2175.

Labitzke, K., 1977: Comparison of the stratospheric temperature distribution over Northern and Southern Hemispheres. COSPAR Space Research, XVII, 159-165.

Labitzke, K., 1980: Climatology of the stratosphere and mesosphere. Phil. Trans. Roy. Soc. Lond., A296, 7-18.

Labitzke, K., 1981: Stratospheric-mesospheric midwinter disturbances: a summary of observed characteristics. J. Geophys. Res., 86, 9679-9687.

Labitzke, K., and J. Barnett, 1973: Global time and space changes of satellite radiances received from the stratosphere and lower mesosphere. J. Geophys. Res., 78, 483-496.

Labitzke, K., and B. Goretzki, 1982: A catalogue of dynamic parameters describing the variability of the middle stratosphere during the northern winters. MAP, 5, edited by C. Sechrist, Jr., 188pp. Available from SCOSTEP Secretariat, University of Illinois, 1406 W. Green Street, Urbana, Illinois 61801.

Lau, N.-C., 1978: On the three-dimensional structure of the observed transient eddy statistics of the Northern Hemisphere wintertime circulation. J. Atmos. Sci., 35, 1900-1923.

Lau, N.-C., and A. Oort, 1981: A comparitive study of observed Northern Hemisphere circulation statistics based on GFDL and NCAR Analyses. Part I: The time-mean fields. Mon. Wea. Rev., 109, 1380-1403.

Leovy, C., 1964: Simple models of thermally driven mesospheric circulations. J. Atmos. Sci., 21, 327-341.

Lin, B.-D., 1982: The behavior of winter stationary planetary waves forced by topography and diabatic heating. J. Atmos. Sci., 39, 1206-1226.

Lindzen, R., 1981: Turbulence and stress due to gravity wave and tidal breakdown. J. Geophys. Res., 86, 9707-9714.

Lindzen, R., E. Batten and J.-W. Kin, 1968: Oscillations in atmospheres with tops. Mon. Wea. Rev., 96, 133-140.

London, J., R. Bojkov, S. Oltmans, and J. Kelley, 1976: Atlas of the global distribution of total ozone, July 1957-June 1967. NCAR Tech. Note NCAR/TN/113+STR, National Center for Atmospheric Research, Boulder, Colorado. Available from NTIS #PB 258882/AS.

London, J., J. Frederick and G. Anderson, 1977: Satellite observations of the global distribution of stratospheric ozone. J. Geophys. Res., 82, 2543-2556.

Madden, R., 1975: Oscillations in the winter stratosphere: Part 2. The role of horizontal eddy heat transport and the interaction of transient and stationary planetary-scale waves. Mon. Wea. Rev., 103, 717-729.

Maeda, K. and D. Heath, 1973: Asymmetries of the upper stratosphere ozone distribution between two hemispheres. J. Atmos. Sci., 40, 1353-1359.

Mahlman, J., J. Levy, and W. Moxim, 1980: Three-dimensional tracer structure and behavior as simulated in two ozone precursor experiments. J. Atmos. Sci., 37, 655-685.

Mahlman, J. and R. Sinclair, 1979: Recent results from the GFDL troposphere-stratosphere-mesosphere general circulation model. Proc. of ICMUA Sessions and IUGG Symposium 18, XVII IUGG General Assembly, Canberra, Australia.

Manabe, S. and B. Hunt, 1968: Experiments with a stratospheric general circulation model. Mon. Wea. Rev., 96, 477-502.

Manabe, S. and J. Mahlman, 1976: Simulation of seasonal and interhemispheric variations in the stratospheric circulation. J. Atmos. Sci., 33, 2185-2217.

Matsuno, T., 1970: Vertical propagation of stationary planetary waves in the winter Northern Hemisphere. J. Atmos. Sci., 27, 871-883.

Matsuno, T., 1971: A dynamical model of the stratospheric sudden warming. J. Atmos. Sci., 28, 1479-1494.

McGregor, J. and W. Chapman, 1979: Stratospheric temperatures and geostrophic winds during 1973-1974, Quart. J. Roy. Meteor. Soc., 105, 241-261.

McNulty, R., 1976: Vertical energy flux in planetary-scale waves: observational results. J. Atmos. Sci., 33, 1172-1183.

McPeters, R., 1980: The behavior of ozone near the stratopause from two years of BUV observations. J. Geophys. Res., 85, 4545-4550.

Miller, A., 1970: The transfer of kinetic energy from the troposphere to the stratosphere. J. Atmos. Sci., 27, 388-393.

Muench, H., 1965: On the dynamics of the winter stratospheric circulation. J. Atmos. Sci., 22, 349-360.

Nastrum, G., B. Balsley and D. Carter, 1982: Mean meridional winds in the mid- and high latitude summer mesosphere. Geophys. Res. Lett., 9, 139-142.

Naujokat, B., 1981: Long-term variations in the Stratosphere of the Northern Hemisphere during the last two sunspot cycles. J. Geophys. Res., 86, 9811-9816.

Newell, R., 1968: The general circulation of the atmosphere above 60km. Meteor. Monogr., No. 31, Amer. Meteor. Soc., 98-113.

Newell, R., 1972: Climatology of the stratosphere from observations. Climatic Impact Assessment Program: Proceeding of the Survey Conference, February 15-16, 1972, 165-185. Available from the Dept. of Transportation. DOT-TSC-OST-72-2.

Newell, R., D. Vincent, T. Dopplik, D. Ferruzza and J. Kidson, 1969: The energy balance of the global atmosphere. The Global Circulation of the Atmosphere, G. A. Carlas, Ed., Roy. Meteor. Soc., 42-90.

Newell, R. and M. Richards, 1969: Energy flux and convergence patterns in the lower and middle stratosphere during the IOSY. Quart. J. R. Met. Soc., 95, 310-328.

Nordberg, W., L. Katchen, J. Theon, and W. Smith, 1965: Rocket observations of the structure of the mesosphere. J. Atmos. Sci., 22, 611-622.

Oort, A., 1964: On the energetics of the mean and eddy circulations in the lower stratosphere. Tellus, 16, 309-327.

Oort, A., 1982: Global Atmospheric Circulation Statistics, 1958-1973. NOAA Prof. Pap. No. 14, U.S. Govt. Print. Off.

Oort, A., and E. Rasmusson, 1971: Atmospheric circulation statistics. NOAA Prof. Pap. 5, U.S. Govt. Print. Off.

Palmer, T., 1982: Properties of the Eliassen-Palm flux for planetary scale motions. J. Atmos. Sci., 39, 992-997.

Park, J. and J. London, 1974: Ozone photochemistry and radiative heating of the middle atmosphere. J. Atmos. Sci., 31, 1898-1916.

Phillips, N., 1957: A coordinate surface having some special advantage for numerical forecasting. J. Meteor., 14, 184-185.

Plumb, R., 1983: A new look at the energy cycle. J. Atmos. Sci., 40, 1669-1688.

Plumb, R., 1982: Zonally symmetric hough modes and meridional circulations in the middle atmosphere. J. Atmos. Sci., 39, 983-991.

Quiroz, R., 1979: Stratospheric temperatures during solar cycle 20. J. Geophys. Res., 84, 2415-2420.

Quiroz, R., 1980: Variations in zonal mean and planetary wave properties of the stratosphere and links with the troposphere. Pageoph., 118, 416-427.

Quiroz, R., 1983: The isolation of stratospheric temperature change due to the El Chichon volcanic eruption from nonvolcanic signals. J. Geophys. Res., 88, 6773-6780.

Ramanathan, V., and R. Dickinson, 1979: The role of stratospheric ozone in the zonal and seasonal radiative energy balance of the Earth-troposphere system. J. Atmos. Sci., 36, 1084-1104, 1979.

Randall, W., and J. Stanford, 1983: Structure of medium-scale atmospheric waves in the Southern Hemisphere summer. J. Atmos. Sci., 40, 2312-2318.

Reed, R., 1966: Zonal wind behavior in the equatorial stratosphere and lower mesosphere. J. Geophys. Res., 71, 4223-4233.

Reiter, E., and D. Westhoff, 1981: A planetary-wave climatology. J. Atmos. Sci., 39, 732-750.

Richards, M., 1967: The energy budget of the stratosphere during 1965. Planetary Circulations Project, MIT Rep. No. 21, Contract AT(30-1)2241 (NTIS MIT-2241-38).

Rottger, J., 1980: Structure and dynamics of the stratosphere and mesosphere revealed by VHR Radar investigations. Pageoph., 118, 494-527.

Russell, G., and J. Lerner, 1981: A new finite-differencing scheme for the tracer transport equation. J. App. Meteor., 20, 1483-1498.

Sato, Y., 1980: Observational estimates of Eliassen and Palm flux due to quasi-stationary planetary waves. J. Meteor. Soc. Japan, 58, 430-435.

Schoeberl, M. and D. Strobel, 1978: The response of the zonally averaged circulation of the middle atmosphere. J. Atmos. Sci., 35, 577-591.

Scott, A., 1972: Mesospheric temperatures and winds during a stratospheric warming. Phil. Trans. Roy. Soc. Lond., A271, 547-557.

Smith, A., 1983: Stationary waves in the winter stratosphere: seasonal and interannual variability. J. Atmos. Sci., 40, 245-261.

Spahr, J., K. Yamazaki, M. Suarez, C. Mechoso, and A. Arakawa, 1982: A study of the sensitivity of numerical forecasts to an upper boundary in the lower stratosphere. Mon. Wea. Rev., 110, 1984-1993.

Staff, Upper Air Branch, 1967, 1969, 1970, 1971: Weekly synoptic analyses, 5-, 2-, and 0.4mb surfaces for 1964, 1965, 1966, 1967 and 1968. ESSA Tech. Reps. WB-2, WB-3, WB-4, WB-12, and NOAA Tech. Rep. NWS-14, National Weather Service, Washington, D.C. Available from NTIS #N70-32342 and N71-36971.

Staff, Upper Air Branch, 1967, 1969: Monthly mean 100-, 50-, 30-, and 10mb charts for 1964, 1965, 1966, 1967. ESSA Tech. reps. WB-1 and WB-11, National Weather Service, Washington, D.C. Available from NTIS #N70-10624.

Taljaard, J., H. van Loon, H. Crutcher, and R. Jenne, 1969: Climate of the Upper Air, Vol. 1. NAVAIR 50-1C-55 (U.S. Govt. Print. Office).

Tenenbaum, J., 1982: Integrated and spectral energetics studies of the GLAS General Circulation Model. Mon. Wea. Rev., 110, 962-980.

Theon, J., W. Smith, J. Casey, and B. Kirkwood, 1972: The mean observed meteorological structure and circulation. NASA TR-R-375, 69pp. Available from NTIS #N72-20551.

Trenberth, K., 1980: Planetary waves at 500mb in the Southern Hemisphere. Mon. Wea. Rev., 108, 1378-1389.

U.S. Committee on Extension to the Standard Atmosphere, 1962: U.S. Standard Atmosphere, 1962. U.S. Govt. Printing Office.

van Loon, H., 1980: Transfer of sensible heat by transient eddies in the atmosphere of the Southern Hemisphere: an appraisal of the data before and during FGGE. Mon. Wea. Rev., 108, 1774-1781.

van Loon, H., and R. Jenne, 1972: The zonal harmonic standing waves in the Southern Hemisphere. J. Geophys. Res., 77, 992-1003.

van Loon, H., K. Labitzke, and R. Jenne, 1972: Half-yearly wave in the stratosphere. J. Geophys. Res., 77, 3846-3855.

van Loon, H., R. Jenne, and K. Labitzke, 1973: Zonal harmonic standing waves. J. Geophys. Res., 78, 4463-4471.

Wallace, J., and V. Kousky, 1968: Observational evidence of Kelvin waves in the tropical stratosphere. J. Atmos. Sci., 25, 900-907.

Wang, P., S. Hong, M. Wu, and A. Deepak, 1982: A model study of the temporal and spatial variations of the zonally-averaged ozone heating rates. J. Atmos. Sci., 39, 1398-1409.

Wehrbein, W. and C. Leovy, 1982: An accurate radiative heating and cooling algorithm for use in a dynamical model of the middle atmosphere. J. Atmos. Sci., 39, 1532-1544.

Williams, B., 1968: Synoptic analysis of the upper stratospheric circulation during the late winter storm period of 1966. Mon. Wea. Rev., 96, 549-

World Meteorological Organization, 1981: The stratosphere 1981: theory and measurements. WMO Global Ozone Research and Monitoring Project Rep. No. 11. Copies available from WMO, Case Postale No. 5, Geneva 20, Switzerland.

Zimmerman, S. and T. Keneshea, 1981: Turbulent heating and transfer in the stratosphere and upper mesosphere. MAP, 2, 311-322. S. Avery, editor. Available from SCOSTEP Secretariat, University of Illinois, 1406 W. Green Street, Urbana, Illinois 61801.